2-1-2015

Functional nanostructred photoanodes for solar fuel production

Ahmad Mohyeldin Mohamed

The American University in Cairo

School of Sciences and Engineering

Nanotechnology Program

Functional Nanostructured Photoanodes for Solar Fuel Production

A Thesis in

Nanotechnology

By

Ahmad Mohyeldin Mohamed

Submitted in Partial Fulfillment of the Requirements

For the Degree of

Master's of Nanotechnology

July 2015

The thesis of Your Name was reviewed and approved* by the following:

Nageh K. Allam
Associate professor. Department of Physics, The American University in Cairo.
Director, Energy and Materials lab (EML).
Thesis Advisor
Chair of Committee

Mohammad AlFiky
Assistant professor, Department of Physics, The American University in Cairo.

Hassan Ahmed
Associate professor at Suez University.

Hanadi Salem
Professor, Department of Mechanical Engineering, The American University in Cairo.
Moderator

*Signatures are on file in the Graduate School

ABSTRACT

Improving the efficiency of water splitting process is one of the main obstacles that are facing the generation of renewable energy. Charge carriers separation is always coupled with low visible light absorption and stability of the materials used. Various efforts have been done in order to construct a full system of different materials that can absorb visible light efficiently, with an enhanced electron hole separation process for an efficient water splitting. However, most of the reported systems suffer either from crystal mismatch between the multiple materials the use of long linkers that promote the recombination of the carriers. In this thesis, we are introduce a new system of titania nanotubes that are functionalized with graphene quantum dot, as a photosensitizer and an efficient charge carrier collector and transporter.

In the first part of the thesis, one-dimensional TiO_2 nanotubes photoanodes were investigated. We are able to produce ultra thin walled titania nanotubes, for the first time. Thin walled titania nanotubes showed higher quantum efficiency; about 50% compared to 15 % for conventional thick-walled nanotubes, with a 50% enhancement in the photocurrent. This enhancement is mainly attributed to the very small wall thickness (3 nm), allowing the diffusion of the charge carriers across the wall, regardless the potential across the region.

In the second part, the effect of hydrogen annealing on the optical and electrical properties of the thin-walled nanotubes was investigated. It was found hydrogen annealing for 4 hours passivate the trap states on the surface of titania, while annealing for longer times acts to create more defect states, larger carrier concentration, larger dark

current, higher resistance. In addition, we introduced a new concept by adding KOH and hydrogen annealing resulted in lower resistance and higher charge carrier concentration and photocurrent.

In the third part, we produced graphene quantum dots, and for the first time, we were able to functionalize graphene quantum dots with different groups (mercapto propanoic acid, and malonyl group). We also introduced a new anchoring method for graphene quantum dots on the surface of titania. The photocurrent was enhanced by 50%, and the reasons were discussed in details.

Finally, we showed the possible new applications for titania nanotubes that are functionalized with our graphene quantum dots.

Table of contents

LIST OF FIGURES

LIST OF TABLES

ACKNOWLEDGEMENTS

I would like to thank everyone who helped me to reach this step.

It is really hard to express my gratitude to Dr. Nageh Allam, who changed my whole life. His inspiring attitude and adventurous spirit gives me hope, motivation, and pushes me forward. He is the only one who believed that I can work with semiconductors even no one believed so. He is always patient and supportive with everyone. He is unique with his manners and ethics; he is full of positive energy that appears everywhere in his lab. I am totally proud to be one of his students.

I would like to thank my professors at AUC, especially Dr. Hanadi Salem for her patience during teaching or during the guidance, she really paid lots of efforts to create this interdisciplinary program. Also, I would like to thank Dr. Adham Ramadan, Dr. Wael Mamoduh and Dr. Mohamed Serry.

I would like to thank all the EML members, they are not just work colleagues, but they turned to be real brothers and sisters. The working atmosphere in the EML is unique, and I believe it is hard to compare it to somewhere else.

I would like to thank all Yousef Jameel center members for their help and cooperation during our research.

The collaboration and hosting of Dr. Mostafa el Sayed in Georgia Tech is greatly acknowledged. Dr. Mostafa provided me with all his lab and clean room facilities, also I would like to thank Steven and Sajan from LDL for their cooperation.

I owe special gratitude to my mom, dad, my sister, Jana and Ali for their patience and support, I know that I always give them hard time, but I promise to give them back as much as I can.

Chapter 1

1) Introduction and Scope of the Thesis

1.1 Energy problems

Energy is the basis of the whole world's activity. The advancement in industry and economy is totally dependent on the availability of an energy source. The world consumes highly concentrated energy forms that are embedded by nature irresponsibly [1,2]. The improper use of natural energy sources negatively affect the quality of life, leading to miserable results in terms of pollution, damaging nature or even diminishing the natural resources [3]. Generally, there are four main real time problems:

1) Disruption of the eco-system: Everything in nature is in equilibrium with its environment, and once the human disrupts this equilibrated system for his own needs, the whole system suffers. Deforestation and damping rivers lead to change in moisture content, killing thousands of habitant animals and organisms. By disrupting one item in the eco system, there would be a great chance for the whole system to collapse.

2) Depletion of resources: The non-renewable, cheap energy resources are valuable, and they are not owned by any generation. Consuming this valuable energy sources by one generation, without using it to find new ways for renewable energy is considered a disaster. Saudi Arabia had one of the largest amounts of ground water in the world that was pure

drinking water [4]. However, due to the lack of planning and studying, most of the ground water was consumed in faming in less than 50 years, leading Saudi Arabia one to be of the poorest countries in the world in terms of water/population.

3) Centralization: Population tends to gather around the energy sources, and hence, cities with natural energy reserves will be highly populated, while small rural areas will suffer from lack of business and governmental care. This difference is obvious when a petrol rich state like Texas is compared to Wyoming [5].

4) Wars: Several wars are initiated for conquering non-renewable resources, especially in the Middle east. What is happening in Iraq now is a consequence of having one of the highest natural reserves for oil in the world.

1.2 Energy Strategy

Based on the above discussion, it is essential for the whole world to change the energy strategy, from consuming the highly concentrated reserves to the efficient use of current reserves and shifting to new renewable energy sources [6]. There are lots of promising renewable energy sources that show a great promise and development. Solar energy is one of the largest sources that are not efficiently utilized till now. A small example can show the problem. Sub Sahara (African countries) have wide areas that are totally hit by the sun for most of the day, yet 5% of Sub Saharan countries only have access to electricity [7]. The strange contradiction here is that those countries are suffering

from endless wars and geopolitical problems, that are mainly arising because on the energy sources (fossil fuels). On the other hand, a country like Bangladesh [8] started an optimistic plan to change 80,000 homes/month to solar energy, and now more than 3 million homes (off grid) are having electricity, moreover more than 150,000 new jobs were created for these applications.

With the great advancement in the solar energy technologies and by increasing the number of population depending on it, the price of solar energy decreased in the past few years, to be leveled with fossil fuels and [9] sometimes-cheaper. The main concern of energy and the main advantage of fossil fuel compared to renewable sources is the ability to store it. Currently, it is very hard to store solar energy for long time, as a result the world is starting to head towards new forms of solar energy that can be easily and efficiently stored.

1.3 Hydrogen fuel

Hydrogen is one of the proposed solutions as a clean energy source. It is considered as a water by-product, easily transported and stored [10]. Huge investments being directed towards the development of hydrogen fuel in different size vehicles. Yet, the main barrier that must be overcome before hydrogen becomes the main source of energy is its economic production. Till now, hydrogen production is considered as a costly process. This high cost arises mainly in the form of the energy needed to produce hydrogen. Generally, hydrogen requires at least twice as much energy as electricity, twice the tonnage of coal, twice the number of nuclear plants, or twice the field of PV panels to perform an equivalent unit of work [11,12]. Most of today's hydrogen is produced from natural gas, which is only an interim solution since it discards 30% of the energy in one

valuable but depletable fuel (natural gas) to obtain 70% of another (hydrogen) [12]. The challenge is to develop more appropriate methods based on sustainable energy sources, methods that do not employ electricity as an intermediate step.

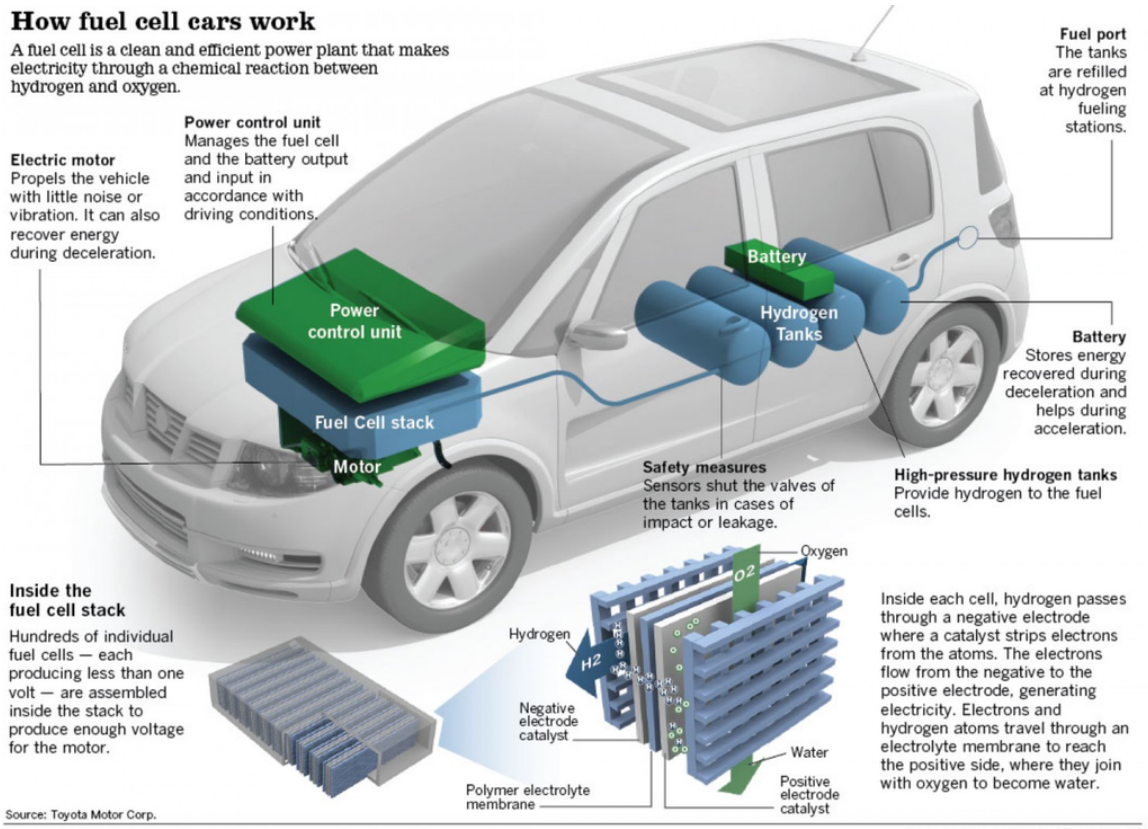

Fig. 1-1: How the fuel cells in cars work [13].

The most cost-efficient method for producing hydrogen fuel is by steam reforming. Hydrocarbons (natural gas) are treated under very high temperature that leads to chemical break down of the hydrocarbons into hydrogen [11]. This process is still producing hydrogen with higher prices if compared to other energy sources, and there are additional costs to get rid of the dangerous by-products. Water electrolysis is another way

to produce hydrogen, although its cost is higher, but the quality of the produced hydrogen is also higher.

There is a strong need to find new ways that produce cost-effective hydrogen fuel. Using solar light to produce hydrogen, known as water splitting, can be the solution for this problem.

1.4 Nanotechnology

Relying on nanotechnology to produce efficient photoanodes that can absorb the visible sun light and convert it into electricity to be used to split water molecules into oxygen and hydrogen, a similar process to water electrolysis, is very promising.

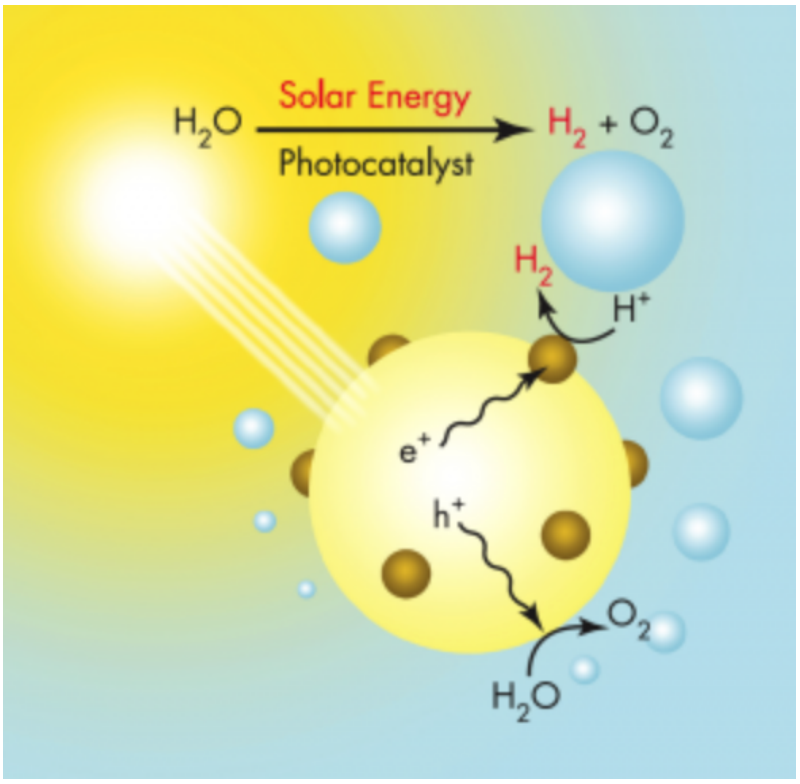

Fig. 1-2: a schematic representation of water splitting process [11].

2 Scope and objective of the thesis:

Our main scope is to develop nanostructred photoanodes with enhanced charge carriers transport, visible light absorption characteristics, and stable.

Chapter 2 Reviews the literature for recent advances in TiO_2 nanotubes, black titania and graphene quantum dots.

Chapter 3 Reveals the scientific background for the physical and chemical aspects that directly affects the efficiency of the produced photoanodes.

Chapter 4 Deals with different synthesis procedures and conditions used in the thesis.

Chapter 5 Presents results and discussion for our findings in the ultra thin walled titania nanotubes.

Chapter 6 Presents our findings regarding the black titania.

Chapter 7 Shows the results of producing and functionalizing graphene quantum dots and their application in water splitting.

Chapter 8 Conclusions and future work.

References

1. Pindyck RS. The structure of world energy demand. *MIT Press Books*. 1979;1.

2. Smil V. Energy in world history. 1994.

3. Szidat S, Jenk TM, Synal H, et al. Contributions of fossil fuel, biomass‐burning, and biogenic emissions to carbonaceous aerosols in zurich as traced by 14C. *Journal of Geophysical Research: Atmospheres (1984–2012)*. 2006;111(D7).

4. Konikow LF, Kendy E. Groundwater depletion: A global problem. *Hydrogeol J*. 2005;13(1):317-320.

5. Weber JG. The effects of a natural gas boom on employment and income in colorado, texas, and wyoming. *Energy Econ*. 2012;34(5):1580-1588.

6. Shariatzadeh F, Mandal P, Srivastava AK. Demand response for sustainable energy systems: A review, application and implementation strategy. *Renewable and Sustainable Energy Reviews*. 2015;45:343-350.

7. Bazilian MD. Power to the poor. *Foreign Affairs*. 2015;94(2):133-138.

8. Rashid R. Towards sustainable energy development in bangladesh-the perspective of renewable energy technology. *Journal of Modern Science and Technology*. 2015;3(1).

9. Koroneos C, Dompros A, Roumbas G, Moussiopoulos N. Life cycle assessment of hydrogen fuel production processes. *Int J Hydrogen Energy*. 2004;29(14):1443-1450.

10. Nicoletti G, Arcuri N, Nicoletti G, Bruno R. A technical and environmental comparison between hydrogen and some fossil fuels. *Energy Conversion and Management*. 2015;89:205-213.

11. Haryanto A, Fernando S, Murali N, Adhikari S. Current status of hydrogen production techniques by steam reforming of ethanol: A review. *Energy Fuels*. 2005;19(5):2098-2106.

12. Hanley ES, Glowacki BA, Nuttall WJ, Kazantzis N. Natural gas–synergies with hydrogen. . 2015.

13. Munk S. Toyota to'kick-start'hydrogen fuel cell market. *Engineering & Technology*. 2015;10(1):15-15.

Chapter 2

Literature review

2.1 Titania nanotubes

Titanium dioxide is considered as one of the most attractive materials that can be used in various applications [1]. Despite its wide band gap (3.2eV for anatase), it is still used widely in various photovoltaic applications [2]. With the emergence of the nanotechnology era, and the ability to tune the material's physical properties by changing its size and shape, different forms of titania nanostructures have been produced in order to fit with various applications. Titania nanoparticles, nanorods and nanotubes are competing together especially in the photovoltaic applications. For Dye synthetized solar cells (DSSC) [3], where large surface area is required to achieve high loading density for the dye on the surface of titania, nanoparticles are considered to be the best. However, the use of nanoparticles can be problematic due to the random connection between the nanoparticles, which leads to increased recombination rate of electrons and holes. Therefore, using nanoparticles is not the best solution for water splitting [4]. 1D nanostructures can solve the problem of the random movement and recombination of electrons and holes, by separating the electron-hole movement directions, in order to achieve higher quantum efficiency (Scheme 2-1). Nanowires and nanotubes are the main representatives of the 1D nanostructures in literature. Being cylindrical in shape, with very high aspect ratio (length to diameter ratio), and confined in two dimensions to the nanoscale, the rules of quantum confinement apply on the electrons and holes in such structures [3]. Unlike quantum dots, is

totally confined to the nanoscale, the length of nanotubes or nanowires can be in the micron range, which offers an additional advantage compared to the quantum dots. This will enable to transport of the confined electrons and holes over long distances and even can shuttle electrons and holes to other substrates. Generally, nanowires are longer than the nanotubes, and due to physical consideration in water splitting mechanism; nanotubes are more preferred to nanowires due to the limited absorption coefficient of the material. Very long nanowires will experience dark areas, which will act as recombination centers. Our main focus in this work is on using titania nanotubes for water splitting application [5].

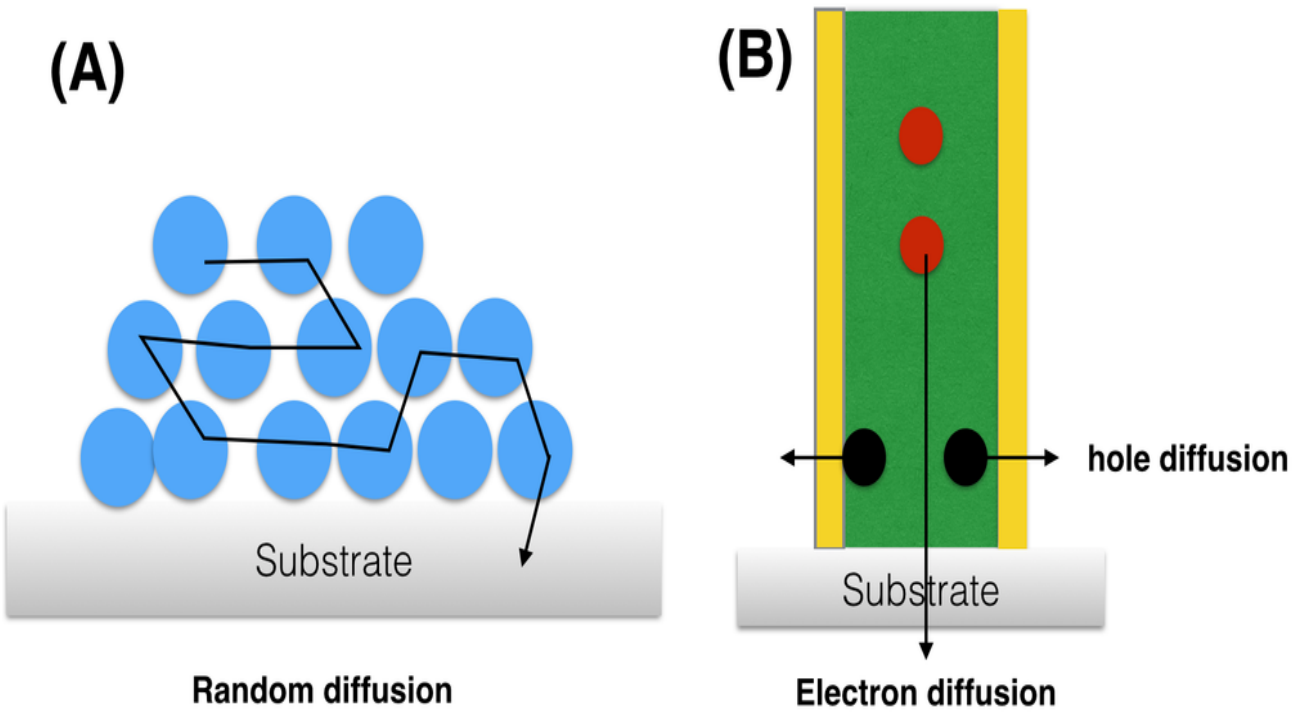

Scheme 2-1: Electron and hole diffusion in (A) nanoparticles (B) and nanotubes.

Geometric consideration for titania nanotubes:

There are several parameters that should be controlled in order to obtain highly efficient titania nanotubes for anodes for water splitting application. The three main factors are the tube length, pore diameter and wall thickness [3]. Before addressing the three main factors, it is important to shed the light on other different structural and compositional factors that can affect the whole water splitting.

The orderness of the nanotubes was first addressed by Zwilling et al, [6,7] who was the first to produce ordered nanotubes structures and to shed the light on the importance of having highly ordered material. Zwilling et al. called his nanostructure as a nanoporus but actually it was nanotubes of 500 nm, using chromic acid as an electrolyte (Fig. 2-1).

They also related the formation of the nanotubes to the presence of the fluoride ions.

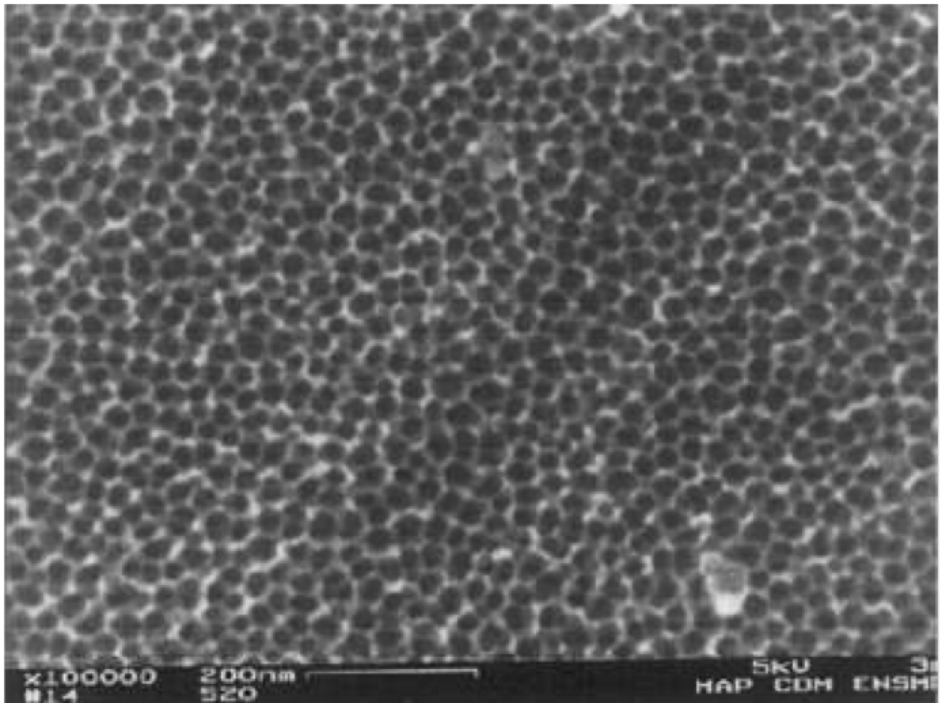

Fig. 2-1: Nanoporous layer that was first shown by Zwilling et al.

Several trials were initiated after this work in order to improve the side wall homogeneity and the orderness of the nanotubes. Kelly et al. in 1979 [8] was the first to address this problem, as they showed that using small concentration of fluoride ions enhances the surface orderness and the homogeneity of the nanotube side walls. Macak et al. [9-11] worked on improving and understanding the real factors behind the synthesis of nanotubes. They showed the effect of pH on the nanotube length, and recommended the use of non-aqueous solvents to passivate the side walls inhomogeneity and increase the aspect ratio of the formed tubes. Macak el al. were able to produce hexagonal nanotubes using ethylene glycol as a non aqueous electrolyte and ammonium floride as the etchant (Fig. 2-2).

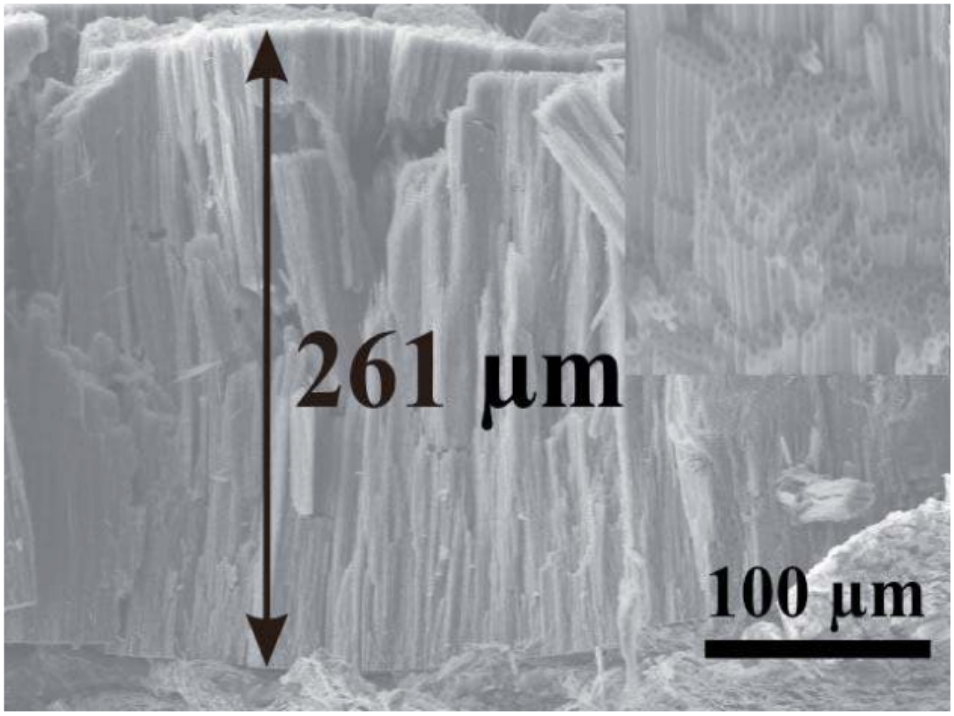

Fig. 2-2: Very long titania nanotubes produced by Macak et al [11].

Roy et al. [5] also studied the effect of the fluoride ion concentration in ethylene glycol, together with the voltage effect on the length of the nanotubes. It was deduced that increasing both the applied voltage and the fluoride ion concentration increases the length of the nanotubes and their order (Fig.2-3).

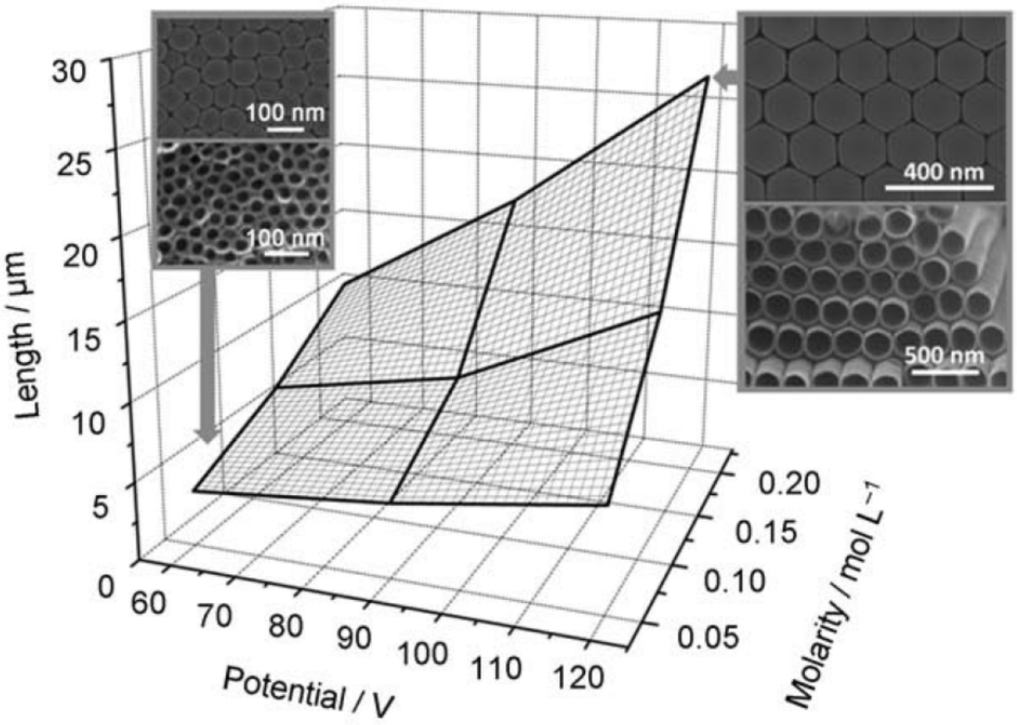

Fig. 2-3: Effect of changing anodization parameters on the tube orderness [5].

Several research groups studied the effect of the anodization time on the tube length (length of the oxide layer) using different electrolytes or even mixtures of organic and in organic electrolytes [12-15](Fig. 2-4).

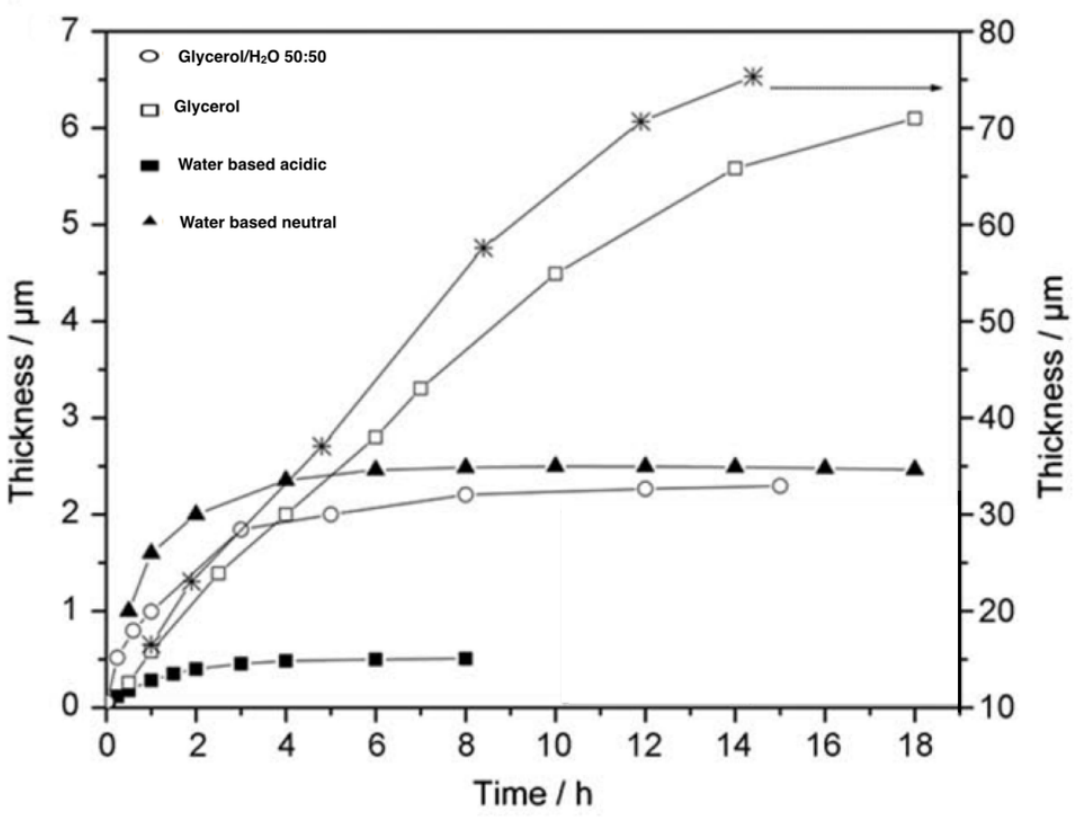

Fig. 2-4: Titanium dioxide nanotubes at different electrolytes and effect on nanotubes thickness [5,13-15].

Other groups reported the effect of the applied voltage on the tube diameter, as one of the crucial factors for efficient water splitting. The use of aqueous or protic electrolytes led to the formation nanotubes with smaller diameter [5] (Fig. 2-5).

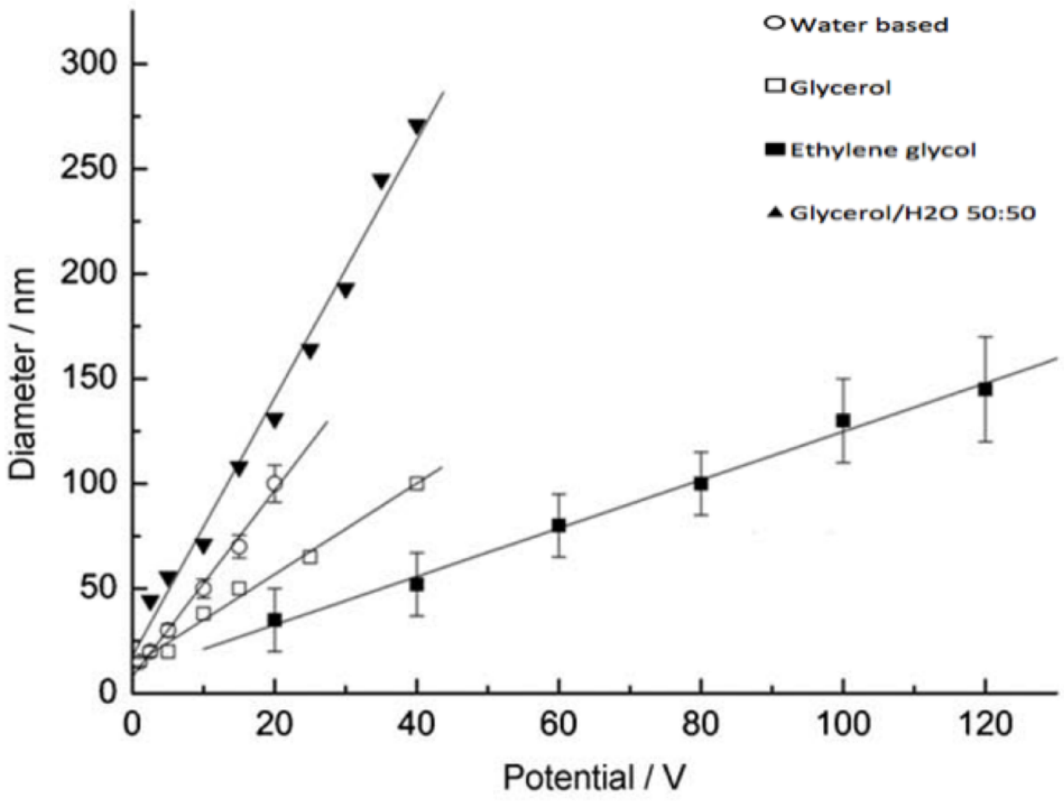

Fig. 2-5: Effect of changing electrolyte and voltage on the diameter of the nanotubes.

Grimes et al [3,16] were interested in improving the nanotubes aspect ratio and properties. The group published large number of papers dealing with titania nanotubes synthesis parameters that directly affects the length, pore size and wall thickness of the nanotubes. Shankar et al. [17]showed the effect of using different cations (5 different cations) on the nanotube length, wall thickness and pore size. He used formamide-based electrolyte and floride ions as etchant. He found that using bulky cations restricts the formation of thick interfacial layer, which is responsible for blocking the ion transfer; as a result longer nanotubes are formed.

Table 1: The effect of adding cations to different electroytes and its effect on the geometric parameters of the nanotubes [17].

cation	molar (M) cation concentration	anodization duration (hr)	outer diameter (nm)	wall thickness (nm)	nanotube length (μm)
		(a) Anodization Potential = 35 V			
H^+	0.14	101	256	21	5.6
H^+	0.27	48	214	20	7.3
NH_4^+	0.14	88	208	17	29.2
NH_4^+	0.27	30	159	15	37.4
Na^+	saturated solution (~0.04)	48	48	18	9.6
Bu_4N^+	0.27	48	190	22	68.9
		(b) Anodization Potential = 20 V			
H^+	0.27	48	99	22	2.9
NH_4^+	0.14	55	90	19	14.4
NH_4^+	0.27	24	90	17	19.6
Bu_4N^+	0.27	34	90	16	35.2
		(c) Anodization Potential = 15 V			
NH_4^+	0.14	110	81	29	8.2
Bu_4N^+	0.27	46	80	15	20.0
$BnMe_3N^+$	0.27	42	70	18	7.2

Mor et al. [4] were able to modify the length and the wall thickness of titnaia nanotubes simply by varying the temperature. Increasing the temperature from 5°C to 50°C, the wall thickness and the length of the nanotubes decreases by a factor of 4 and 2, respectively.

Table 2 : Effect of changing the anodization temperature of the nanotube's wall thickness and length [4].

anodization temp	wall thickness (nm)	tube length (nm)
5 °C	34	224
25 °C	24	176
35 °C	13.5	156
50 °C	9	120

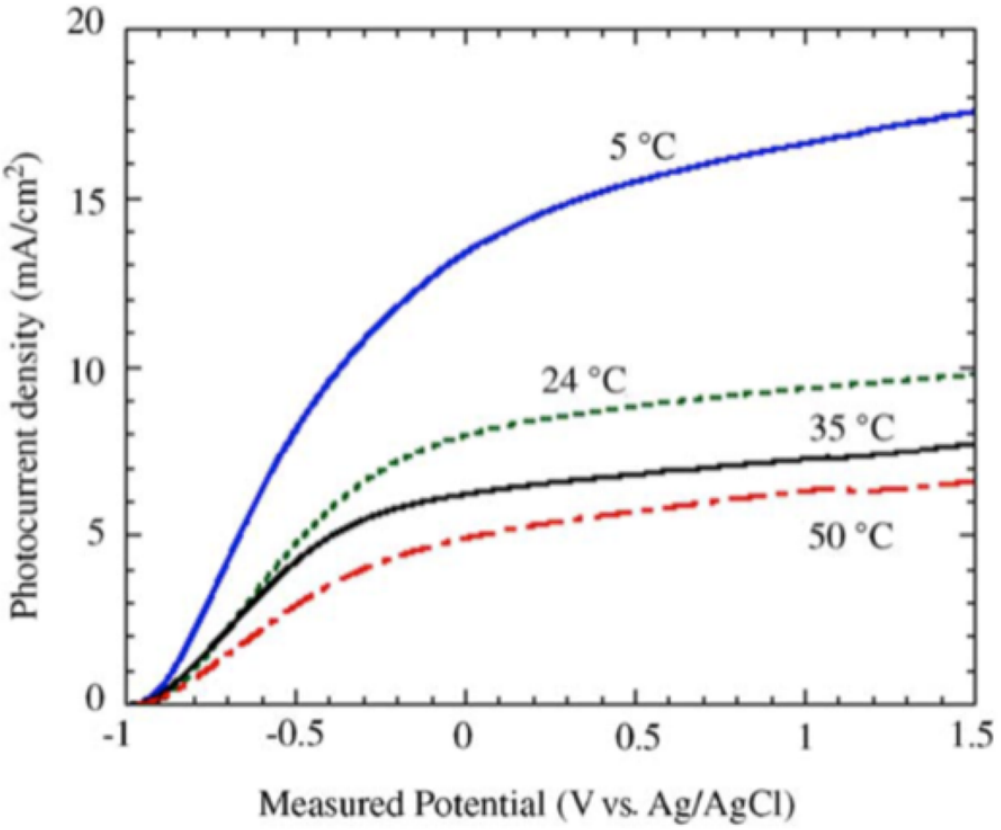

Fig. 2-6: Photocurrent response of nanotubes produced at different temperatures[4].

Moreover, the photocurrent was measured for the different nanotubes produced at different temperatures (Fig. 2-6). It was found that the nanotubes with the smallest wall thickness and length achieved the highest photocurrent under UV light. This finding sheds the light on the importance of the wall thickness factor in determining the efficiency of the photocurrent produced.

Till now, there is no reported method that can produce titania nanotubes with high aspect ratio and at the same time with a thin wall thickness. Recently, Amer et al. [18] (Fig. 2-7) were able to produce very well aligned zirconia nanotubes using a mixture of aqueous and non aqueous electrolyte (glycerol based), with floride ions as the etchant.

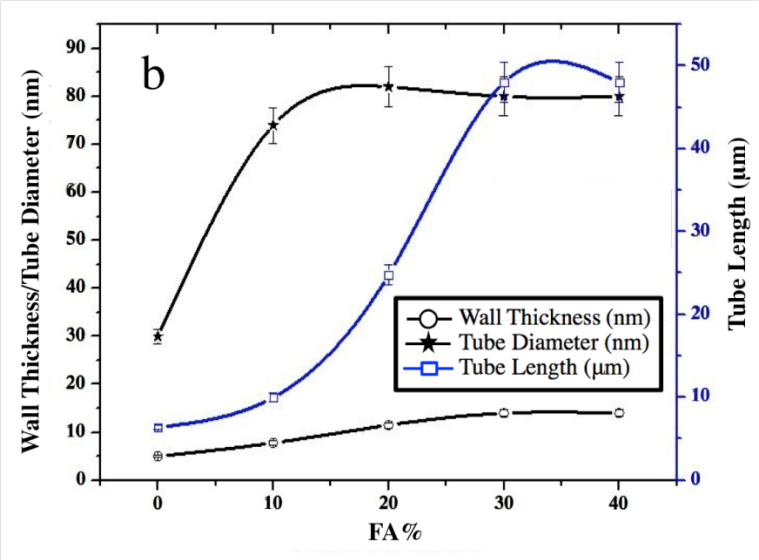

Fig. 2-7: Effect of changing formamide, fluoride and water content in the electrolyte directly affects the wall thickness and the length of the nanotubes [18].

2.2 Black titania:

The concept of black titania was first introduced in 2011 by Chen et al. [19] in their widely famous paper published in Science. The concept of black titania as indicated in the aforementioned paper is based on forming new mid gap defect states by reducing the oxygen via hydrogenation, which reduces the band gap of titania by 1.54 eV. Although similar work was publish by 1965 by Cornemeyer [20] on titania nanoparticles (Fig. 2-8), but it was not cited in this work. Later, Wang et al. [21] introduced their concept about hydrogen annealing and its effect on water splitting using titania nanowires and nanotubes (Fig. 2-9).

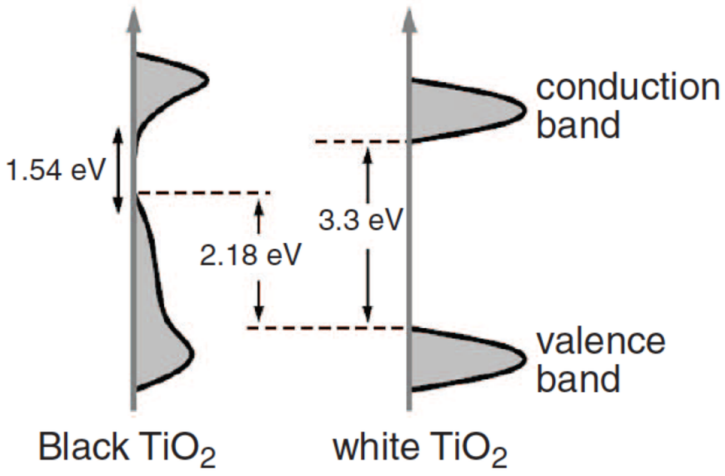

Fig. 2-8: Difference between the band diagram in black and white titania [19].

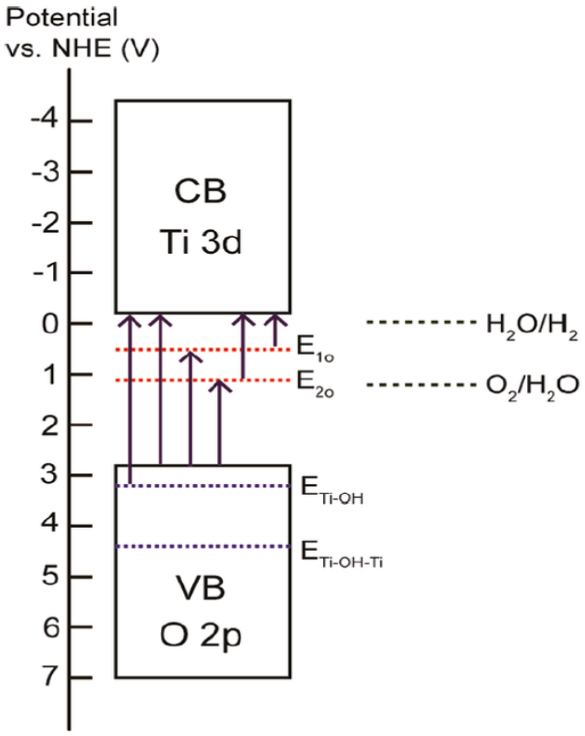

Fig. 2-9: The two oxygen defect states created below the conduction band of titania [21].

Based on Cornemeyer [20] experiments who was able to define the oxygen vacancies that are created below the conduction band (shallow and deep defects), they started to define the effect of both defect states on the water splitting process [21]. They found that both states are not straddling the water oxidation and reduction potential. In addition the deep defect states act as charge carriers recombination center, which are thought to reduce the produced photocurrent. On the other hand, the created defect states increase the charge carrier density of titania, as proven by Mott-Schottky analysis. Also, the measured photocurrent showed an improvement together with the quantum efficiency. Schmuki et al. [22] showed a quite improvement in photocurrent via hydrogen annealing of the nanotubes in three different cases, hydrogen followed by argon, high-pressure hydrogen, and air annealed samples (Fig. 2-10). They concluded that the argon followed by hydrogen showed the highest absorbance and photocurrent responses.

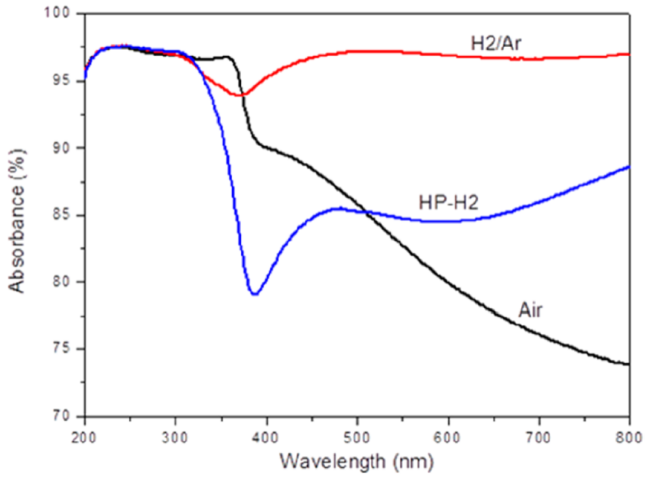

Fig. 2-10: UV-visible absorption spectra for three titania nanotubes annealed under air, high pressure hydrogen and hydrogen followed by air [22].

It's clear that most of the articles are not focusing on the exact mechanism or how the improvement takes place; instead the main focus is on producing higher photocurrent. The papers cited above showed totally different conflicting results and improvement rates.

Surprisingly, Tusi et al. [23] showed that hydrogen annealing passivates the surface trap states, on contrary to all what have been published before. they strengthened their argument by annealing the material with hydrogen and lithium and measured Mott-Schottky response to find that the conductivity is higher for hydrogen annealed samples with improved electron lifetime and current transient.

The aforementioned controversial reports indicated that the real problem is in the full understanding of the hydrogen effect.

We noted that every published paper uses its own technique in hydrogen annealing without describing the experimental details. Therefore, we believe that this is the real reason behind the contradicting results in literature.

2.3 Graphene quantum dots:

Although it is newly discovered and produced, graphene took its place as one of the hottest topics in nanotechnology. Owing to its very high conductivity and electron mobility, in addition to its high mechanical strength, graphene can act as a co-catalyst or charge carrier reservoir [24]. Unfortunately, graphene hydrophobicity hindered such processes. On the other hand, graphene oxide was introduced a solution for this problem, not just that but also a new band gap is formed in graphene oxide due to the incorporation of O2p by oxidizing graphene. This reaction opened a new avenue for new applications for graphene oxide, even as a photoactive material [25-27].

Kim et al [28]. introduced a composite made of reduced graphene oxide and titania nano-sheets. The interaction occurred by electrostatic self-assembly between the negatively charged reduced graphene oxide and the positively charged titania nano-sheets. They proved theoretically and experimentally that there is an exchange in electrons that takes place between titania and reduced graphene oxide. Moreover, they speculated that there might be a band gap reduction of titania, due to the enhanced visible light absorption (Fig. 2-11 and 2-12).

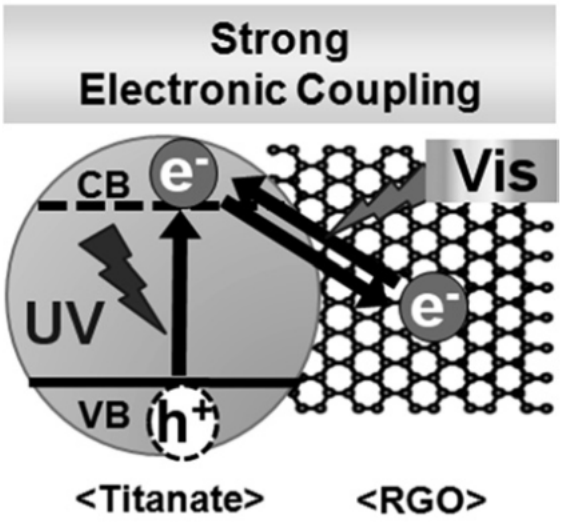

Fig. 2-11: Electronic coupling that is formed between titania nanosheets conduction and reduced graphene oxide [28].

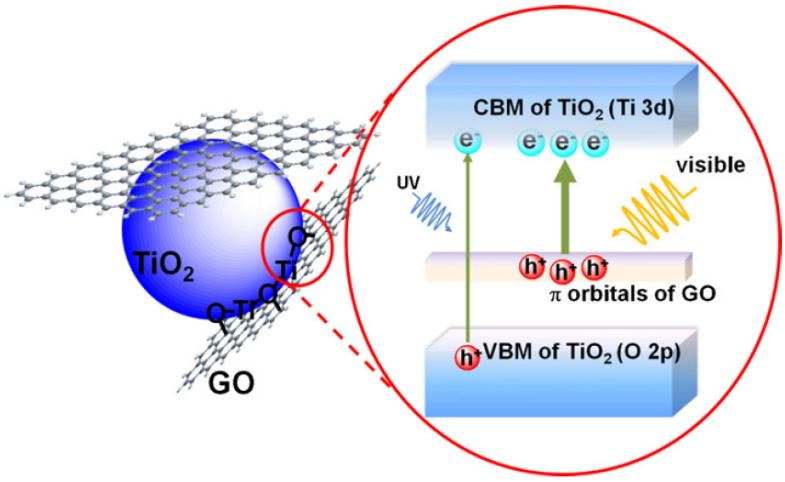

Fig. 2-12: Band gap reduction of titania by the O2p of graphene oxide [28].

Iwase et al. [29] (Fig. 2-13) were able to use graphene oxide as an electron mediator between $BiVO_4$ and Ru-$SrTiO_3$:Rh, which resulted in a three-fold increment in photocurrent density.

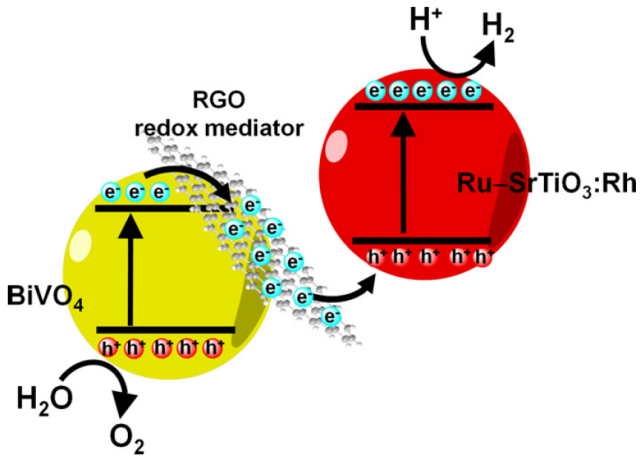

Fig. 2-13: Using reduced graphene oxide as an electron mediator between $BiVO_4$ and Ru-$SrTiO_3$:Rh [29].

Yeh at al. [30] (Fig. 2-14) did Mott-Schottky analysis to determine the Fermi level of graphene oxide of different oxidation states (valence band). They found that by increasing the

oxidation level, the Fermi levels tend to shift to more positive values (vs Ag/AgCl), while the conduction band remains intact. In the tree cases of different oxidation levels shown below, both the valence and conduction band straddles the water oxidation and reduction potentials, which means its suitable for water splitting reaction.

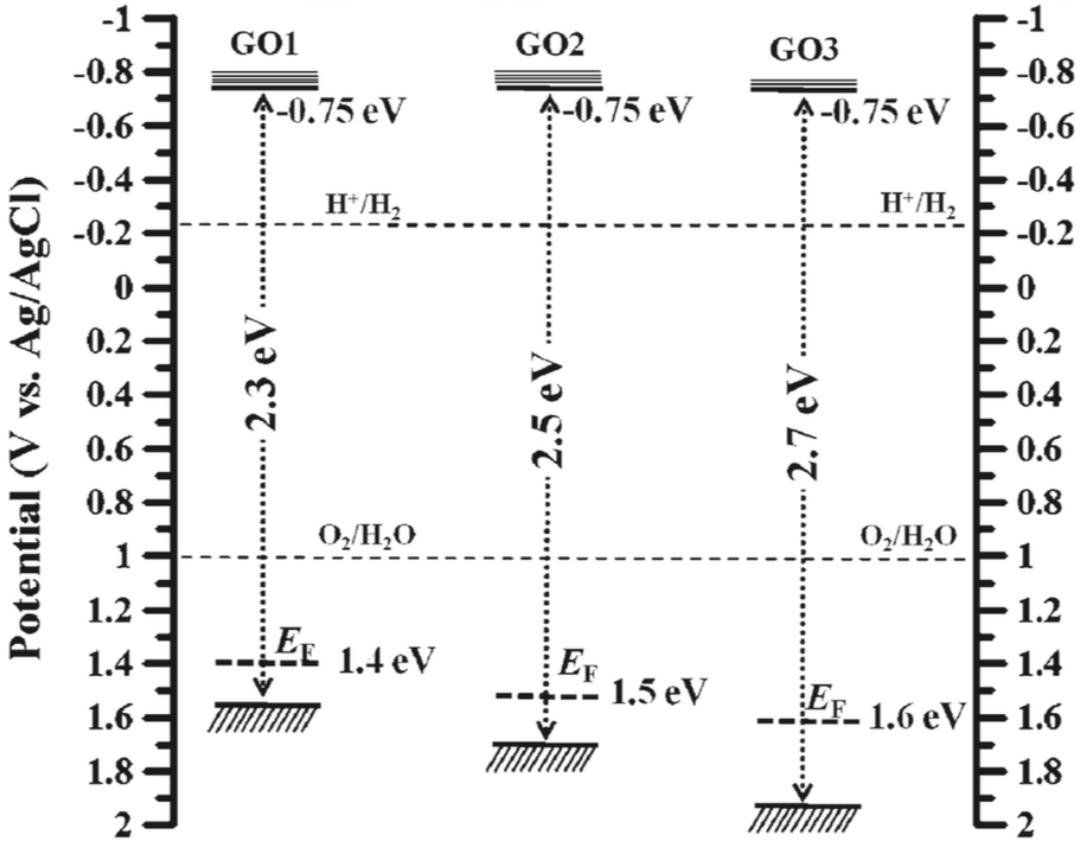

Fig. 2-14: Degree of oxidation of graphene oxide and its direct reflection on the band gap of graphene oxide [30].

In summary, to use graphene oxide as a photosensitizer, the maximum band gap reduction that could be attained is achieved by reducing graphene oxide to reach a band gap of 2.3 eV (absorption edge at 539 eV). It still not satisfactory for a material like graphene.

Graphene quantum dots are thought to be the magical material that will allow the efficient tuning of the band gap to the complete visible absorption. Semi conductor quantum dots are well known for their" size dependent optical properties", where the size of the band gap changes inversely with the size of the quantum dots [31].

Several methods are proposed for the synthesis of quantum dots. They mainly depend on the etching of graphene or graphene oxide, either solvothermally or electrochemically, or even via chemical reaction. It is hard to control the size and shape of the produced graphene quantum dots. Bottom up synthesis offers best control on the shape and size of the quantum dots. However, it is very tedious and takes long time to produce [32,33].

It was thought that the quantum confinement would modify the band gap of graphene quantum dots as the case with semi-conductor quantum dots. However, this was not the case, so researchers started to dope graphene quantum dots in order to reduce the band gap and enhance their visible light absorption [34]. Several strategies took place, such as doping with sulfur, or nitrogen or both. Qu et al. [35] were able to co-dope sulfur and nitrogen to graphene quantum dots for the sake of improving the visible light absorption for water splitting application.

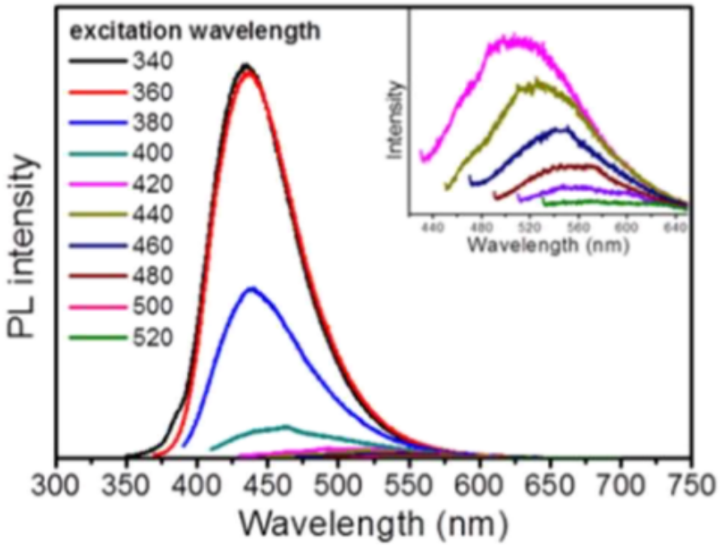

Fig. 2-15: Photoluminescence of Graphene dots co-doped with S and N[35].

They measured the photoluminescence of the co-doped graphene quantum dots, unfortunately, the difference induced by co-doping is minimal. Increasing the wavelength towards the visible region, the emission decreases abruptly till it reaches zero nearly at 500 nm (Fig. 2-15).

Recently, Kundu et al. [36] (Fig. 2-16) were able to dope graphene quantum dots with nitrogen, sulfur and floride. The Uv-vis absorption of the quantum dots showed a tail reaching 590 nm, with the main peak still at 303 nm, which means that there is no real improvement or reduction in the band gap, even after doping with three different atoms.

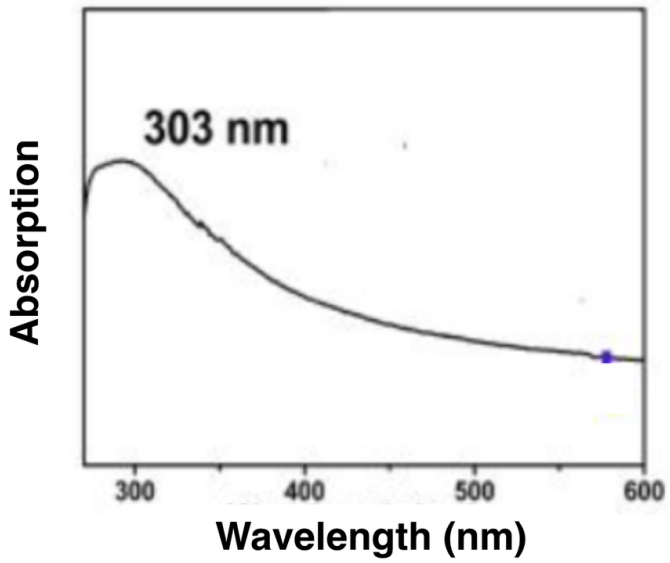

Fig. 2-16: UV-vis of graphene quantum dots co-doped with S, N, F[36].

References

1. Fujishima, A.; Rao, T. N.; Tryk, D. A. Titanium dioxide photocatalysis. *Journal of Photochemistry and Photobiology C: Photochemistry Reviews* **2000**, *1*, 1-21.

2. Manley, D. W.; McBurney, R. T.; Miller, P.; Howe, R. F.; Rhydderch, S.; Walton, J. C. Unconventional titania photocatalysis: Direct deployment of carboxylic acids in alkylations and annulations. *J. Am. Chem. Soc.* **2012**, *134*, 13580-13583.

3. Grimes, C. A.; Mor, G. K. *TiO2 nanotube arrays: synthesis, properties, and applications;* Springer Science & Business Media: 2009; .

4. Mor, G. K.; Shankar, K.; Paulose, M.; Varghese, O. K.; Grimes, C. A. Use of highly-ordered TiO2 nanotube arrays in dye-sensitized solar cells. *Nano letters* **2006**, *6*, 215-218.

5. Roy, P.; Berger, S.; Schmuki, P. TiO2 nanotubes: synthesis and applications. *Angewandte Chemie International Edition* **2011**, *50*, 2904-2939.

6. Zwilling, V.; Darque‐Ceretti, E.; Boutry‐Forveille, A.; David, D.; Perrin, M.; Aucouturier, M. Structure and physicochemistry of anodic oxide films on titanium and TA6V alloy. *Surf. Interface Anal.* **1999**, *27*, 629-637.

7. Zwilling, V.; Aucouturier, M.; Darque-Ceretti, E. Anodic oxidation of titanium and TA6V alloy in chromic media. An electrochemical approach. *Electrochim. Acta* **1999**, *45*, 921-929.

8. Kelly, J. The influence of fluoride ions on the passive dissolution of titanium. *Electrochim. Acta* **1979**, *24*, 1273-1282.

9. Macak, J. M.; Tsuchiya, H.; Taveira, L.; Aldabergerova, S.; Schmuki, P. Glattwandige anodische TiO2‐Nanoröhren. *Angewandte Chemie* **2005**, *117*, 7629-7632.

10. Macak, J. M.; Sirotna, K.; Schmuki, P. Self-organized porous titanium oxide prepared in Na 2 SO 4/NaF electrolytes. *Electrochim. Acta* **2005**, *50*, 3679-3684.

11. Macak, J. M.; Albu, S. P.; Schmuki, P. Towards ideal hexagonal self‐ordering of TiO2 nanotubes. *physica status solidi (RRL)-Rapid Research Letters* **2007**, *1*, 181-183.

12. Albu, S. P.; Ghicov, A.; Aldabergenova, S.; Drechsel, P.; LeClere, D.; Thompson, G. E.; Macak, J. M.; Schmuki, P. Formation of Double‐Walled TiO2 Nanotubes and Robust Anatase Membranes. *Adv Mater* **2008**, *20*, 4135-4139.

13. Beranek, R.; Hildebrand, H.; Schmuki, P. Self-organized porous titanium oxide prepared in H 2 SO 4/HF electrolytes. *Electrochemical and solid-state letters* **2003**, *6*, B12-B14.

14. Macak, J.; Hildebrand, H.; Marten-Jahns, U.; Schmuki, P. Mechanistic aspects and growth of large diameter self-organized TiO 2 nanotubes. *J Electroanal Chem* **2008**, *621*, 254-266.

15. Masuda, H.; Satoh, M. Fabrication of gold nanodot array using anodic porous alumina as an evaporation mask. *Japanese Journal of Applied Physics* **1996**, *35*, L126.

16. Grimes, C. A., Varghese, O. K., & Ranjan, S. (2008). Light, water, hydrogen: The solar generation of hydrogen by water photoelectrolysis. New York: Springer.

17. Shankar, K.; Mor, G. K.; Fitzgerald, A.; Grimes, C. A. Cation effect on the electrochemical formation of very high aspect ratio TiO2 nanotube arrays in formamide-water mixtures. *The Journal of Physical Chemistry C* **2007**, *111*, 21-26.

18. Amer, A. W.; Mohamed, S. M.; Hafez, A. M.; AlQaradawi, S. Y.; Aljaber, A. S.; Allam, N. K. Self-assembled zirconia nanotube arrays: fabrication mechanism, energy consideration and optical activity. *RSC Advances* **2014**, *4*, 36336-36343.

19. Chen, X.; Liu, L.; Yu, P. Y.; Mao, S. S. Increasing solar absorption for photocatalysis with black hydrogenated titanium dioxide nanocrystals. *Science* **2011**, *331*, 746-750.

20. Cronemeyer, D. Infrared Absorption of Reduced Rutile Ti O 2 Single Crystals. *Physical Review* **1959**, *113*, 1222.

21. Wang, G.; Wang, H.; Ling, Y.; Tang, Y.; Yang, X.; Fitzmorris, R. C.; Wang, C.; Zhang, J. Z.; Li, Y. Hydrogen-treated TiO2 nanowire arrays for photoelectrochemical water splitting. *Nano letters* **2011**, *11*, 3026-3033.

22. Liu, N.; Schneider, C.; Freitag, D.; Hartmann, M.; Venkatesan, U.; Müller, J.; Spiecker, E.; Schmuki, P. Black TiO2 nanotubes: cocatalyst-free open-circuit hydrogen generation. *Nano letters* **2014**, *14*, 3309-3313.

23. Tsui, L.; Saito, M.; Homma, T.; Zangari, G. Trap-state passivation of titania nanotubes by electrochemical doping for enhanced photoelectrochemical performance. *Journal of Materials Chemistry A* **2015**, *3*, 360-367.

24. Geim, A. K.; Novoselov, K. S. The rise of graphene. *Nature materials* **2007**, *6*, 183-191.

25. Nguyen, D. D.; Tai, N.; Lee, S.; Kuo, W. Superhydrophobic and superoleophilic properties of graphene-based sponges fabricated using a facile dip coating method. *Energy & Environmental Science* **2012**, *5*, 7908-7912.

26. Shin, Y. J.; Wang, Y.; Huang, H.; Kalon, G.; Wee, A. T. S.; Shen, Z.; Bhatia, C. S.; Yang, H. Surface-energy engineering of graphene. *Langmuir* **2010**, *26*, 3798-3802.

27. Dreyer, D. R.; Park, S.; Bielawski, C. W.; Ruoff, R. S. The chemistry of graphene oxide. *Chem. Soc. Rev.* **2010**, *39*, 228-240.

28. Kim, I. Y.; Lee, J. M.; Kim, T. W.; Kim, H. N.; Kim, H.; Choi, W.; Hwang, S. A Strong Electronic Coupling between Graphene Nanosheets and Layered Titanate Nanoplates: A Soft‐Chemical Route to Highly Porous Nanocomposites with Improved Photocatalytic Activity. *Small* **2012**, *8*, 1038-1048.

29. Ng, Y. H.; Iwase, A.; Kudo, A.; Amal, R. Reducing graphene oxide on a visible-light BiVO4 photocatalyst for an enhanced photoelectrochemical water splitting. *The Journal of Physical Chemistry Letters* **2010**, *1*, 2607-2612.

30. Yeh, T.; Chan, F.; Hsieh, C.; Teng, H. Graphite oxide with different oxygenated levels for hydrogen and oxygen production from water under illumination: the band positions of graphite oxide. *The Journal of physical chemistry C* **2011**, *115*, 22587-22597.

31. A. P.Alivisatos. Semiconductor clusters, nanocrystals, and quantum dots. *Science* **1996**, *271*, 933-937.

32. Liu, R.; Wu, D.; Feng, X.; Müllen, K. Bottom-up fabrication of photoluminescent graphene quantum dots with uniform morphology. *J. Am. Chem. Soc.* **2011**, *133*, 15221-15223.

33. Shen, J.; Zhu, Y.; Yang, X.; Li, C. Graphene quantum dots: emergent nanolights for bioimaging, sensors, catalysis and photovoltaic devices. *Chemical Communications* **2012**, *48*, 3686-3699.

34. Xu, Q.; Zhou, Q.; Hua, Z.; Xue, Q.; Zhang, C.; Wang, X.; Pan, D.; Xiao, M. Single-particle spectroscopic measurements of fluorescent graphene quantum dots. *ACS nano* **2013**, *7*, 10654-10661.

35. Qu, D.; Zheng, M.; Du, P.; Zhou, Y.; Zhang, L.; Li, D.; Tan, H.; Zhao, Z.; Xie, Z.; Sun, Z. Highly luminescent S, N co-doped graphene quantum dots with broad visible absorption bands for visible light photocatalysts. *Nanoscale* **2013**, *5*, 12272-12277.

36. Pillai, V. K.; Kundu, S.; Ajayan, P. M.; Yadav, R.; Shelke, M. V.; Narayanan, N. T.; Vajtai, R. Synthesis of N, F and S Co-Doped Graphene Quantum Dots. *Nanoscale* **2015**.

Chapter 3

Scientific background

3.1 Thin walled titania:

There are three factors known to affect the efficiency of titania nanotubes; the length, wall thickness and pore size. Increasing the length, the surface area increases, and also the number of generated electrons and holes will increase (diffusion coefficient) [1]. However, the efficiency does not have a linear relationship with length, as by increasing length beyond light diffusion, it acts as recombination site. Therefore, there is a limit for the tube length. The pore size is also another important factor, most of the literature review confirmed that a pore size around 60 nm is optimum for an efficient water splitting reaction [1,2]. The wall thickness is the third important factor that was usually paired with the tube length in literature among the most important factors that affect the nanotubes photo electrochemical properties [3]. The architecture of the nanotubes provides a great advantage in favor of holes being close to the electrolyte surface. Generally, the holes migration to the electrolyte is controlled by the depletion region electric field. Therefore, there must be enough electric field to support the charge transfer and prevents recombination to take place. The presence of large depletion region is highly required in order to provide enough electric field to separate holes from electrons. This depletion region increases with increasing the wall thickness. One of the problems of nanoparticles that their small sizes does not provide the support to form enough electric field across the surface, as a result thick walled titania nanotubes were preferred. Unfortunately, there is another contributing factor that must be considered, which is contradicting with the first

one. The size of the depletion region must be around the hole diffusion length to allow the hole to pass through it and reaches the electrolyte surface, for very thick wall thickness, holes will stuck and will recombine with the electrons. At this controversial point, either we increase wall thickness to get high electric field difference to reduce charge recombination, or at same time the wall thickness should be lower than the diffusion length, to allow hole diffusion without recombination with the electron [1,4,5].

The reported data from the literature also showed the same contradictions. Grimes et al. [1,6] are supporting that the larger the wall thickness, the higher the efficiency of charge carriers separation, while Zhu et al. [7,8] believes that a thinner wall thickness allows better hole diffusion, based on the fact that such very small wall thickness would allow the diffusion of holes through it without the need for potential difference.

Based on those reports, we were encouraged to study the effect of electron and hole diffusion in nanotubes of wall thicknesses less than the diffusion length of charge carriers.

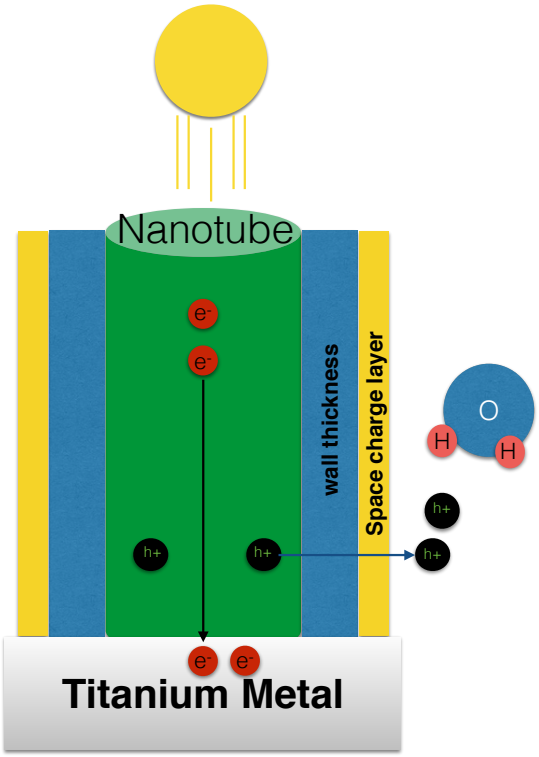

Scheme 3-1: Electron and hole diffusion pathway in ultrathin wall titania nanotubes.

During the fabrication of titania nanotubes, the choice of the electrolyte is one of the varying factors that must be considered. Using aqueous electrolyte can contribute O^{2-} atoms easier than organic electrolytes, which is directly reacted with the metal to form metal oxide [9,10], while it is hard for the non-aqueous electrolyte to give O^{2-} atom for the metal. Therefore, the oxide layer cannot be formed fast as in the case of the aqueous electrolyte. This concept can be witnessed when comparing the anodization current in both aqueous and non-aqueous electrolyte. In the case of aqueous electrolyte, the current starts at very high values and it decreases rapidly due to the fast formation of the semiconducting layer. On the other hand, with the non-aqueous electrolyte, the oxide

layer formation takes longer time and large areas of metal are still exposed to the electrolyte and the current remains high for longer time [2].

Also it is important to shade the light on the difference between using ammonium floride (NH_4F) and hydrogen floride (HF) as an etchant ions [11,12]. HF is a stronger etchant than ammonium fluoride, due to its smaller disassociation constant. This strong etching power results in shorter nanotubes. Ammonium fluoride has larger disassociation constant, and as a result it produces well defined, highly ordered titania nanotubes.

Therefore, we chose an aqueous electrolyte and we added ammonium fluoride as a source of etchant ions in the anodization process.

$$TiO_2 + F^- + H^+ \rightarrow [TiF_6]^{2-} + 2H_2O \qquad (1)$$

$$Ti + H_2O \rightarrow TiO_2 + H^+ + e \qquad (2)$$

There are two main synthesis strategies, either by using formamide-based electrolyte or ethylene glycol-based electrolyte. Formamide-based electrolytes produce bundled nanotubes that are somehow focused on certain islets [1]. Ethylene glycol-based electrolytes, however, results in the formation of highly aligned nanotubes [13]. However, they are very weakly attached oxide layer on the surface of the metal.

Amer et al. [14] were able to produce thin walled Zirconia nanotubes that are highly aligned with very small wall thickness. Based on Amer's assumptions, they used a mixture of the organic and aqueous electrolytes, using glycerol-based electrolyte that contains reduced concentration of formamide and water.

3.2 Anatase titania:

Electrochemical anodization results in the formation of amorphous structures, which are well known for their high charge recombination rate, owing to their poor ordered structure [1]. Hence, it's important to transfer the amorphous structure into crystalline counterpart.

There are various approaches to crystallize the amorphous as-anodized titania nanotubes. Annealing is one of the simplest and direct methods to convert titanium dioxide nanotubes into crystalline structure [15]. There are three crystalline forms of titania, anatase, rutile and brookite [16]. Generally, the anatase and rutile structure are the most popular, while till now there is no specific pathway to produce brookite structure. Figure 3-1 shows [17] the phase diagram of titania. Anatase crystals are predominant till 450 °C, and after 450°C the percentage of rutile to anatase increases i.e.; it is a temperature dependent mechanism.

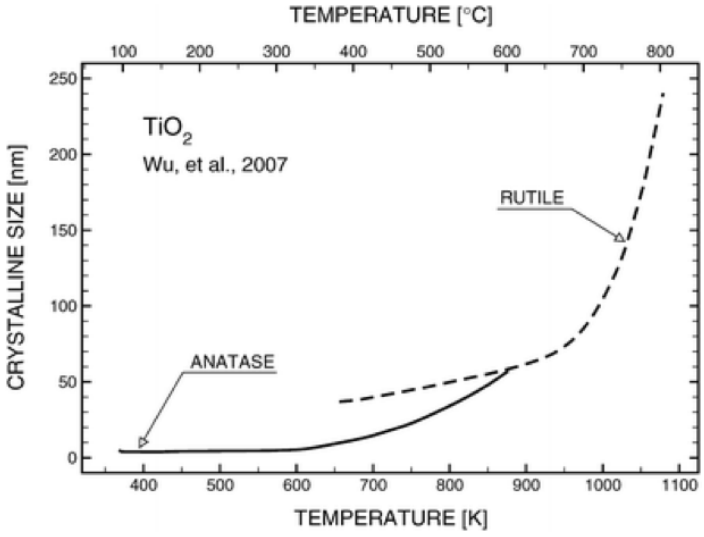

Fig. 3-1: Phase diagram of titania polymorphs [17].

Gibbs free energy is needed to change the structure of Titania from amorphous to crystalline or even from one crystalline form to the other. Titania contains OH groups on its surface, and by applying sufficient heat, the OH groups come closer to each other and a condensation reaction takes place, where water atom is lost, and the particles get closer to each other and become in contact. The heat will allow the small particles to nucleate and grow till densification. Once they densify, the crystallization process starts forming an anatase crystal structure. By increasing the temperature, the grain growth rate will increase, and this excessive heat will give the atomic crystals the freedom to change orientation and rotate, only if they have the space for that and changes to rutile. Generally, this happens when a rutile crystal comes in contact with anatase crystal, so they both merge together forming larger rutile crystallite. Crystal sizes smaller than 14 nm does not have the chance to change their crystal structure to rutile, same for wall thickness [18,19].

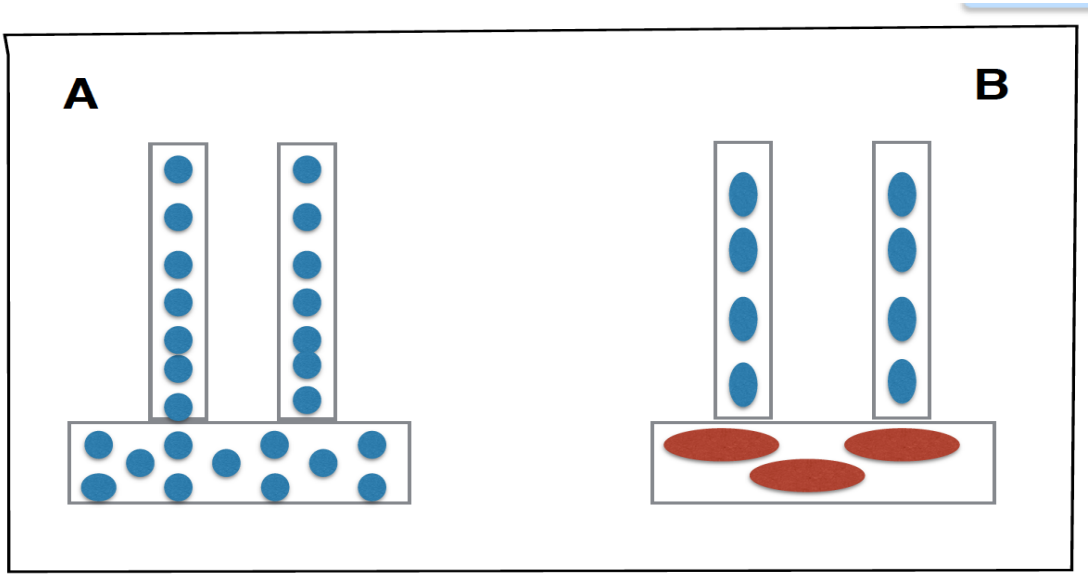

Scheme 3-2: Anatase crystallites (A) and the gradual change in to rutile (B).

Scheme 3-2 shows the anatase structure (A) and its transformation process to rutile (B). The anatase crystallites are smaller, so they can form in any small space (even within the wall thickness). However, the more ordered, larger rutile crystallites require more space to form so they just can not form on the tube walls.

Annealing the samples at high temperature opens a new avenue towards modifying the band gap of semiconductors by annealing under different atmospheres, which can be regarded as doping the material with different atoms of interest in order to reach the desired specs [20].

Away from being anatase or rutile, defect states is one of the most controversial topics in literature, although it is well established several years ago, but still there is lack of understanding of their role in various applications such as water splitting. Annealed titanim dioxide (TiO_{2-x}) always creates defect states by losing oxygen atoms [21].

There are two types of defects that are produced by annealing, in plane defects and bridging defects [22]. The bridging oxygen atom is easier to remove (at temp 450°C) while the in-plane oxygen atoms require higher temperature. In-plane oxygen atom is coordinated with three Ti, while birding oxygen atoms is coordinated with only 2 Ti. As a result, there are two types of oxygen defect states on the band diagram.

It was found that the first defect state (oxygen vacancy E10) is formed at 0.73 eV below the conduction band, which is considered as a shallow state, i.e. increasing charge carrier concentration. The second defect state appears at 1.18 eV below the conduction band, which is nearly in the half way between valence and conduction band (titania band gap is

3.2 eV), forming a deep trap state, that can hinder the electron transfer to the conduction band and leads to reduction in the photocurrent produced (Scheme 3-3).

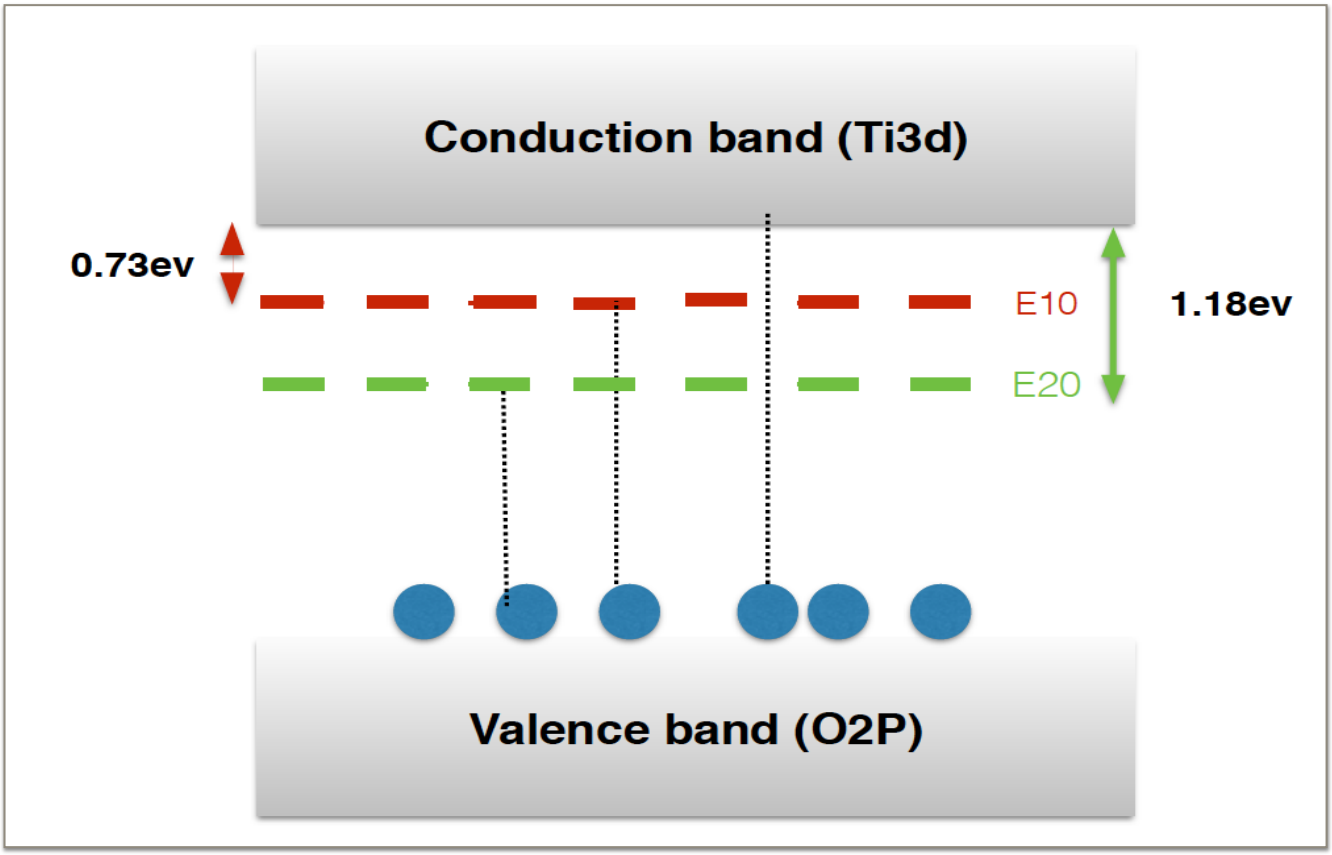

Scheme 3-3 shows the band diagram of titanium dioxide.

In this thesis, we focus on the best optimization for titania nanotubes by annealing under different conditions in order to reach the highest photocurrent, improving visible light absorption, and getting rid of deep trap states that diminishes the photocurrent. We annealed titania under different atmospheres including air (default), oxygen, and hydrogen. In addition, we tried to understand the effect of adding potassium hydroxide during the anodization of titania, KOH and different alkali metals are known to diffuse

between grain boundaries, modifying the shape and size of the nanoparticles, that results in the redistribution of the oxygen atoms on the surface, as a result it increases the charge carrier density and results in a higher open circuit voltage.

3.3 Anatase vs. Rutile:

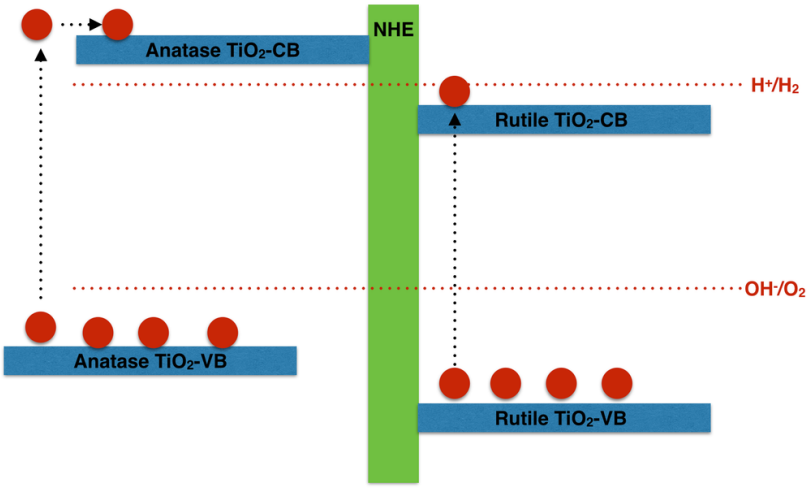

Scheme 3-4:Band structure of anatase and rutile titania.

Anatase titania (3.2 eV) has larger band gap that rutile, Rutile band gap is about 3 eV. It's clear that the rutile (3 eV). Therefore, rutile titania is expected to absorb more light.

Moreover, rutile is a direct band gap semiconductor, while anatase is an indirect band gap semiconductor, which means higher amount of energy and more time is required for anatase titania to excite an electron from the valence band, which results in consuming some of the absorbed energy to change the electron momentum to reach the conduction

band. However, there are two main points to consider here that are related to our application, water splitting. In order to achieve an efficient water splitting, the semiconductor valence and conduction bands must straddle water oxidation and reduction potential; in this regard, anatase is totally straddling the water oxidation and reduction potential, while rutile is obeying only the water oxidation potentials. However, Titania is used as a photoanode, ie. water oxidation process. Therefore, straddling the water reduction potential is not necessary physically, but practically. Thus, it would cost higher amount of electrical bias to reach the flat band potential than in the case of anatase Titania. The other point is about the indirect band gap and charge carrier life time. Water splitting application is dependent on the efficient charge carrier transfer from the conduction band to the metal substrate before recombination process, so by increasing charge carrier life time, we are increasing the amount of charge carriers that can be transferred either from sensitizing material to the substrate or from the substrate to the metal substrate. Usually increasing the charge carrier life time is achieved by doping, which always results in higher dark current and in an inefficient transfer of electrons to the conduction band. This results in a lower photocurrent. Anatase is gifted with an indirect band gap that increases the charge carrier lifetime, avoiding the problems of doping. It is obvious now that anatase titania is the one that satisfies our application [23].

3.4 Annealing under different atmospheres:

As we noted previously, annealing creates oxygen defects on the surface, and there are two different types of oxygen vacancies that are produced as a result of annealing at high temperature. Shallow defects (near conduction or valence band) are highly required, but the deep defect states are undesirable [21]. Different strategies are employed to handle the defect states that are produced during annealing. Oxygen annealing is the conventional treatment this is used since many years ago. Oxygen annealing annihilates all oxygen vacancies, which reduces the charge carrier concentration and reduces the photocurrent [24].

Hydrogen annealing is not a new topic in literature, although it seems, but it was studied 60 years ago by Cornemeyer [21], but recently it evolved again in the scene as a successful candidate for producing what is called " black titania" [25]. Black titania is one of the most controversial topics in literate recently. Various articles started explaining the role of hydrogen with Titania, and the formation of defect states Ti^{3+} (increasing charge carrier concentration), that are responsible for reducing the band gap of titania and shifting its absorption till 600 nm [26-29]. Hydrogen annealing increases the oxygen defect states (E10 and E 20), and as a result the deep defect state (E20) will act as a charge recombination center that will result in a lower photocurrent and a higher dark current. Moreover those defect states (E10 and E20) does not straddle the water oxidation and reduction potential, which means that their use in water splitting is useless [30]. Another group believes that Hydrogen annealing passivates the defect states on the surface and results in higher

photocurrent, but not much as the first group reported. It is obvious that there is a poor understanding for the effect of hydrogen annealing on titania [31].

First of all, most of the reports in literature ignore the effect of annealing conditions, such as temperature and flow rate. Most of the literature reports care only about producing higher photocurrent. We totally believe that we cannot compare literature data one to the other by this simple way. First of all, we have to quantify the variable conditions that take place during the annealing process.

3.5 Graphene quantum dots:

Graphene quantum dots are made out of Graphene, which is one atom thick layer extracted from Graphite. This layer is made out of tightly bonded Carbon atoms that are arranged in hexagonal structure (Ball and stick model) [32]. Before 2004, this structure was thought to be non realistic, as it is thermally impossible to have such 2D structure in nature, but Geime and Novoselov in 2004 were able to extract the first graphene layer and proved the aforementioned structure [33]. There are thousands of articles that have been published since then trying to explore graphene and its properties. Carbon is a semi metal, with 2 inner shell electrons and 4 outer shell electrons. Generally, the outer shell electrons shares in chemical reactions, but in Graphene 3 of the 4 outer shell electrons are bound to 3 neighboring carbon atoms, leaving the remaining electron for electrical conductivity. The overlap of those π orbitals enhance the bonding in graphene and they totally control the electronic properties of graphene. It was found that there are 6 dirac points over graphene, which renders the conductivity quite low at these points, that's why its essential to dope graphene in order to improve this property [34]. The mechanical

properties of graphene also attracted considerable attention, and this is mainly due to its very high strength (130 to 400 megapascal of A36 steel), with its very low weight, which is about 0.77 mg/cm^2 (1000 times lighter than paper) and elasticity [35]. This magical combination was not found in any other material. It is noteworthy to indicate that those properties are based on theoretical models as large-scale production contains defects and such defects affects the properties of graphene. The only side effect with graphene is its optical property i.e. Its band gap is nearly zero, which renders it useless when it comes to optical applications [33].

A part of the thesis, will discuss the properties of graphene quantum dots, especially the optical and the electronical properties.

Graphene quantum dots are gaining an increasing interest, especially for optical applications, such as solar cells, water splitting, and even bio imaging, although there are lots of concerns of using carbon-based products in the human body and the consequences of that.

Although there are large numbers of scientific research papers and articles that are published daily on the graphene quantum dots, there is still no real understanding of physics of graphene quantum dots that is responsible for their properties. Also, till now well-known procedure or even any evidence on the ability to engineer the band gap of graphene quantum dots, despite thousands of articles which are talking about the band gap engineering with contradicting photo luminance results and absorption spectra. Therefore, It is very interesting to study this controversial point and discovering what is the real reason behind the properties of those quantum dots.

Graphene oxide showed U.V absorption, with weak visible absorption. The photoluminescence of graphene oxide can be divided in to 2 main peaks, first centered at about 400 nm, which is called IP2, and other larger peak at 600 nm, which is IP1 [36]. It was proven that both peaks are contributed from 2 different electronic states, and as a result, several researches were curious to determine the origin of both peaks, and it was found out that the ip1 is originating from the n-π*, which is originating from the bound oxygen groups and forming defect states on the surface, while the IP2 is originating from the new π-π*, which is the original band gap of graphene. From here we can deduce that the functionalization is the main source of band gap engineering, which we will discuss it later in this chapter.

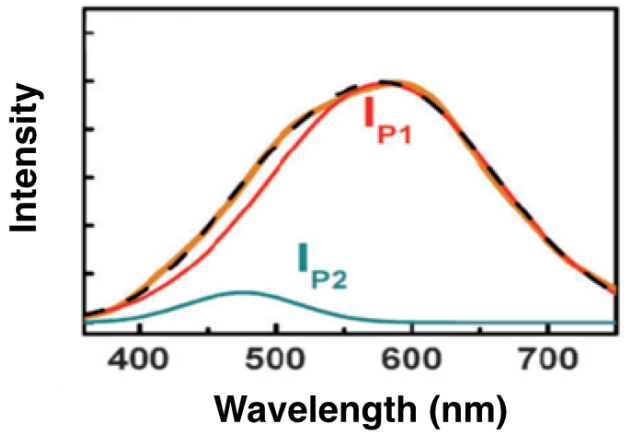

Figure3-2: Typical photoluminescence curve for graphene oxide [36].

Quantization evolved as another solution for the optical properties problem [37]. Quantum dots are nanoparticles that are smaller than Bohr radius, which is the distance between the nucleus and nearest electron in an atom. Reducing the particle size to such level deviates

it from classical physics laws to the quantum level. Quantum dots exhibit squeezing of the energy levels and formation of new quantized energy levels continuum, which is size dependent. Squeezing the quantum dots more (reducing their size), the band gap increases and by increasing their size (limited by Bohr radius), the band gap decreases. Semi conductor quantum dots showed very high luminesce and efficiency, although the stability of the quantum dots is questionable. Quantization of graphene quantum dots was thought similar results, unfortunately, graphene quantum dots showed quiet different absorption and emission behavior than other semi conductor quantum dots, and this arises generally because of their carbonic nature.

References

1. Grimes, C. A.; Mor, G. K. *TiO2 nanotube arrays: synthesis, properties, and applications;* Springer Science & Business Media: 2009; .

2. Mor, G. K.; Varghese, O. K.; Paulose, M.; Shankar, K.; Grimes, C. A. A review on highly ordered, vertically oriented TiO 2 nanotube arrays: fabrication, material properties, and solar energy applications. *Solar Energy Mater. Solar Cells* **2006***, 90*, 2011-2075.

3. Macak, J.; Hildebrand, H.; Marten-Jahns, U.; Schmuki, P. Mechanistic aspects and growth of large diameter self-organized TiO 2 nanotubes. *J Electroanal Chem* **2008***, 621*, 254-266.

4. Gao, X.; Chen, J.; Yuan, C. Enhancing the performance of free-standing TiO 2 nanotube arrays based dye-sensitized solar cells via ultraprecise control of the nanotube wall thickness. *J. Power Sources* **2013***, 240*, 503-509.

5. Yuan, X.; Zheng, M.; Ma, L.; Shen, W. High-speed growth of TiO2 nanotube arrays with gradient pore diameter and ultrathin tube wall under high-field anodization. *Nanotechnology* **2010***, 21*, 405302.

6. Varghese, O. K.; Ranjan, S. *Light, Water, Hydrogen: The Solar Generation of Hydrogen by Water Photoelectrolysis;* Springer: 2008; .

7. Zhu, K.; Neale, N. R.; Miedaner, A.; Frank, A. J. Enhanced charge-collection efficiencies and light scattering in dye-sensitized solar cells using oriented TiO2 nanotubes arrays. *Nano letters* **2007***, 7*, 69-74.

8. Zhu, K.; Vinzant, T. B.; Neale, N. R.; Frank, A. J. Removing structural disorder from oriented TiO2 nanotube arrays: reducing the dimensionality of transport and recombination in dye-sensitized solar cells. *Nano Letters* **2007***, 7*, 3739-3746.

9. Beranek, R.; Hildebrand, H.; Schmuki, P. Self-organized porous titanium oxide prepared in H 2 SO 4/HF electrolytes. *Electrochemical and solid-state letters* **2003***, 6*, B12-B14.

10. Albu, S. P.; Ghicov, A.; Macak, J. M.; Schmuki, P. 250 µm long anodic TiO2 nanotubes with hexagonal self-ordering. *physica status solidi (RRL)-Rapid Research Letters* **2007***, 1*, R65-R67.

11. Shankar, K.; Mor, G. K.; Prakasam, H. E.; Yoriya, S.; Paulose, M.; Varghese, O. K.; Grimes, C. A. Highly-ordered TiO2 nanotube arrays up to 220 µm in length: use in water photoelectrolysis and dye-sensitized solar cells. *Nanotechnology* **2007***, 18*, 065707.

12. Prakasam, H. E.; Shankar, K.; Paulose, M.; Varghese, O. K.; Grimes, C. A. A new benchmark for TiO2 nanotube array growth by anodization. *The Journal of Physical Chemistry C* **2007**, *111*, 7235-7241.

13. Macak, J. M.; Sirotna, K.; Schmuki, P. Self-organized porous titanium oxide prepared in Na 2 SO 4/NaF electrolytes. *Electrochim. Acta* **2005**, *50*, 3679-3684.

14. Amer, A. W.; Mohamed, S. M.; Hafez, A. M.; AlQaradawi, S. Y.; Aljaber, A. S.; Allam, N. K. Self-assembled zirconia nanotube arrays: fabrication mechanism, energy consideration and optical activity. *RSC Advances* **2014**, *4*, 36336-36343.

15. Fröschl, T.; Hörmann, U.; Kubiak, P.; Kučerová, G.; Pfanzelt, M.; Weiss, C. K.; Behm, R.; Hüsing, N.; Kaiser, U.; Landfester, K. High surface area crystalline titanium dioxide: potential and limits in electrochemical energy storage and catalysis. *Chem. Soc. Rev.* **2012**, *41*, 5313-5360.

16. Hu, Y.; Tsai, H.; Huang, C. Effect of brookite phase on the anatase–rutile transition in titania nanoparticles. *Journal of the European Ceramic Society* **2003**, *23*, 691-696.

17. Nowotny, J. Titanium dioxide-based semiconductors for solar-driven environmentally friendly applications: impact of point defects on performance. *Energy & Environmental Science* **2008**, *1*, 565-572.

18. Neupane, M. P.; Park, I. S.; Lee, M. H.; Bae, T. S.; Watari, F. Influence of heat treatment on morphological changes of nano-structured titanium oxide formed by anodic oxidation of titanium in acidic fluoride solution. *Biomed. Mater. Eng.* **2009**, *19*.

19. Varghese, O. K.; Gong, D.; Paulose, M.; Grimes, C. A.; Dickey, E. C. Crystallization and high-temperature structural stability of titanium oxide nanotube arrays. *J. Mater. Res.* **2003**, *18*, 156-165.

20. Ma, Q.; Qin, T. P.; Liu, S. J.; Weng, L. Q.; Dong, W. Y. Morphology and photocatalysis of mesoporous titania thin films annealed in different atmosphere for degradation of methyl orange. *Applied Physics A* **2011**, *104*, 365-373.

21. Cronemeyer, D. Infrared Absorption of Reduced Rutile Ti O 2 Single Crystals. *Physical Review* **1959**, *113*, 1222.

22. Ghosh, A. K.; Wakim, F.; Addiss Jr, R. Photoelectronic processes in rutile. *Physical Review* **1969**, *184*, 979.

23. Luttrell, T.; Halpegamage, S.; Tao, J.; Kramer, A.; Sutter, E.; Batzill, M. Why is anatase a better photocatalyst than rutile?-Model studies on epitaxial TiO2 films. *Scientific reports* **2014**, *4*.

24. Hardcastle, F. D.; Ishihara, H.; Sharma, R.; Biris, A. S. Photoelectroactivity and Raman spectroscopy of anodized titania (TiO 2) photoactive water-splitting catalysts as a function of oxygen-annealing temperature. *Journal of Materials Chemistry* **2011**, *21*, 6337-6345.

25. Chen, X.; Liu, L.; Yu, P. Y.; Mao, S. S. Increasing solar absorption for photocatalysis with black hydrogenated titanium dioxide nanocrystals. *Science* **2011**, *331*, 746-750.

26. Huo, J.; Hu, Y.; Jiang, H.; Li, C. In situ surface hydrogenation synthesis of Ti3 self-doped TiO2 with enhanced visible light photoactivity. *Nanoscale* **2014**, *6*, 9078-9084.

27. Liu, H.; Ma, H.; Li, X.; Li, W.; Wu, M.; Bao, X. The enhancement of TiO 2 photocatalytic activity by hydrogen thermal treatment. *Chemosphere* **2003**, *50*, 39-46.

28. Zheng, Z.; Huang, B.; Meng, X.; Wang, J.; Wang, S.; Lou, Z.; Wang, Z.; Qin, X.; Zhang, X.; Dai, Y. Metallic zinc-assisted synthesis of Ti 3 self-doped TiO 2 with tunable phase composition and visible-light photocatalytic activity. *Chemical Communications* **2013**, *49*, 868-870.

29. Lu, X.; Wang, G.; Zhai, T.; Yu, M.; Gan, J.; Tong, Y.; Li, Y. Hydrogenated TiO2 nanotube arrays for supercapacitors. *Nano letters* **2012**, *12*, 1690-1696.

30. Wang, G.; Wang, H.; Ling, Y.; Tang, Y.; Yang, X.; Fitzmorris, R. C.; Wang, C.; Zhang, J. Z.; Li, Y. Hydrogen-treated TiO2 nanowire arrays for photoelectrochemical water splitting. *Nano letters* **2011**, *11*, 3026-3033.

31. Liu, N.; Schneider, C.; Freitag, D.; Hartmann, M.; Venkatesan, U.; Müller, J.; Spiecker, E.; Schmuki, P. Black TiO2 nanotubes: cocatalyst-free open-circuit hydrogen generation. *Nano letters* **2014**, *14*, 3309-3313.

32. Abergel, D.; Apalkov, V.; Berashevich, J.; Ziegler, K.; Chakraborty, T. Properties of graphene: a theoretical perspective. *Adv. Phys.* **2010**, *59*, 261-482.

33. Geim, A. K.; Novoselov, K. S. The rise of graphene. *Nature materials* **2007**, *6*, 183-191.

34. Neto, A. C.; Guinea, F.; Peres, N.; Novoselov, K. S.; Geim, A. K. The electronic properties of graphene. *Reviews of modern physics* **2009**, *81*, 109.

35. Lee, C.; Wei, X.; Kysar, J. W.; Hone, J. Measurement of the elastic properties and intrinsic strength of monolayer graphene. *Science* **2008**, *321*, 385-388.

36. Chien, C.; Li, S.; Lai, W.; Yeh, Y.; Chen, H.; Chen, I.; Chen, L.; Chen, K.; Nemoto, T.; Isoda, S. Tunable photoluminescence from graphene oxide. *Angewandte Chemie International Edition* **2012**, *51*, 6662-6666.

37. Leutwyler, W. K.; Bürgi, S. L.; Burgl, H. Semiconductor clusters, nanocrystals, and quantum dots. *Science* **1996**, *271*, 933-937.

Chapter 4

Materials and Experimental Methods

4.1 Materials and Supplies:

Titanium metal foils with thickness 0.25 mm and purity of 99.95 % were purchased from Sigma Aldrich. Graphite crystalline powder with particle size about-325 mesh, and a purity of 99% was purchased from Alfa Aser. Hydrogen and Oxygen gas cylinders were purchased from Airgas Company. The quantum dot functionalization and characterization was done in a collaborative work with Georgia Institute of Technology. Other chemicals used in the following experiments are bought from Sigma aldrich

4.2 Potentiostatic anodization:

Prior to anodization step, the working electrode (titanium foil) is thoroughly cleansed by sonicating in a water bath in acetone, ethanol followed by D.I water. Anodization was performed in an electrochemical cell, where the anode (titanium) is connected to the positive pole and the counter electrode (Platinum) is connected to the negative pole of the cell. We used Agilent E3612A DC power supply for anodization, where the voltage is increased by a rate of 0.2V/sec. Two different electrolytes were used, the first is formamide-based, which is used to produce the conventional nanotubes, and the second one is glycerol-based for the thin-walled nanotubes. Both electrolytes contained ammonium floride as an etchant.

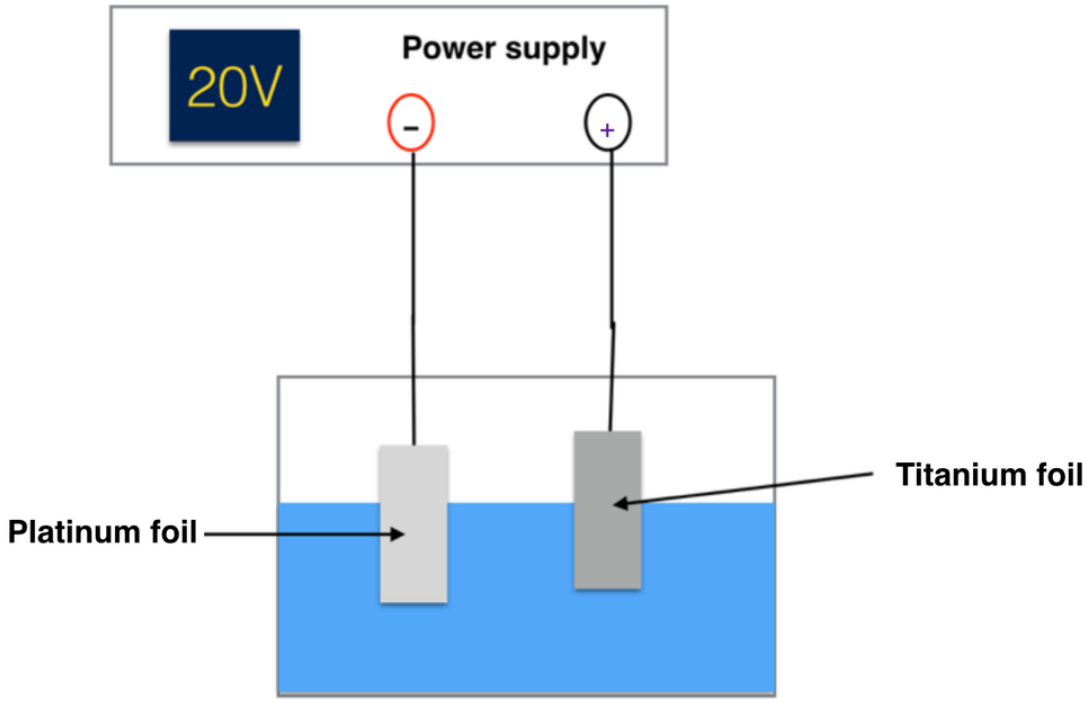

Scheme 4-1: The anodization setup

4.3 Thermal annealing:

Thermal annealing of the amorphous nanotubes formed by anodization is a critical step. We used Lindberg blue M furnace to anneal the samples at 450°C , with an upward ramp rate of 1°C/ min, for 4, 6, 8 and 10 hours using different atmospheres. For oxygen and hydrogen, we used MKS GM50A flow meter to control the flowing gas and allow a constant flow rate of 20 SCCM during the whole annealing process.

4.4 Synthesis of graphene quantum dots:

Graphene quantum dots were synthetized in a two-step process, first oxidized by oxidizing graphite into graphite oxide, and followed by exfoliation to graphene and producing quantum dots.

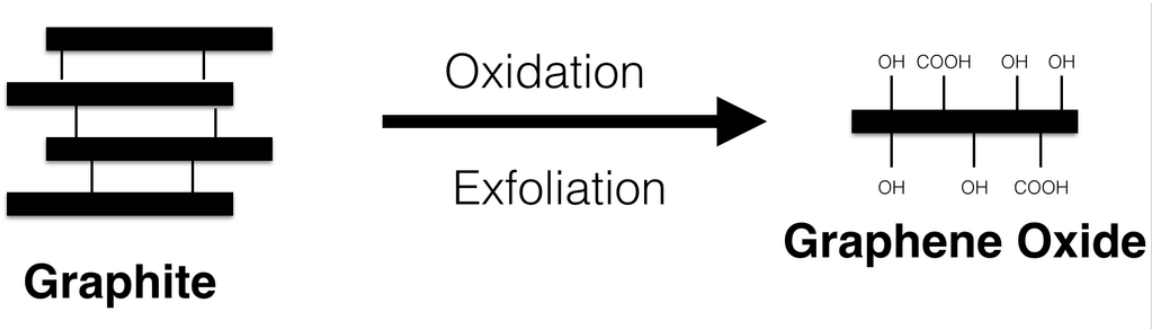

Scheme 4-2: Oxidation process and the exfoliation from graphite to graphene oxide.

The oxidation process "Modified Hummers Method" [1]can be divided into two main steps; the preoxidation step and the oxidation step. The peroxidation is performed using sulfuric acid, phosphorus pentoxide and potassium persulfate, while the oxidation step involves the actual oxidation of Graphite by using sulfuric acid, potassium permneganate, and hydrogen peroxide. Between the two steps and after the last step, the product must be neutralized by washing with distilled water and filtering it on 0.2 micron nylon filter paper (Sigma Aldrich). Graphite oxide is formed with a brown yellowish color, graphite oxide is formed, and then exfoliation process takes place, where graphite oxide (0.2mg/ml) is sonicated with dimethyl formamide for one hour to produce graphene oxide. Graphene oxide is etched under high temperature (200°C) with dimethyl formamide to produce graphene quantum dots [2].

Dialysis tubing was used to obtain a uniform size and expel the excess acids and salts during the reaction purify the produced quantum dots.

4.5 Functionalizing the graphene quantum dots:

In order to be able to anchor graphene quantum dots to other materials, we functionalized those dots with mercapto propanoic acid.

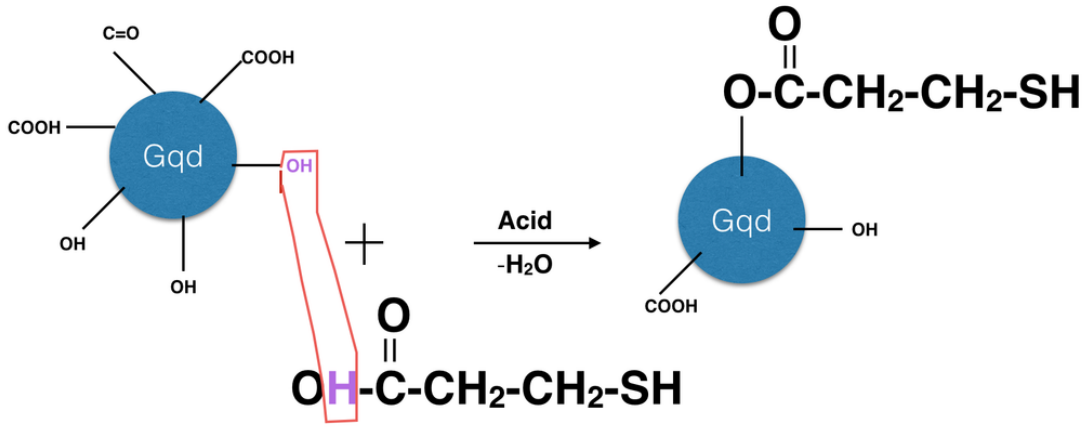

Scheme 4-3: Fischer esterification of graphene quantum dots with mercaptopropanoic acid.

We functionalized the surface of the Graphene quantum dots with mercaptopropanoic acid by an ester linkage, relying on the abundance of the hydroxyl groups on the surface of the graphene quantum dots. Fischer esterification requires the presence of a carboxylic acid group and a hydroxyl group in an acidic media that acts as a catalyst for the reaction [3]. First, the acid protonates the carbonyl group of the carboxylic acid, which renders the O of the carbonyl group more electrophilic, to allow the nucleophilic attack by the rich Hydroxyl group, followed by the removal of water

molecules which protaonates the ester then it deprotonates. The problem of Fischer esterification is that it is totally reversible during the synthesis procedure, but once the ester bond is formed, it is stable.

As a result, care should be taken during the reaction because any small mistake would disrupt the whole reaction. The actual working procedure that we added the graphene quantum dots in a conical flask together with mercapto propanoic acid (ratio between OH and COOH must be 1:1). It should be noted that adding excess of quantum dots is highly required during the synthesis process to enhance the bond formation. Then, the catalyst acid is added. We used sulfuric acid in small drops. Excess acid used can lead to breaking the ester linkage and disrupt its formation, so adding the acid should be very cautious. The mixture is heated at 80° C for 2 hours, excess heat should also be avoided because ester linkage can be broken easily. After heating for 2 hours, the mixture must be neutralized to pH 7, as the acidic condition can destroy the ester linkage. However, it should be noted that strong alkaline conditions can also break the ester linkage, as a result a very dilute solution of Sodium bicarbonate is titrated on the mixture till it becomes neutral. Afterwards, in order to separate the functionalized and non-functionalized Graphene quantum dots, they are added into a separating funnel containing a 2-phase system made out of chloroform (lower phase) and water (upper phase). It's expected that adding a thiol functional group on the surface of the Graphene quantum dots imparts a lipophilic property for the quantum dots. Therefore, instead of partitioning with water molecules, it moves to a similar phase, as chloroform is an organic solvent. The non-functionalized graphene quantum dots can then move simply to the water phase, owing to their oxygenated surface. After separating the functionalized graphene quantum dots,

they should be subject to dialysis to ensure that excess reactants are removed from the solution. However, since Chloroform disrupts the dialysis tubing, Chloroform should be substituted with water, and this can be performed by Rotary evaporator using ethanol as an intermediate between chloroform and water, since water and Chloroform are immiscible. After this step, the sample can be dialyzed for one week to ensure the purification of the final product.

4.6 Electrophoretic depositon:

After the efficent synthesis and charactarization of the titania nanotubes and the functionalized graphene quantum dots, we chose the electrophoretic depositon technique for the attaching. Electrophoretic depositon is a simple technique that relies on the generation of opposite charges between the substrate and solute molocules, which leads to an attraction between them under the influnece of an external bias.

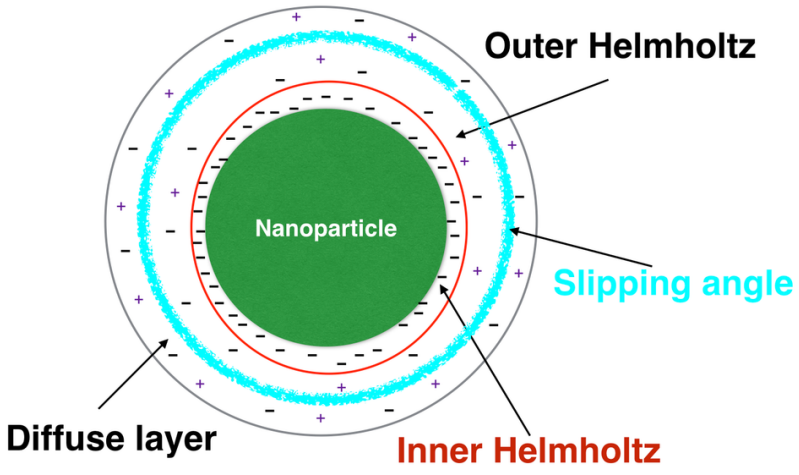

Fig. 4-1: Double layer formed on a nanoparticle.

Fig. 4-1 shows the 3 main layers that are formed on the surface of any particle when immersed in a solution [4,5]. The first layer is Inner Helmholtz layer, which is a compact layer of opposite charges to the particle, usually this layer is very thin, just few atoms thick. This is followed by the outer Helmholtz layer, which is larger than the inner one but still containing similar charges as the inner layer and opposite to the particle. The third layer is the diffuse layer, which is formed of a normal gradient of the solvent ions without any preferential charged ions.

The layer between the outer helmholz and the diffuse layer is called the slipping angle, from which we can derive the zeta potential and determine the stability of the particle and its susceptibility to adhesion or agglomeration. Hamaker equation gives a better understanding of the parameters affecting the deposition technique [6].

$$w = \frac{2 \times C \times \varepsilon_0 \times \varepsilon_r \times \zeta \times E \times t}{3 \times \eta \times L}$$

where, w is the deposition weight of the particles on the surface of the electrode, C is the concentration of the particles in solution, ε_0 is the permittivity of vacuum, ε_r is the relative permittivity of the solvent, ζ is the zeta potential determined from the slipping angel, η is the viscosity of the solvent, L is the distance between the 2 electrodes (anode and cathode), E is the applied voltage, while t is the deposition time. From Hamaker equation, it is easier to predict the deposition process and to control it. If we consider the solvent and solute are not changing, then we will have only three variables, which are the concentration of the solute, the applied potential and deposition time.

For the solvent, polar solvents are highly appealing, specially water. Water offers fast depositon and low agglomeration rate, but unfortunately, water electrlolysis occurs at

1.2 V, and hydrogen bubbles will start appearing at the cathode. This can disrupt the deposition process or affect the concentration by losing water molecules.

In case of using organic solvents, the mobility of the solute will be smaller and will require very high voltage (140 V) to initiate the reaction, in addition to their negative environmental impact and cost.

Other issue that favors water on organic solvents is the control of pH, which is a crucial factor for electrophoretic deposition. The presence of carboxylic acid group in alkaline media will cause deprotonation of the H and formation of carboxylate anion (COO-), while in acidic media it neutralizes and no anion is formed. It is easy to control the pH with water, but actually there is no pH measured for organic solvent, usually acids or bases are added to the organic solvents in order to enhance the acidity or the basicity of the media respectively.

Unlike polar particles, organic particles like graphene quantum dots are non polar, and no intrinsic charges are expected. Consequently, the overall charge of the particle is determined from the surface groups. In our case, graphene quantum dots contain carboxylic acid groups, hydroxyl groups, and the functionalized mercapto propanoic acid. In basic media like water, it is expected that the weak acid like carboxylic acid group and the thiol group (mercapto propanoic acid) get deprotonated, leaving anion on the surface. These anions formed on the surface can be integrated with the inner Helmholtz layer, as a result the overall charge of the particle and double layer is negative. By applying current, the negatively charged particles are forced to move to the oppositely charged anode, in our case is titania nanotubes, depositing on its surfac. This process is followed by annealing the deposited quantum dots in a muffle at 90° C for 2 hours.

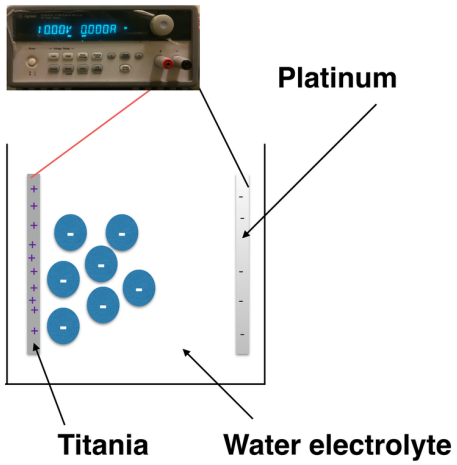

Scheme 4-4: Setup of the electrophoretic deposition process.

The morphology of the samples was examined using a field emission scanning electron microscope FESEM-Zeiss SEM Ultra 60. Transmission electron microscopy (TEM) was done via JEOL 4000EX high-resolution electron microscope (HREM) 400kV The compositional analysis of the samples was investigated using X-ray photoelectron spectroscopy (XPS) on a Thermo Scientific K-alpha XPS with an Al anode. The spectra were charge referenced to O 1s at 532 eV. Raman measurements were performed on a Raman microscope (ProRaman-L Analyzer) with an excitation laser beam wavelength of 532 nm.

X-ray diffraction was done on PANalytical X'Pert PRO XRD diffractometer.

4.7 Optical and photoelectrochemical measurements:

Photoluminescence is measured by using Shimadzu RF-5301 PC spectrofluorimeter operating in the wavelength region between 220 and 750 nm.

For photoelectrochemical investigations, the annealed samples are connected to a copper sheet via conductive silver paste, and connected to a three electrode system which is made of an anode (titania), cathode (platinum counter electrode) and calomel reference electrode. The cell has one quartz surface to allow efficient light transport. The electrolyte used is 1M KOH in order to increase the conductivity of the water. This cell is connected to a potentiostat Biologic Sp200, where an applied bias from -1V to 1V is supplied to the anode. The cell is aligned with a light source Xenon lamp with a power of 300 W and supplied with an Air Mass1.5 filter to simulate the solar light hitting the earth surface. The position of the light source is adjusted to produce a focused light on the anode with a power 100mW/cm^2. By applying light and bias, electrons and holes are produced on the anode, the holes oxidize the electrolyte, while the electrons transfer through the wiring to the cathode, where they reduce the oxidized water molecules and produce hydrogen.

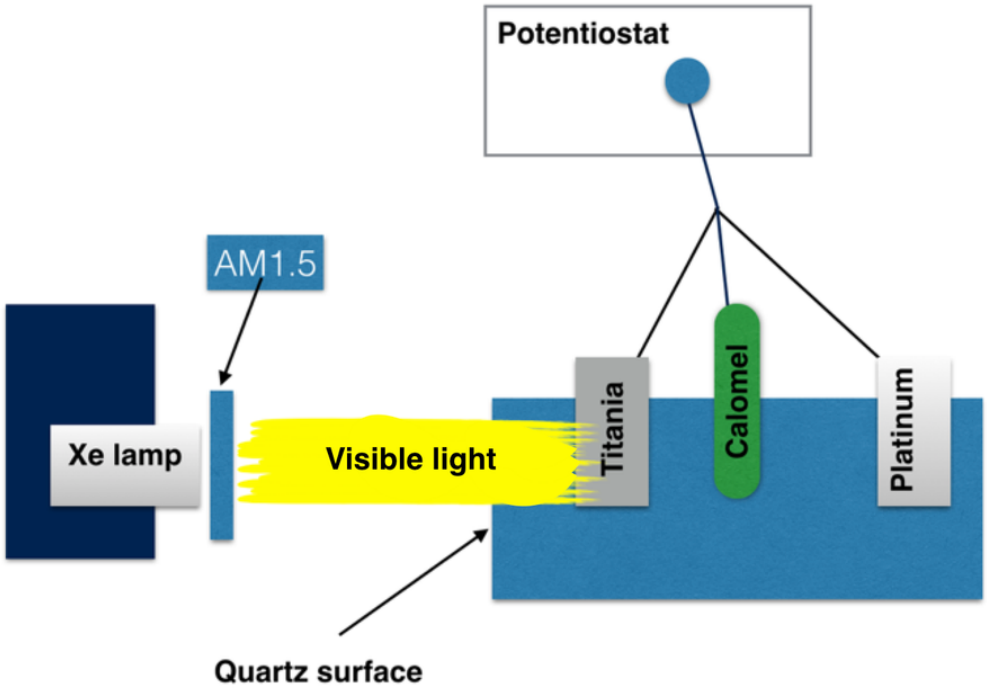

Scheme 4-5: Setup for photoelectrochemical technique, composed of 3- electrode cell.

Incident photon-to-current efficiency (IPCE) is another technique that is used to define the quantum efficiency of the photoanode without an applied bias. The measurement was performed by New port QEPVSI-B. It is a 2 electrode system, where titania (anode) is placed in front of platinum (counter electrode) and both are immersed in an electrolyte made of 1 M KOH. A built in monochromator unifies the beam hitting the sample and the detector detects the absorbed electron at each wavelength, and integrates the result into quantum efficiency.

4.8 Electrochemical impedance spectroscopy:

It was measured by Biologic Sp-200, using a three-electrode system: titania as the anode, platinum as the counter electrode and a calomel reference electrode. Impedance spectroscopy was done under dark conditions for all samples for a frequency ranging from 10 mHz to 1000 kHz, for a voltage ranging from -1 to 0.6 V, the number of measured cycles was unified to be 21 cycles.

Nyquist plot was drawn from this technique and Mott-Schottky plots were generated on the Nyquist plot data in order to define the flat band potential and the charge carrier density.

References

1. Chen, T.; Zeng, B.; Liu, J.; Dong, J.; Liu, X.; Wu, Z.; Yang, X.; Li, Z. In *In High throughput exfoliation of graphene oxide from expanded graphite with assistance of strong oxidant in modified Hummers method;* Journal of Physics: Conference Series; IOP Publishing: 2009; Vol. 188, pp 012051.

2. Zhu, S.; Zhang, J.; Qiao, C.; Tang, S.; Li, Y.; Yuan, W.; Li, B.; Tian, L.; Liu, F.; Hu, R. Strongly green-photoluminescent graphene quantum dots for bioimaging applications. *Chem.Commun.* **2011***, 47*, 6858-6860.

3. Li, X.; Eli, W. A green approach for the synthesis of long chain aliphatic acid esters at room temperature. *Journal of Molecular Catalysis A: Chemical* **2008***, 279*, 159-164.

4. Chan, D. Y.; Mitchell, D. J. The free energy of an electrical double layer. *J. Colloid Interface Sci.* **1983***, 95*, 193-197.

5. Yates, D. E.; Levine, S.; Healy, T. W. Site-binding model of the electrical double layer at the oxide/water interface. *Journal of the Chemical Society, Faraday Transactions 1: Physical Chemistry in Condensed Phases* **1974***, 70*, 1807-1818.

6. Besra, L.; Compson, C.; Liu, M. Electrophoretic deposition on non-conducting substrates: the case of YSZ film on NiO–YSZ composite substrates for solid oxide fuel cell application. *J. Power Sources* **2007***, 173*, 130-136.

Results and discussions

Chapter 5

Thin walled titania nanotubes

Controlling the length and the diameter of [1]TiO_2 nanotubes has shown tremendous positive effects on the performance of the material in solar energy conversion. However, the effect of wall thickness was poorly discussed in literature [1,2], despite the fact that it is one of the determinant factors controlling the dynamics of charge carriers, especially in photoelectrochemical water splitting systems. Most of the published articles are dealing with wall thicknesses that are greater than the diffusion length of charge carriers in titania [1-4]. Herein, we report the first demonstration of the fabrication of vertically aligned titania nanotube arrays with very thin walls (3-5 nm) and their use for solar water splitting. The thin-walled nanotubes facilitate the diffusion of the photogenerated holes to the semiconductor/electrolyte interface during water splitting, allowing for efficient separation of charge carriers.

The diffusion length of charge carriers in titania is around 10 nm [1], and until now there is no reproducible method to produce titania nanotubes with wall thickness that is considerably lower than the diffusion length. Inspired by the work of Amer et al [5], who were able to fabricate thin-walled ZrO_2 nanotubes, we used a mixture of non-aqueous (glycerol) and aqueous (water) electrolytes to anodize titanium in order to achieve titania nanotubes with ultrathin walls. The detailed experimental set-up and

This chapter was published in Chem Comm as: Chem Comm. DOI: 10.1039/C5CC04539H.

conditions are summarized in Chapter 4. In order to show the effect of the wall thickness, two sets of samples were fabricated; namely thick-walled nanotubes (NT1) using the conventional anodization method and thin-walled nanotubes (NT2) using our modified fabrication method.

Figure 1 shows FESEM images of the fabricated NT1 and NT2. The thin-walled nanotubes (Fig.5-1(a)) are highly ordered, tightly packed with wall thicknesses ranging between 3 and 6 nm, length of ~ 1 μm, and inner diameter of 60±5 nm. In contrast, the thick-walled nanotubes (Fig.5-1(b)) are not well-aligned with irregular outer diameters that contain ridges and circumferential serrations, similar to those usually seen upon anodizing Ti in formamide-based electrolytes. The difference in homogeneity and packing between NT1 and NT2 can be related to the use of highly viscous electrolyte (glycerol) in case of NT1 as was detailed elsewhere [2,6,7].

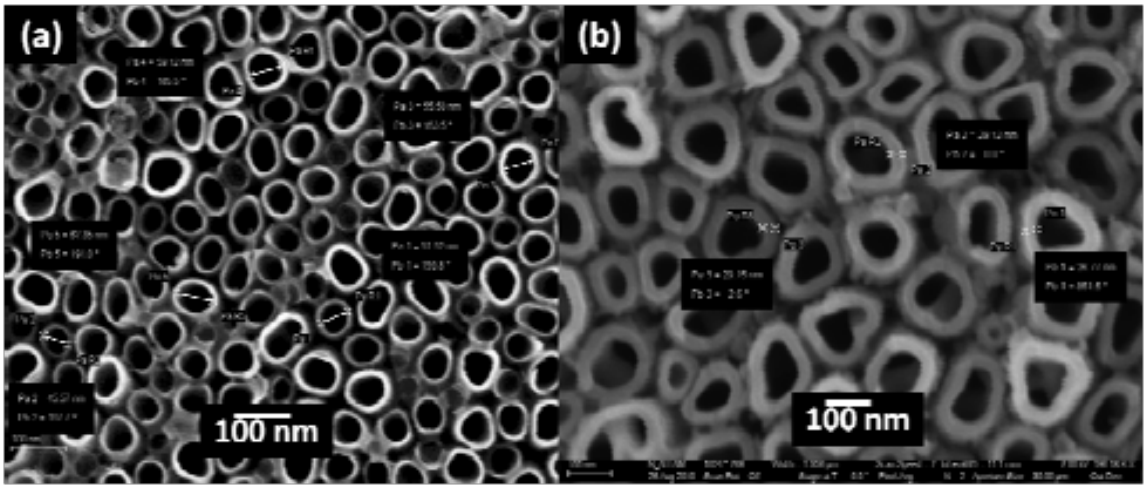

Fig 5-1: FESEM images of (a) thin-walled and (b) thick-walled titania nanotubes.

As the as-anodized nanotubes are amorphous, we annealed them in air to crystallize them. Figure 2 shows the obtained XRD pattern of the annealed thin-walled nanotubes at 450°C for 4h. A characteristic peak is observed at 2Θ=25° that is related to the (1 0 1) crystalline anatase phase, which is consistent with the anatase titania in literature [8]. The most prominent peak shown is the one representing the (1 0 5) crystalline phase. The (1 0 5) crystalline facet is considered an active facet unlike the (1 0 1) facet. The predominance of the high energy facet (1 0 5) increases the hydrogen bonding on the surface of the titania, which results in increasing the barrier for forming larger crystal structure [9], as a result smaller crystal size are formed in this structure Using Scherer equation, the crystallite size was about 7.12 nm.

$$Size = \frac{k \times \lambda}{\beta \cos\theta} \qquad (1)$$

Where, the size of nanoparticle is in nm, k is constant and nearly equals 1, λ is the wavelength of the Cu anode and it equals 1.54 Å, β is the FWHM of the peak in radians, and θ is the diffraction angle divided by 2 in degrees.

With lattice parameters of a= 2.414 nm and c= 3.56 nm, giving a stress along a = 5.38 and along c = 2.74.

$$c = \frac{kl}{2\sin\theta} \qquad (2)$$

$$\frac{1}{d_{khl^2}} = \frac{4}{3}\frac{h^2+k^2+hk}{a^2} + \frac{l}{c^2} \qquad (3)$$

The relative standard deviation of the determined average particle size is ~5% and the instrument broadening was corrected for using NIST 640c silicon. Note that the obtained

crystallite size for the thin-walled nanotubes (7 nm) is much smaller than that reported for the conventionally prepared thick-walled nanotubes (40-70 nm). Such a small grain size has an effect on the photocatalytic activity of the material will be explained later [10].

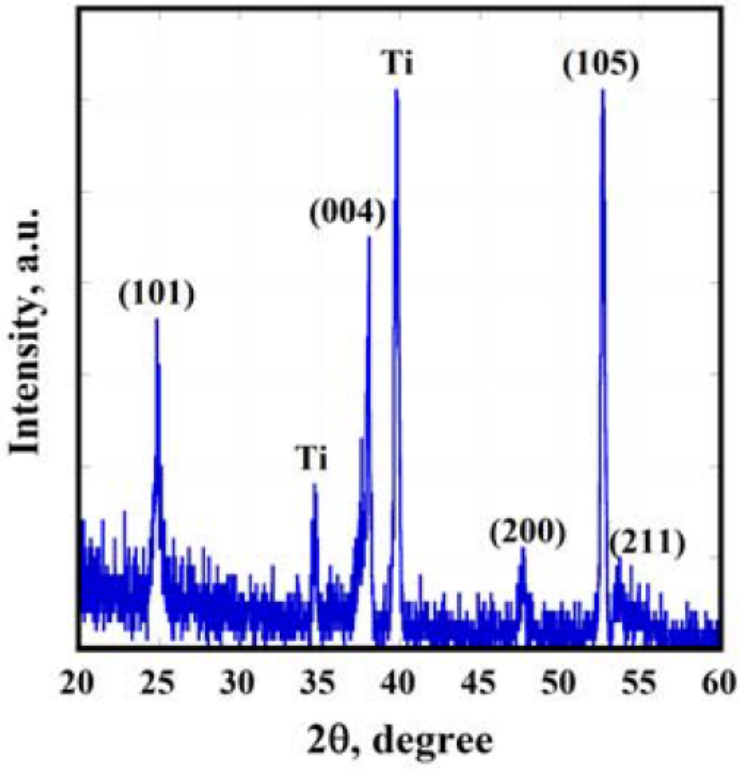

Fig 5-2: XRD pattern of the annealed thin-walled nanotubes.

To get more insights into the composition of the thin-walled nanotubes, we have performed x-ray photoelectron spectroscopy (XPS) analysis for the annealed samples using a Thermo Scientific K-alpha XPS with an Al anode. Spectra were charge referenced to O 1s at 532 eV. The formation of oxide is evident from the O 1s and Ti 2p

peaks with the molar ratio of Ti/O being close to the stoichiometric proportion. Note that both Ti $2p_{3/2}$ and $2p_{1/2}$ peaks are observed (Figure 5-3(a)) with a separation of 5.7 eV, which confirm the presence of Ti^{4+}. The O 1s spectrum (5-3(b)) is composed of two peaks appearing at 530.9 and 532.1 eV that are characteristic of Ti oxide (Ti-O-Ti) and chemisorbed OH groups on the nanotube's surface, respectively [9,10].

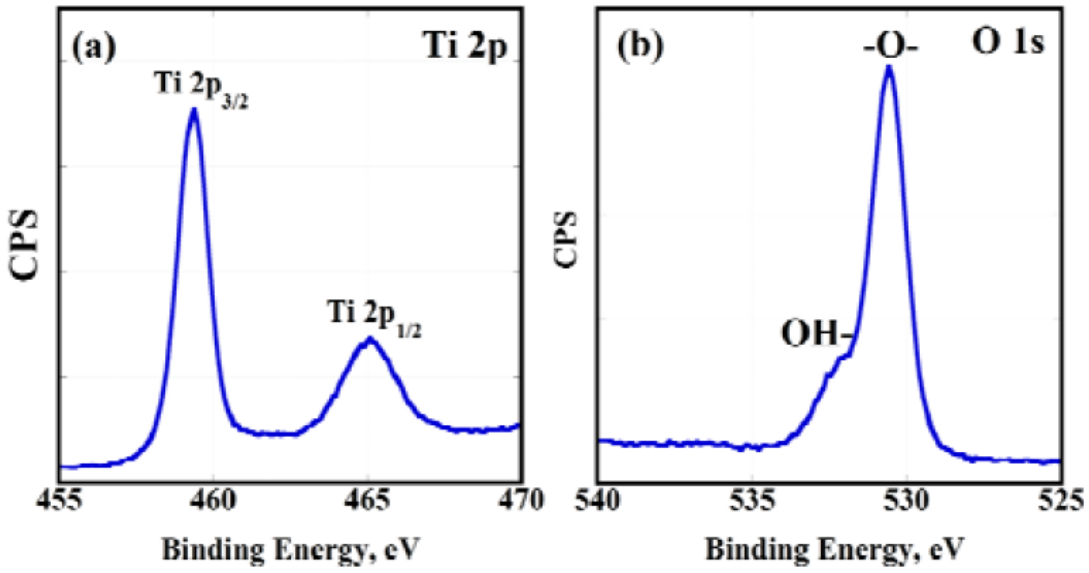

Fig 5-3: XPS spectra of thin-walled titania nanotubes.

The effect of the wall thickness on the charge carrier dynamics and the performance of titania nanotubes is still unclear in literature. On one side, it is reported that thick wall thickness would ensure the creation of large depletion region (space charge region) and consequently there would be an enough electric potential difference

between the sides of the wall (potential drop) [1,4]. The generated electric field in that case would directly result in separation of charge carriers and preventing recombination. The potential drop ($\Delta\varphi_o$) across the wall thickness can be calculated using Eq. 4:

$$\Delta\Phi_0 = kTr_0^2 / 6eL_D \qquad (4)$$

where r is half the wall thickness and L_D is the Debye length, which can be calculated using Eq. 5:

$$L_D = \left[\varepsilon_0 \varepsilon kT / 2e^2 N_D\right]^{1/2} \qquad (5)$$

where N_D is the charge carrier density, ε and ε_o are the dielectric constant and the permittivity in air for titania, respectively (23). In this case, there must be a minimal band bending of 50 mV in order to prevent the charge recombination. This band bending (ω) can be consumed by having an efficient depletion region to accommodate the band bending, which can be calculated using Eq. 6:

$$\omega = \sqrt{\frac{2\varepsilon\varepsilon_0 V_B}{eN_D}} \qquad (6)$$

Where V_B is the amount of band bending took place. As the wall thickness of the nanotubes supports only a potential depletion zone that is half its width, a wall thickness of ~24 nm is needed [1,4].

On the other side, a thinner wall thickness would result in a lower band bending with the band potential being very close to the flat band potential. However, the thin wall thickness would prevent the formation of a large depletion region, and consequently there would not be enough potential drop across the wall, leading to less separation of the

photogenerated charge carriers [1,11]. When the wall thickness is less than the diffusion length in titania, which is thought to be about 10 nm, only in this case, there is no electric diffusion layer needed to separate electrons and holes, as the holes simply diffuse through the tube walls to the semiconductor/electrolyte interface [1], see scheme 3-1.

To test the validity of either assumptions mentioned above, the thin-walled and thick-walled titania nanotubes have been used as photoanodes in a three electrode electrochemical cell to split water in a 1 M KOH electrolyte solution. Figure 5-4a shows the variation of the photocurrent density *versus* applied bias. The photocurrent produced by the thin-walled titania nanotubes is almost twice that produced by thick-walled nanotubes under the same conditions, highlighting the better charge dynamics for the thin-walled nanotubes. However, the dark current in case of thick-walled nanotubes is lower than that of the thin-walled counterparts. The high dark current in case of thin-walled nanotubes can be related to the smaller crystallite size (7 nm) compared to that of thick walls (40-60 nm). Small crystallite size produces large number of under coordinated Ti atoms on the grain surface. In order to counteract this down coordination, Ti atoms absorb water molecules, leading to a distortion of the crystal structure. This distortion results in the heading of the negative centres to the interior of the grain and the positive centres to the outside, which can be manifested by the formation of parallel surface defect dipole and the increase of dipole-dipole repulsion [10,12]. This defect dipole was shown to increase the dark current. Another privilege of the thin-walled nanotubes is that the onset potential is lower than that for the thick-walled nanotubes. This can mainly be attributed

to the better charge kinetics and lower resistance as confirmed later via electrochemical impedance measurements [13].

Incident Photon to current collection efficiency (IPCE) experiments were performed without an applied bias in order to better understand the charge carriers collection efficiency in both thin and thick-walled nanotubes. The experiments were performed in a two-electrode cell with the nanotubes film as the working photoelectrode and platinum foil as a counter electrode in 1 M KOH solution. The IPCE was calculated using Eq. 7, where λ is the wavelength of incident light, j_{ph} is the photocurrent density under illumination at λ and I_o is the incident light intensity at λ.

$$\boldsymbol{IPCE}\% = \frac{|\boldsymbol{j_{ph}}(\boldsymbol{mA/cm^2})| \times \boldsymbol{1239.8}(\boldsymbol{V \times nm})}{\boldsymbol{I_0}(\boldsymbol{mW/cm^2}) \times \boldsymbol{\lambda}(\boldsymbol{nm})} \qquad (7)$$

Figure 5-4b shows the obtained IPCE, where the thin-walled nanotubes show higher collection efficiency (47%) than the thick-walled nanotubes (15%). These results clearly show the direct effect of reducing the wall thickness on enhancing the charge carrier separation and collection. Also, it is evident that controlling the tube thickness is more effective than relying on the potential depletion region for thick-walled nanotubes.

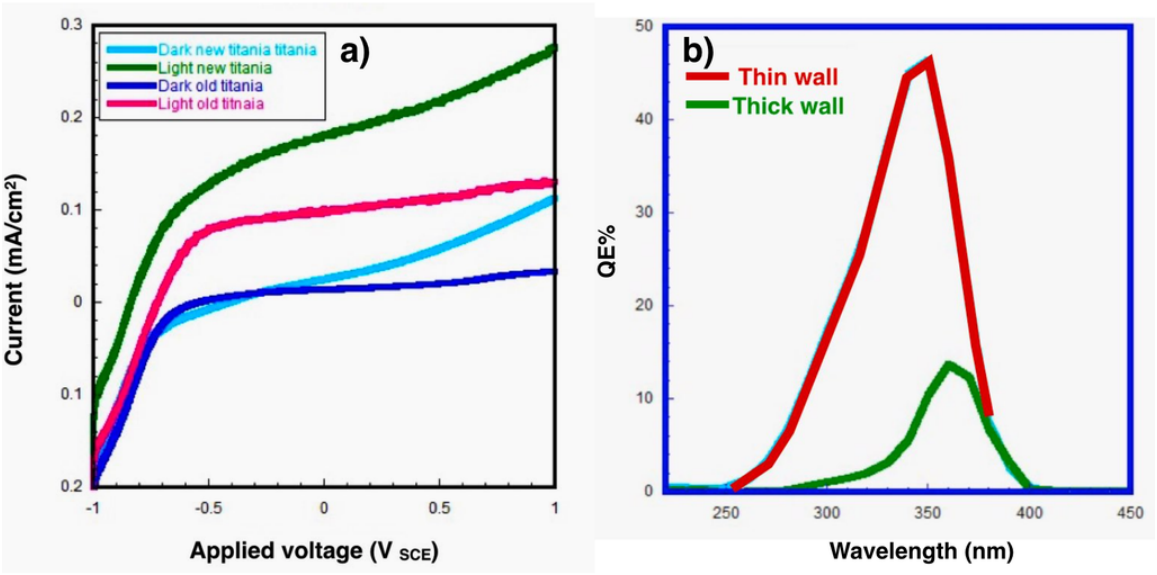

Fig. 5-4: (a) I-V and (b) IPCE characteristics of thin-walled and thick-walled titania nanotubes measured in 1M KOH aqueous solutions under dark and illuminated (AM 1.5) conditions.

To get more insights into the effect of wall thickness on the properties of titania nanotubes, electrochemical impedance spectroscopy measurements were done using Biologic SV-200 for both thin and thick-walled nanotubes at 0.6V. Figure 5 shows the obtained Nyquist plots. The thin-walled titania shows higher conductivity compared to the thick-walled counterparts, which confirms the efficient charge carrier transport for the thin-walled nanotubes. This was asserted by the Mott-Schottky analysis, which revealed a flat band potential of -0.7 V *versus* SCE with charge carrier density of 5×10^{18} cm^{-3}. The obtained flat band potential and carrier density are in agreement with those reported in literature [14].

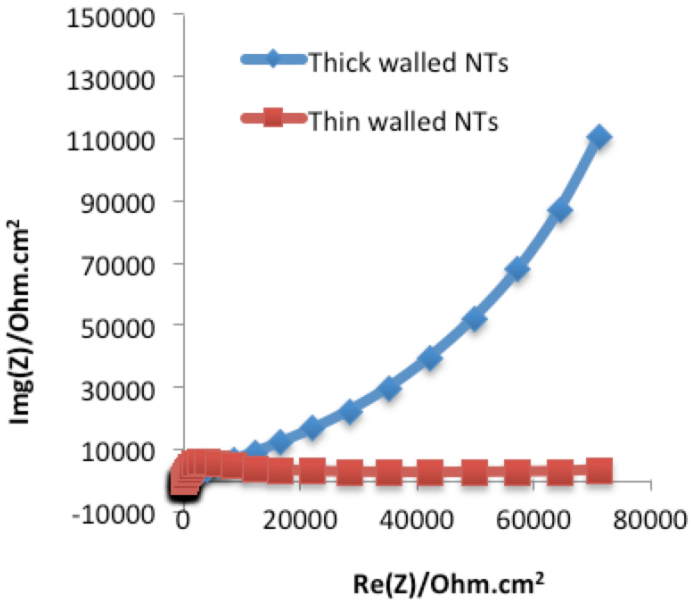

Fig. 5-5: Nyquist plot of both thin and thick-walled titania nanotubes.

In summary, a new synthetic approach to produce thin-walled titania nanotubes, with wall thickness less than the charge carriers diffusion length, is presented. The calculated crystallite size for the thin-walled nanotubes is as small as 7nm, leading to the creation of a large number of under coordinated Ti atoms on the grain surface and consequently high dark current. The thin-wall nanotubes showed almost double the photocurrent of the thick-wall nanotubes upon their use in water splitting arrangement. The IPCE and electrochemical impedance measurements confirmed the superiority of the thin-walled nanotubes over their thick-walled counterparts. The Mott-Schottky analysis revealed a flat band potential of -0.7 V *versus* SCE with charge carrier density of 5×10^{18} cm^{-3}. Our work confirmed the importance of using ultra thin- walled titania nanotubes as photoanodes for efficient solar water splitting.

References

1. Grimes, C. A.; Mor, G. K. *TiO2 nanotube arrays: synthesis, properties, and applications;* Springer Science & Business Media: 2009; .

2. Liang, S.; He, J.; Sun, Z.; Liu, Q.; Jiang, Y.; Cheng, H.; He, B.; Xie, Z.; Wei, S. Improving photoelectrochemical water splitting activity of TiO2 nanotube arrays by tuning geometrical parameters. *The Journal of Physical Chemistry C* **2012**, *116*, 9049-9053.

3. WU, C.; ZHUO, Y.; ZHU, P.; CHI, B.; PU, J.; LI, J. Tunable fabrication of TiO2 nanotube arrays with high aspect ratio and its application in dye sensitized solar cell. *Journal of inorganic materials* **2009**, *5*, 006.

4. Gao, X.; Chen, J.; Yuan, C. Enhancing the performance of free-standing TiO 2 nanotube arrays based dye-sensitized solar cells via ultraprecise control of the nanotube wall thickness. *J. Power Sources* **2013**, *240*, 503-509.

5. Amer, A. W.; Mohamed, S. M.; Hafez, A. M.; AlQaradawi, S. Y.; Aljaber, A. S.; Allam, N. K. Self-assembled zirconia nanotube arrays: fabrication mechanism, energy consideration and optical activity. *RSC Advances* **2014**, *4*, 36336-36343.

6. Kapusta-Kołodziej, J.; Tynkevych, O.; Pawlik, A.; Jarosz, M.; Mech, J.; Sulka, G. D. Electrochemical growth of porous titanium dioxide in a glycerol-based electrolyte at different temperatures. *Electrochim. Acta* **2014**, *144*, 127-135.

7. Kar, P. Effect of anodization voltage on the formation of phase pure anatase nanotubes with doped carbon. *Inorganic Materials* **2010**, *46*, 377-382.

8. Du, G.; Chen, Q.; Che, R.; Yuan, Z.; Peng, L. Preparation and structure analysis of titanium oxide nanotubes. *Appl. Phys. Lett.* **2001**, *79*, 3702-3704.

9. Ahmad, M. I.; Bhattacharya, S. Size effect on the lattice parameters of nanocrystalline anatase. *Appl. Phys. Lett.* **2009**, *95*, 1906.

10. Li, G.; Boerio-Goates, J.; Woodfield, B. F.; Li, L. Evidence of linear lattice expansion and covalency enhancement in rutile TiO2 nanocrystals. **2004**.

11. Zhao, Z.; Yi, C.; Lantz, K.; Stiff-Roberts, A. Effect of donor-complex-defect-induced dipole field on InAs⁄GaAs quantum dot infrared photodetector activation energy. *Appl. Phys. Lett.* **2007**, *90*, 233511.

12. Macák, J. M.; Tsuchiya, H.; Schmuki, P. High-Aspect-Ratio TiO2 Nanotubes by Anodization of Titanium. *Angewandte Chemie International Edition* **2005**, *44*, 2100-2102.

13. Van de Krol, R.; Goossens, A.; Schoonman, J. Mott-Schottky Analysis of Nanometer-Scale Thin-Film Anatase TiO2. *J. Electrochem. Soc.* **1997**, *144*, 1723-1727.

14. Endut, Z.; Hamdi, M.; Basirun, W. J. An investigation on formation and electrochemical capacitance of anodized titania nanotubes. *Appl. Surf. Sci.* **2013**, *280*, 962-966.

Chapter 6

Crystallization and Surface treatment

In this chapter, two strategies are investigated to enhance the performance of titania NTs as photoanode material in photoelectrochemical water splitting. The first strategy was to identify the best annealing conditions that result in structurally and optically active titania. The second strategy was alkali metal treatment of the NTs to passivate the inherent defects.

6.1 Black titania:

In this part, we compared the samples that are annealed under air, hydrogen and oxygen at different annealing times but similar temperatures.

Fig. 6-1 shows the dark and illuminated currents for the annealed titania NTs samples for 4 HRS. The dark and light currents are separated, in order to get in depth analysis and to get an idea about the best annealing conditions suiting our goal.

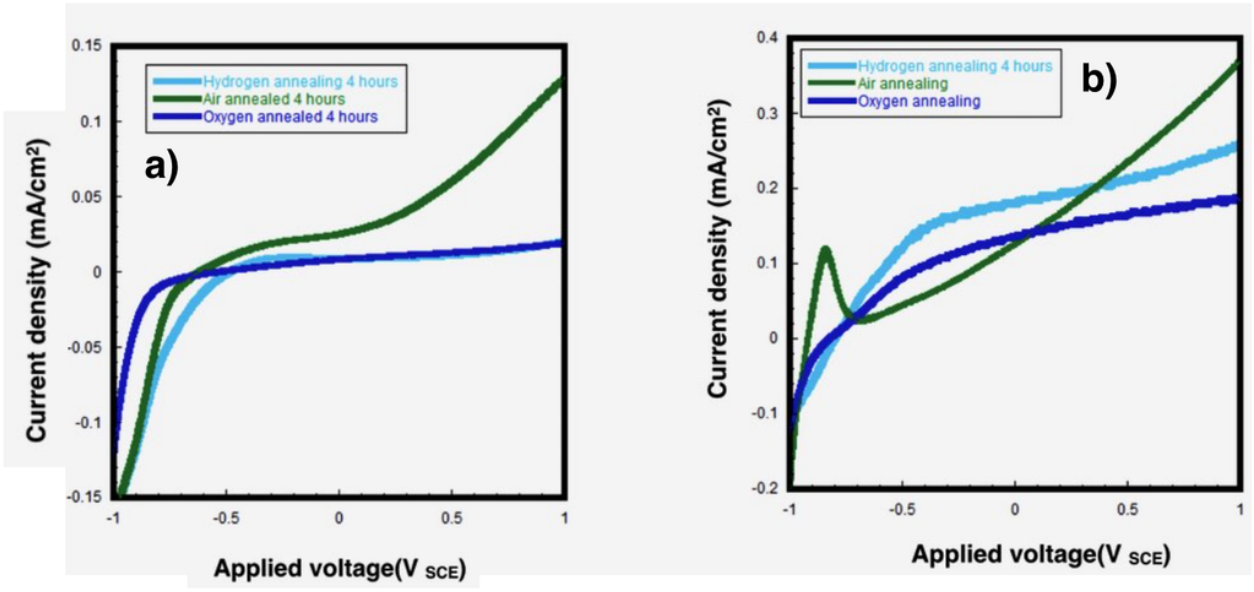

Fig. 6-1: (a) Dark and (b) the photocurrents (b), for air, hydrogen and oxygen-annealed samples, in 1M KOH as an electrolyte.

As shown in Fig 6-1, the dark current for 4 hours hydrogen annealed sample is similar to oxygen annealed sample, which means they both annihilated the defect states on the surface, leading a lower dark current reading compared to air annealed titania. From the photocurrent in Fig 6-1(b), hydrogen annealed samples have nearly similar photocurrents, while the oxygen annealed sample produced lower photocurrent. It seems that the hydrogen annealing for 4 hours annihilated defect states on titania, mostly the deep defect states, because this annihilation was accompanied by a minimal reduction in photocurrent and a considerable reduction in dark current [1].

As we increase the annealing time, from 4 hours to 8 hours, Titanium metal turn to form a thin hydride, which is easily broken. Moreover we found that large number of defect states are created with the longer annealing time. This effect was confirmed by measuring

the photocurrent. Fig 6-2 shows the abrupt increase in the dark and light currents for the 8 hours hydrogen annealed titania. Although the light current is not as high as reported before (1-5 mA) [2]. It is still higher than what is expected for titania nanotubes. In addition, the open circuit voltage is shifted more positive (from -0.82 to -0.6).

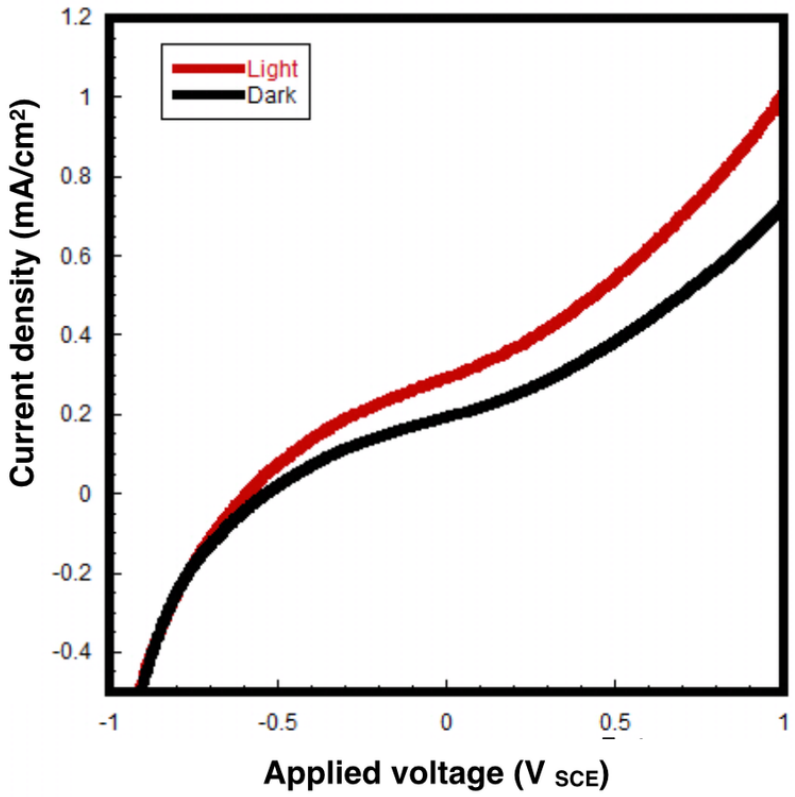

Fig. 6-2: Dark and photocurrent for 8 hours hydrogen annealed titania in 1M KOH.

IPCE data shown in Fig. 6-3 confirm the findings. Air annealed titania has about 45% quantum efficiency, while the 4 hours hydrogen annealed samples achieves nearly 80%. On contrary the 8 hours annealed sample gives only 10% quantum efficiency, which proves the concept of formation of deep defect states that prevent the efficient transfer of

the excited electrons. All the aforementioned findings can indicate the formation of new defect states by annealing for 8 hours under hydrogen. Only few papers discussed the increase in dark current by hydrogen annealing [3], but we return back to the same problem that there are no specific parameters that were set for annealing, or even conditions or gas flow rate.

By zooming into the small region that is beyond 400 nm in the IPCE graph, we found that the 8 hours annealed sample has an absorbance tail beyond 600 nm, while the other two samples have no absorbance at this region.

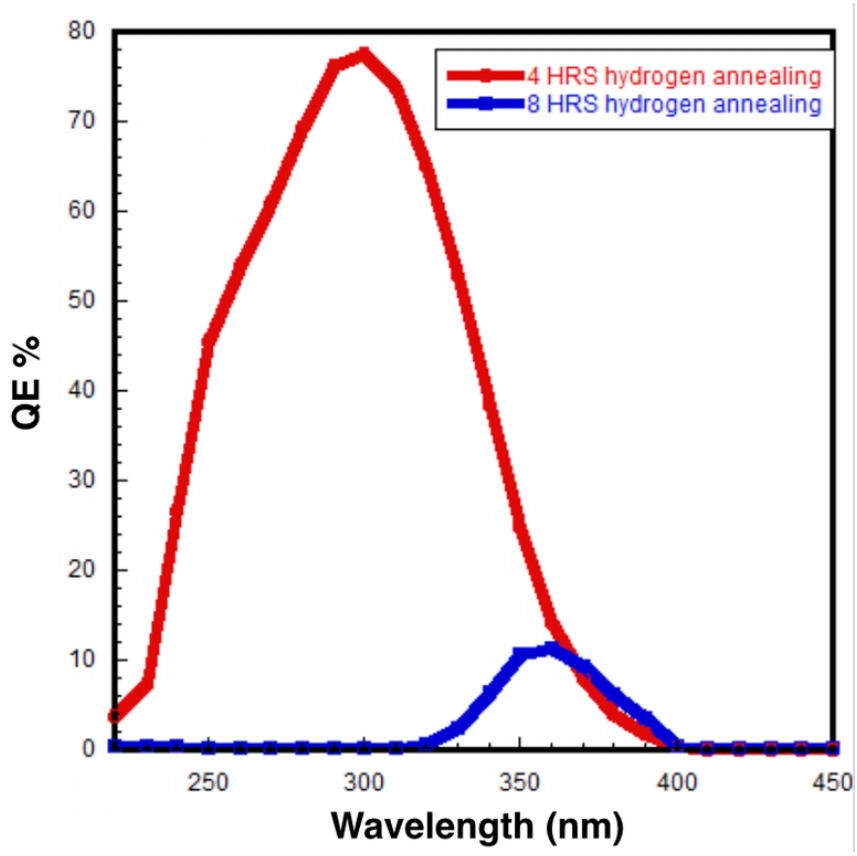

Fig. 6-3: IPCE for titania nanotubes annealed under air and hydrogen atmospheres for 4 and 8 hours measured in 1M KOH in a 2-electrode cell.

It seems that annealing for 8 hours under hydrogen, enabled the formation of black titania, which absorbs in the visible region. Surprisingly, we could not find any IPCE data in literature having higher quantum efficiency for black titania in this visible region. Most of the reported data have similar quantum efficiency values, which arises question marks for the relevance of such very small quantum efficiency to the great enhancement in the photocurrent.

To get more insights in to the obtained results, electrochemical impedance spectroscopy measurements were performed. Fig. 6-4 shows the obtained Nyquist plots and the corresponding Mott-Schottky analysis.

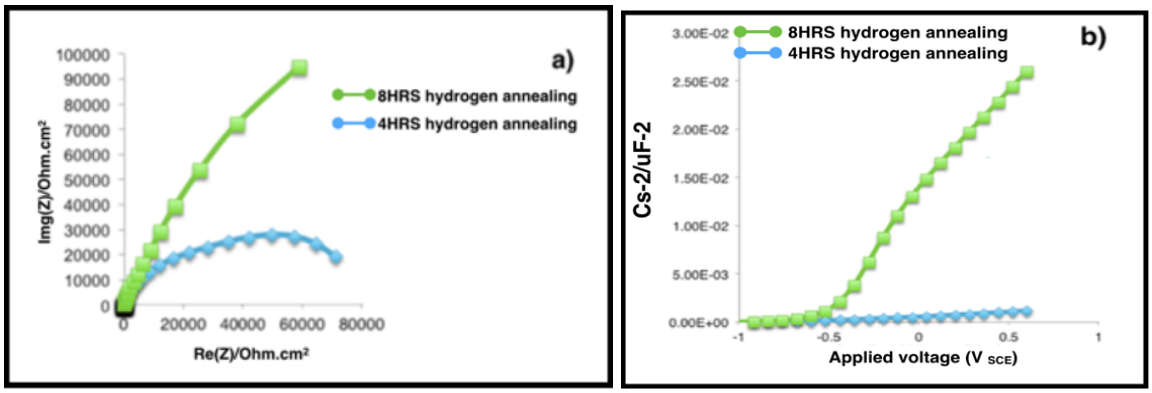

Fig.6-4: (a) Nyquist plot for 4 and 8 hours hydrogen annealed titania, (b) Mott-Schottky for 4 and 8 hours hydrogen annealed titania.

Nyquist plot for 4 and 8 hours annealed titania shows the huge difference in conductivity between them. The 4 hours shows very high conductivity compared to the 8 hours annealed sample. This can be attributed to the lower number of defect states exist in the 4 hours annealed samples, which directly results in higher conductivity.

Mott Schottky curves were drawn for both 4 and 8 hours hydrogen annealed nanotubes. Note the very high steepness of the 8 hours annealed sample compared to the 4 hours annealed sample. Consequently, the 8 hours hydrogen annealed samples have the highest charge carrier density followed by the 4 hours hydrogen annealed sample. Again, this proves that annealing for 8 hours creates defect states that increase the charge carrier density. The charge carrier density jumps from $14\times10^{18}cm^{-1}$ for the 4 hours to $23\times10^{21}cm^{-1}$ for the 8 hours hydrogen annealed sample.

6.2 Surface treatment:

We studied the effect of potassium hydroxide as a reducing agent during the anodization process. The resulted nanotubes were then annealed under hydrogen atmosphere for 4 hours.

We were expecting to have higher charge carrier density. Creation of more defect states most probably a behaviour similar to the 8 hours hydrogen annealing. The photocurrent for this sample was measured and compared to a normal 4 hours hydrogen annealed sample.

The KOH treated sample produced higher photocurrent and dark current compared to the 4 hours hydrogen annealed sample, Fig. 6-5. This can be atributed directly to the formation of new defect states due to the use of a strong reducing agent (KOH) that removes O atoms from TiO_2. Althought the photocurrent difference is not quite high, the dark current increased.

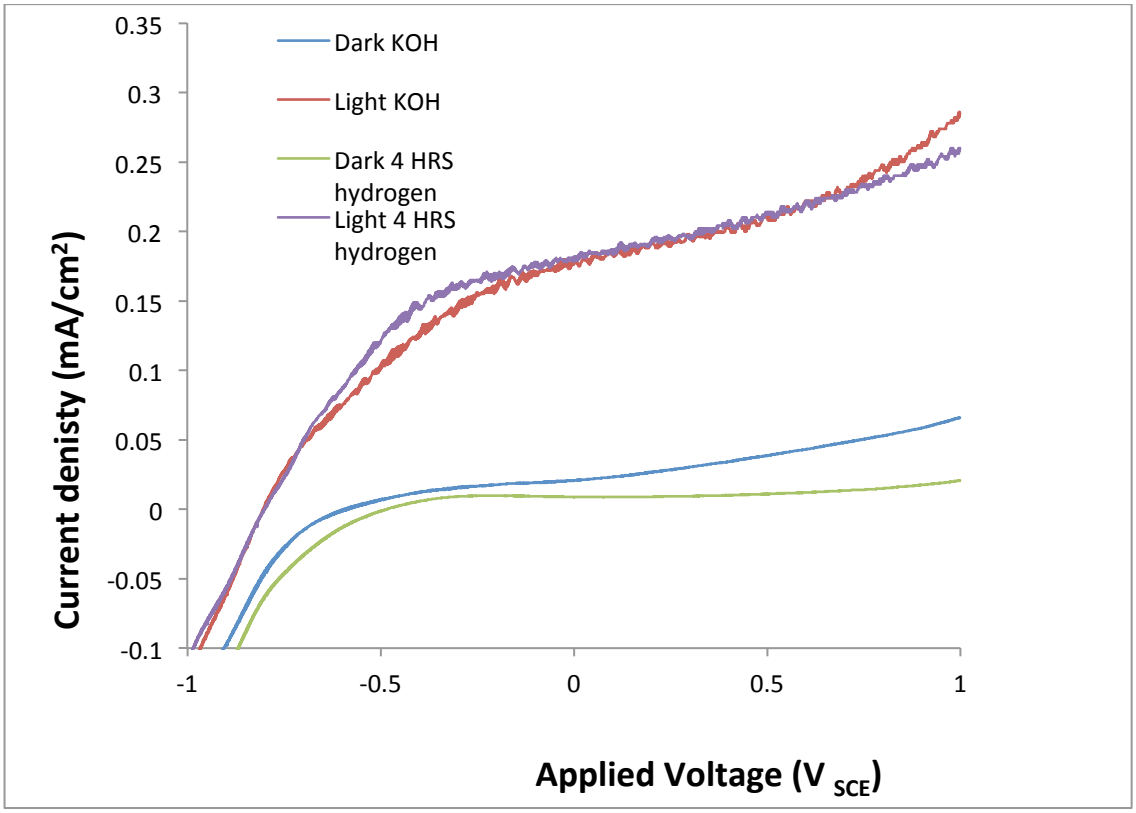

Fig. 6-5: Dark and photocurrent of two titania samples annealed under hydrogen atmosphere for 4 hours, one anodized in the presence of KOH, while the other without KOH.

The IPCE for the 4, 8 and KOH hydrogen annealed samples is displayed in Fig. 6-6. The KOH annealed samples achieved a quantum efficecy about 55%, lying between the 4 and 8 hours hydrogen annealed samples. This can be indicative for the formation of defect states but not as much as the 8 hours hydrogen annealed sample. By zooming in to the area beyond 400 nm, we can find that the wavelenght is extended by 50 nm compared to the 4 hours hydrogen annealed sample, but did not reach the 8 hours hydrogen annealed sample.

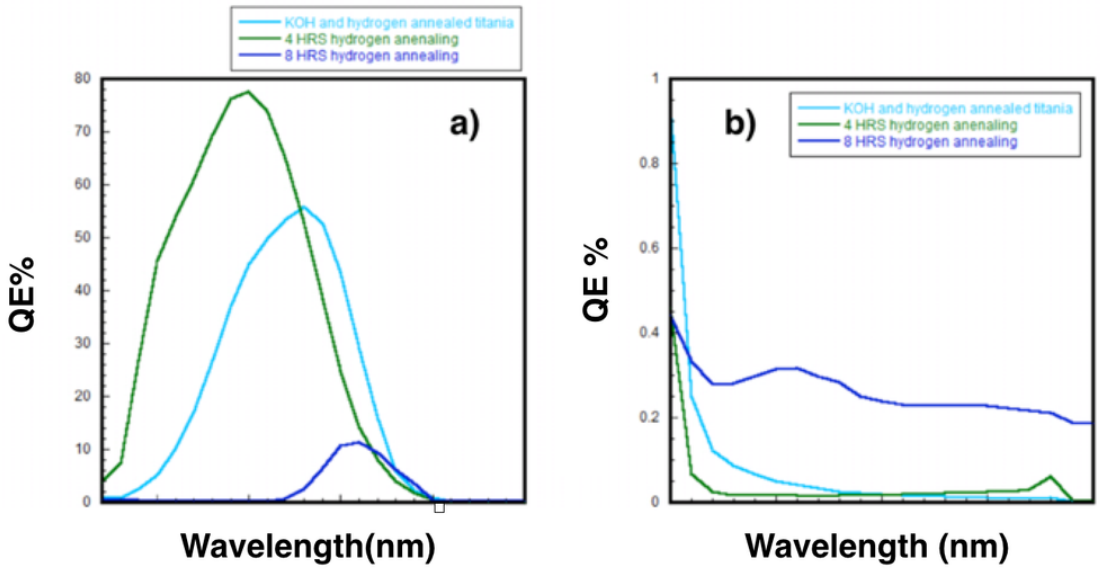

Fig.6-6: IPCE for KOH anodized samples and annealed for 4 hours under hydrogen atmosphere, together with 4 and 8 hours hydrogen annealed samples (a). (b) is a zoom in preview for IPCE data (a) for the region beyong 400 nm.

In order to confirm our results, impedance measurments were performed as shown in fig. 6-7, KOH 4 hours hydrogen annealend titania showed higher conductivity than the 4 hrs hydrogen annealed sample (Fig. 6-7(a)), conforming that KOH passivates the defect states more than hydrogen annealing alone. Mott Schottky analysis for the 3 set of samples is shown in Fig. 6-7(b). The steepest curve is for the 8 hours hydrogen annelead followed by the KOH and finally the 4 hours hydrogen annealed sample. By measuring the charge carrier denisty of the KOH hydrogen annealed sample, it was found to be $2.15\times10^{21}\mathrm{cm}^{-1}$, which is the higher than the 4 hous hydrogen annelaed sample and comparable to 8 HRS hydrogen annealed sample.

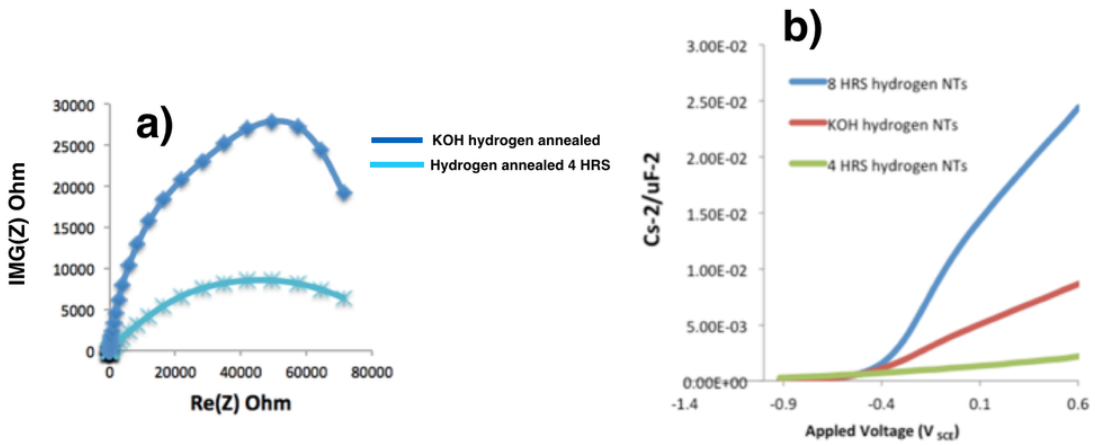

Fig. 6-7: Nyquist plot for the 4 hrs hydrogen annealed sample and KOH 4 hrs hydrogen annealed sample. (b) Mott-Schottky plot for the 4 and 5 hrs hydrogen annealed sample, and the KOH 4 hrs hydrogen annealed.

In Summary, hydrogen annealing process was studied under different exposure times (4 HRS to 8 HRS). It was proved that 4 HRS hydrogen annealing passivates the defect states and reduces the dark current extinsvley, while the 8 HRS hydrogen annealing creates new deep defect states that increases the dark current and the photocurrent. Impedance analysis confirmed the aformentioned findings and the charge carrier denisty increased with increasing the hydrogen annealing time from $14\times10^{18}cm^{-3}$ to $23\times10^{21}cm^{-3}$. Also, the visible light absorption tail was shifted from 400 nm to 600 nm.

Another surface modification was implied for the sake of comparison with hydrogen annealing, by introducing a strong oxidizing agent (KOH), followed by hydrogen annealing. It was found that adding (KOH) passivates most of the defect states, but not as much as the 4 HRS hydrogen annealing. The strong reducing agent also created some

defect states on the surface, with a charge carrier density comparable with the 8 HRS hydrogen annealed titania.

References

1. Tsui, L.; Saito, M.; Homma, T.; Zangari, G. Trap-state passivation of titania nanotubes by electrochemical doping for enhanced photoelectrochemical performance. *Journal of Materials Chemistry A* **2015***, 3*, 360-367.

2. Chen, X.; Liu, L.; Yu, P. Y.; Mao, S. S. Increasing solar absorption for photocatalysis with black hydrogenated titanium dioxide nanocrystals. *Science* **2011***, 331*, 746-750.

3. Wang, G.; Wang, H.; Ling, Y.; Tang, Y.; Yang, X.; Fitzmorris, R. C.; Wang, C.; Zhang, J. Z.; Li, Y. Hydrogen-treated TiO2 nanowire arrays for photoelectrochemical water splitting. *Nano letters* **2011***, 11*, 3026-3033.

Chapter 7

Graphene quantum dots

This chapter highlights the work done to synthetize and functionalizes graphene quantum dots for solar energy conversion.

7.1 Non-functionalized graphene quantum dots:

Fig. 7-1 shows the UV-vis spectra of the non-dialyzed and the dialyzed quantum dots. Two distinct features are obvious from this curve; the peak at 270nm, and the tail that reaches 450 nm. The dialyzed quantum dots show higher absorption if compared to the non-dialyzed sample, which shows how the absorption of the Graphene quantum dots is highly affected by the surrounding media. And this finding is totally conforming what is published in literature [1].

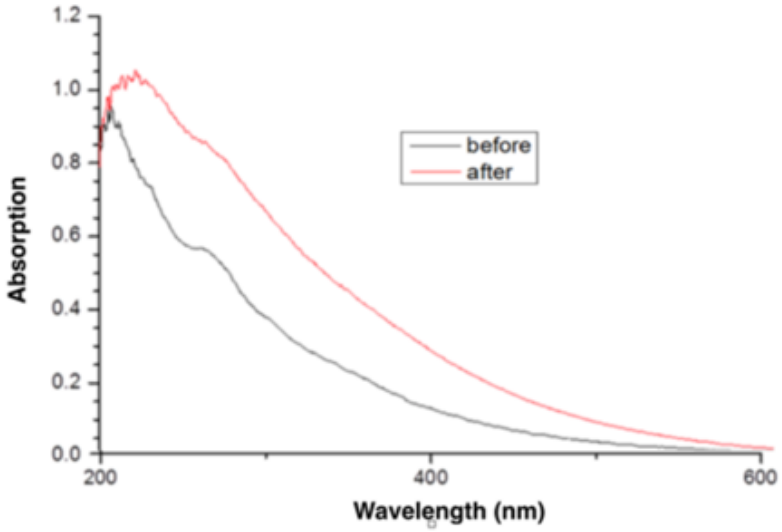

Fig. 7-1: UV-vis absorption of dialyzed and non-dialyzed graphene quantum dots.

Fig. 7-2 shows HRTEM image of the synthetized graphene quantum dots. Note that are not agglomerated, with an average particle size ranging from 7-10 nm. The diffraction pattern showed a d-spacing of 0.25 nm, in agreement with previous reports [2].

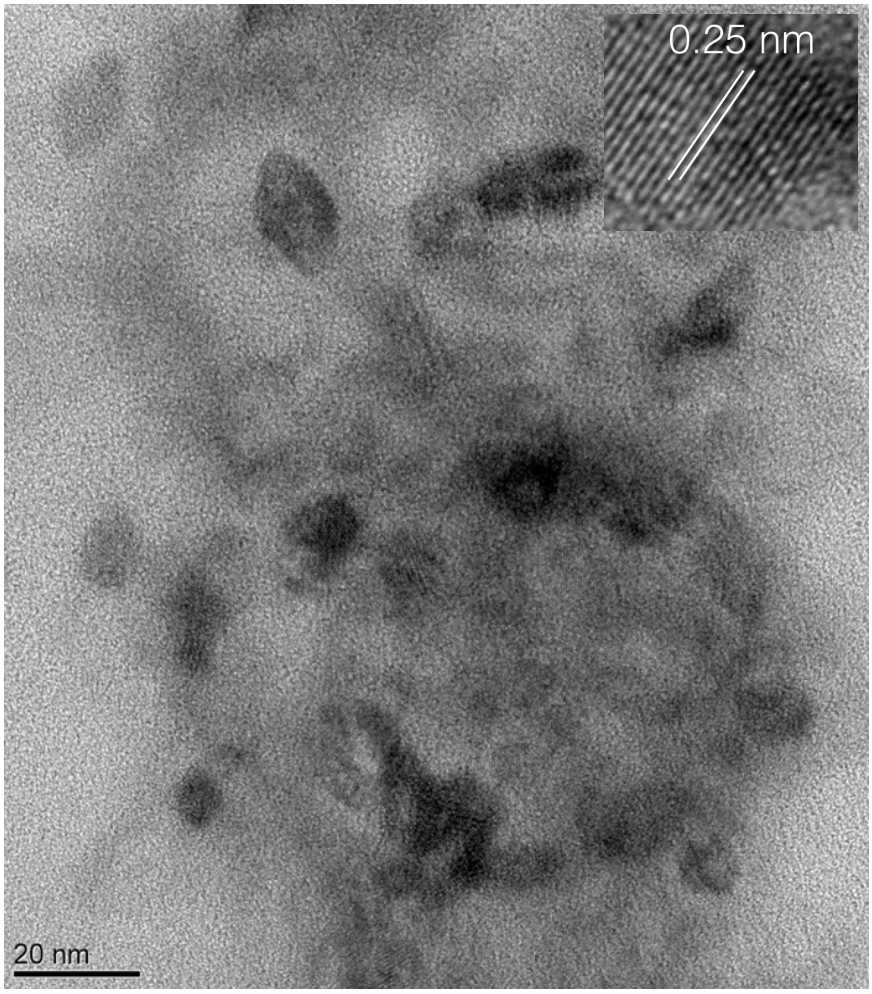

Fig.7-2: Hi-Res TEM image for graphene quantum dots, inset for the diffraction pattern of the graphene quantum dots.

Raman Scattering is a non-destructive technique that was introduced because it is one of the most specific characterization tools. Raman test was performed as

a confirmatory test after each major step during the oxidation of graphite to graphene oxide, to the formation of the quantum dots, Fig. 7-3.

In accordance with the literature, the D band appears at 1380 nm, indicating the outer plane defects and surface defects. The G band also appears at 1550, and indicating the inner plane sp-carbon vibrations. Higher D band is expected for graphene oxide than graphite, due to the presence of oxygenated surface, and same for Quantum dots. The ratio between I_D/I_G bands is considered as a reference for the degree of defects created in the structure and the oxygenation level. Usually the hydrothermally prepared quantum dots shows variable I_D/I_G ratio. Our graphene quantum dots showed I_D/I_G ratio of 1.04, which is in agreement with previous reports [3].

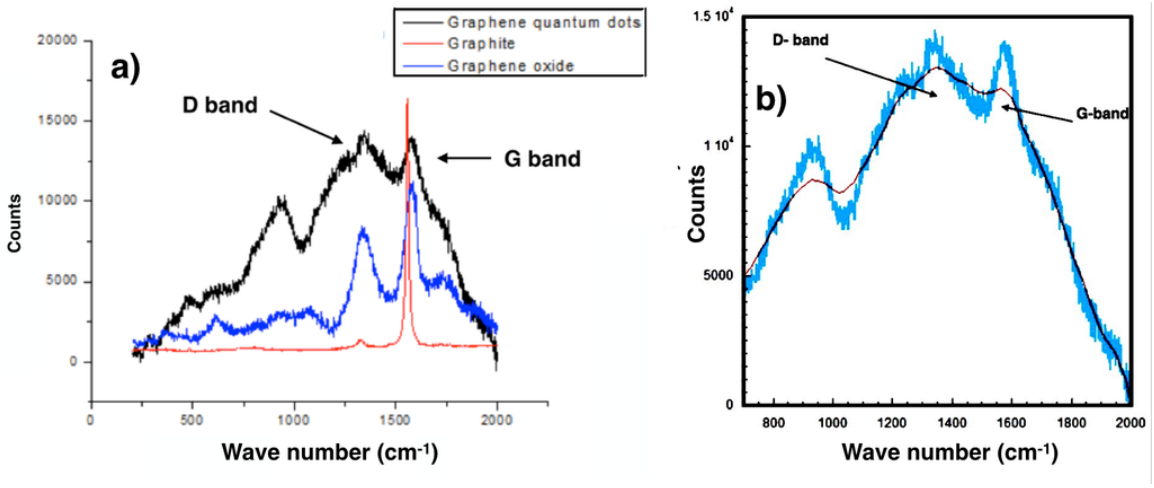

Fig. 7-3: (a) Overlay of Raman spectra for graphene, graphene oxide and graphene quantum dots, and (b) Raman spectra for graphene quantum dots.

In order to get more insights about the chemical composition of the produced quantum dots, FTIR is performed. There are three distinctive peaks for Graphene quantum dots,

which are the OH group at 3420 nm and the COOH carboxylic at both 1720 and 2350 nm [4].

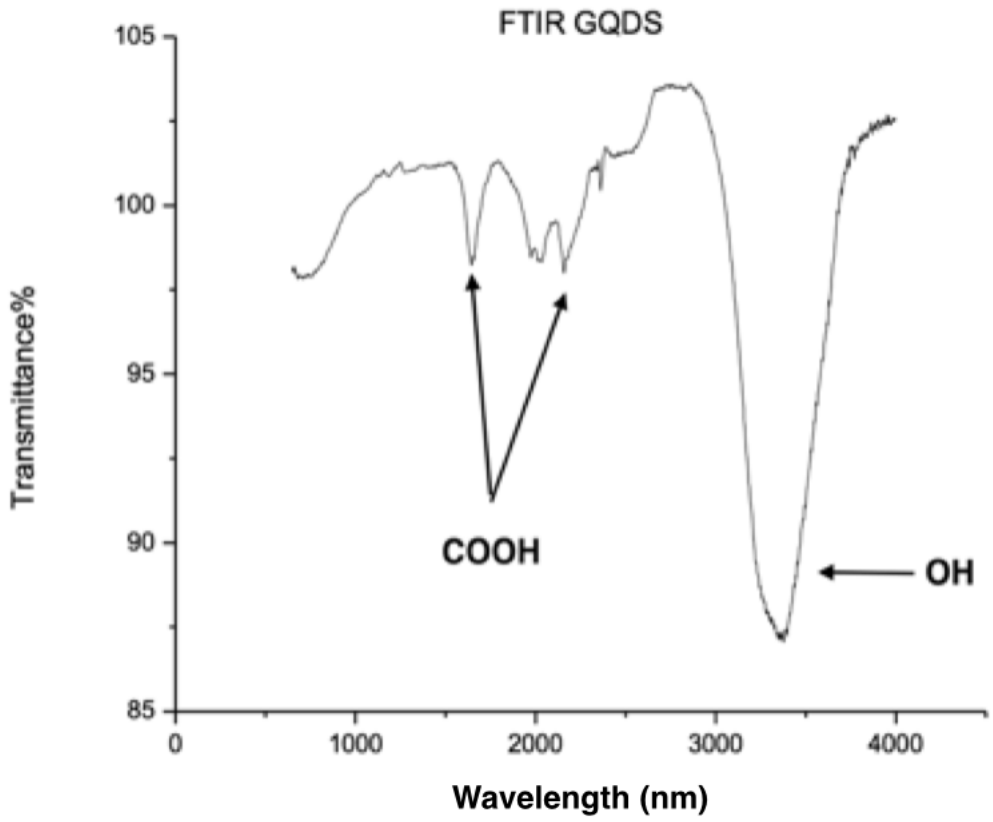

Fig. 7-4: FTIR of the graphene quantum dots.

This was also confirmed via X-ray photoelectron spectroscopy analysis.

XPS results for C1s confirmed the presence of graphene quantum dots by the presence of C-C bond at 286 eV, C-O at 286.5 eV, C=O at 287 eV and COOH at 288 eV, which is in agreement with the previous reports [5].

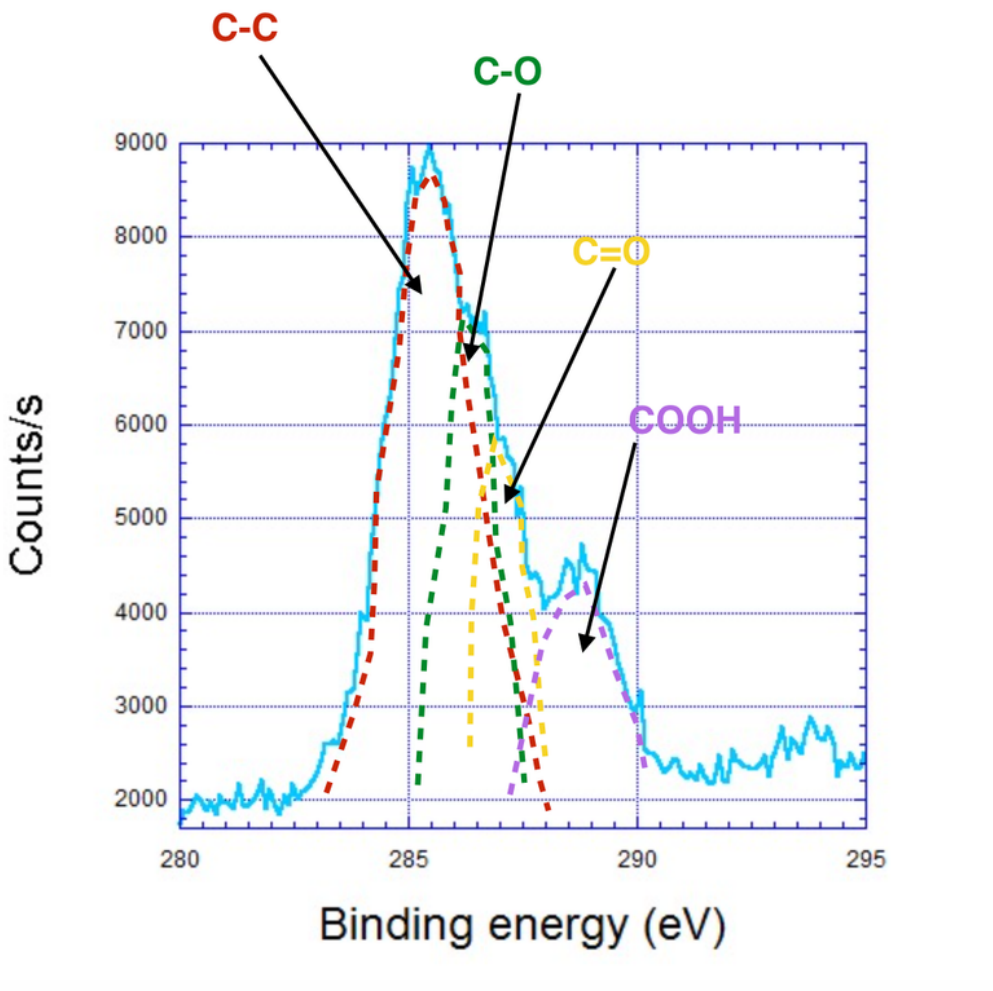

Fig. 7-5: XPS peak for C1s of graphene quantum dots.

The photoluminescence of graphene oxide can be divided into two main peaks: the first is centered at about 400 nm, which is known as I_{P2}, and other larger peak at 600 nm, which is known as I_{P1} [6]. It was proven that both peaks are contributed from two different electronic states, and as a result, several researches were curious to determine the origin of both peaks. It was found that the I_{p1} is originating from the n-π*, which is originating from the bound oxygen groups and forming defect states on the surface. The I_{P2} is originating from the new π-π*, which is the original band gap of

graphene. From here we can deduce that the functionalization is the main source of band gap engineering, but we will discuss it later in details.

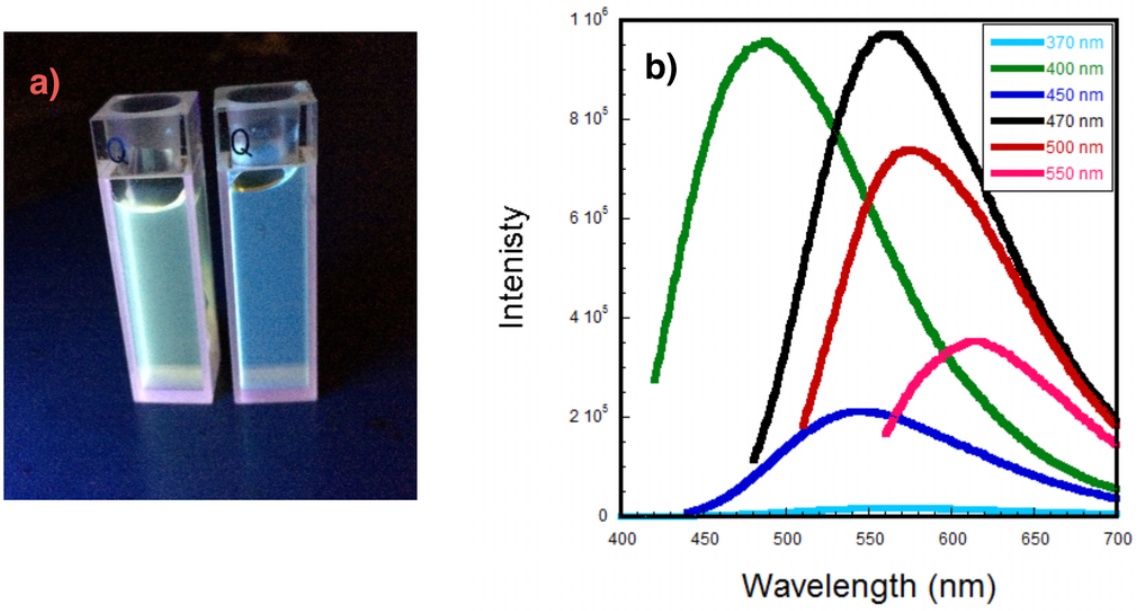

Fig. 7-6: a) Illumination of the graphene quantum dots dialyzed (right) and non dialyzed (left) by UV light (345 nm), and (b) Photoluminescence of graphene quantum dots that are illuminated with different wavelengths (370 nm-550 nm).

Graphene oxide mainly consists of a mixture of sp-2 Carbon bound with oxygen atoms and sp3 defective carbon atoms [7]. Large number of defect states is formed in the band gap of graphene oxide, owing to the low formation energy of π bonding, as a result those new defect states are formed deep in the band tail. It was also found that by reducing those oxygen defects, the number of deep defect states decreases considerably, and I_{P1} emission decreases linearly with the reduction process. Consequently, sp-2 Carbon structure starts

to from new states, which is below the conduction band and they are able to transfer electrons by hoping mechanism [8].

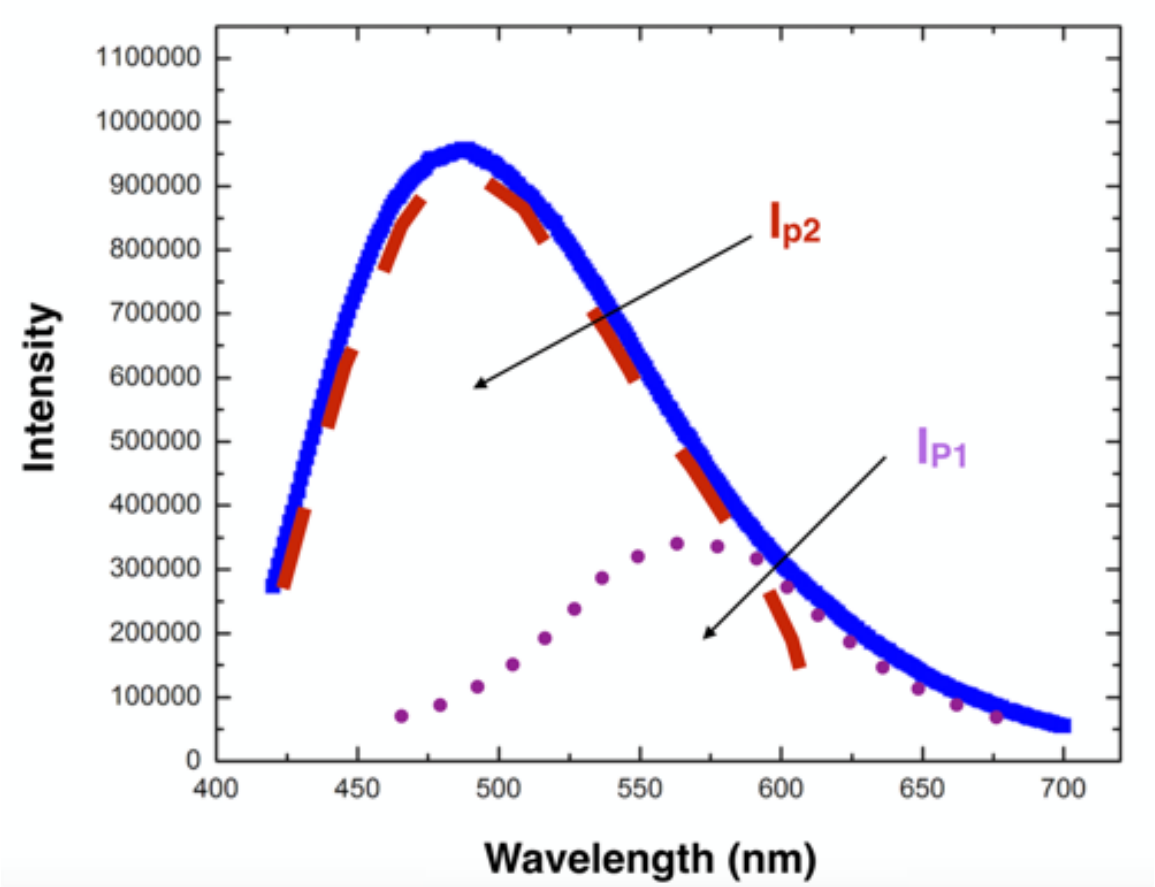

Fig.7-7: Deconvoluted luminescence peak for graphene quantum dots excited at 400nm.

It was found that those carbonic structures are not able to form larger structures because of the energy needed for clustering. In our case, the quantum dots, we found also that there are two main luminescence peaks (Fig. 7-7) similar to graphene oxide (Fig. 3-2). It is important to note that the two assigned peaks I_{P1} and I_{P2} are inverted here, as the I_{P1} is larger and I_{P2} is the smaller for graphene oxide. This is attributed mainly to the nature of

the quantum dots, which is mainly composed of C-C bond with lower number of oxygen groups on the surface than in graphene oxide.

We measured the Time resolved PL of the graphene quantum dots to determine the life time, see Fig. 7-8. It was found that the decay of graphene quantum dots in water is faster than the decay of graphene quantum dots in Dimethyl formamide, and this is attributed to the polarity of the solvent, as reported in literature.

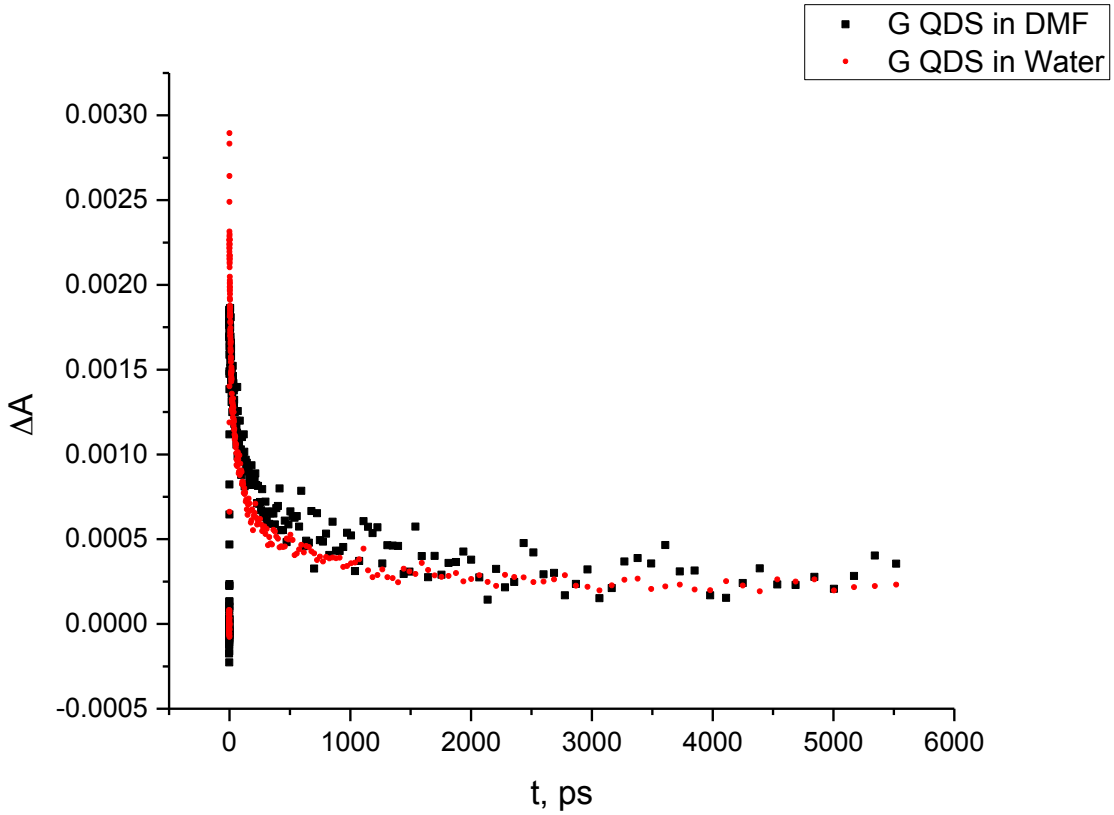

Fig. 7-8: Time resolved Photoluminescence for graphene quantum dots in water and DMF excited @ 370nm.

The current claim that the graphene quantum dots band gap is attributed to the quantum confinement is not applicable. There is no way of comparison between semiconductor quantum dots like CdSe or CdS and graphene quantum dots. CdSe quantum dots exhibits blue shift by reducing their size by 5 nm. This is a considerable shift, unlike the graphene quantum dots, that even by using different sizes of graphene quantum dots, they all show nearly similar absorption and emission. According to literature [1], there is a range of 20-30 nm, which we believe it is mainly due to using different synthesis procedure that introduces new surface functional groups that acts like oxygenation of Graphene, or even by changing the solvent and its effect on the surface states, or by changing pH.

Oxygen introduced new defect states to graphene and attained the photo properties to graphene. Doping with other materials would have similar effects, away from the quantum dot size or any confinement. Qu et al and Yeh el al publsished several articles regarding the effect of functionalizing graphene quantum dots and its effect on red shifting the absorption of the quantum dots [9,10]. Qu et al proposed that doping with sulfur and nitrogen (with lower bands than oxygen) can reduce the band gap of graphene quantum dots to reach 1.9 eV, rendering the material active in the visible region.

As shown in Scheme 7-1,the main band gap reduction took place due to the doped sulfur and nitrogen atoms only and not due to quantization. Moreover, this scheme indicates why different excitation wavelengths of graphene quantum dots, produce emissions that are totally different from the other wavelength. In a semiconductor quantum dot, exciting an electron with an energy that is larger than the conduction band leads to the excitation of the electron and it relaxes by emitting heat till it reaches the lowest unoccupied

molecular orbital, where it relaxes to the valence band and emit a luminescence which equals the band gap in energy. Therefore, in semiconductor quantum dots, whatever excitation wavelength the material is excited with, it will result in similar luminesce as long as the energy provided is larger than the band gap. However, in the case of graphene quantum dots, the presence of defect states within the band gap leads to different excitations according to the energy of the applied source, and as a result we get different emission peaks.

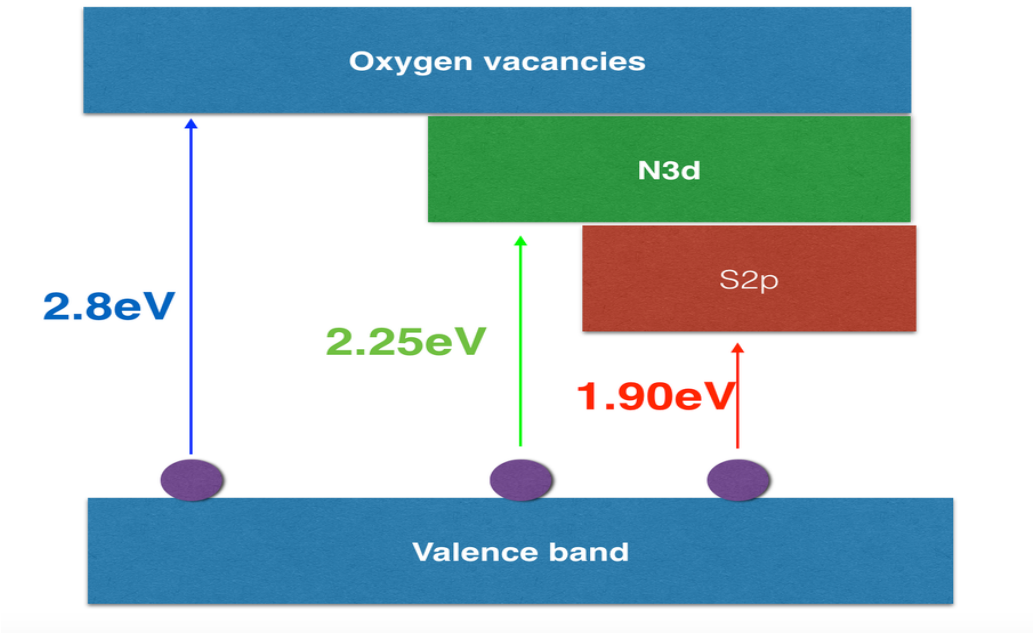

Scheme 7-1: Band gap of graphene quantum dots after doping with N and S.

The solvent used also plays an important rule in the emission [6]. We showed in the previous paragraph that the surface groups and defects play an important rule in determining the red or blue shift in the absorption and emission of the graphene

quantum dots, as a result changing the solvent polarity would affect the surface group that will directly result in changing the absorption and emission shift. Polar solvents are classified into protic or aprotic, protic solvents like water can easily form hydrogen bonding with the carboxylic or hydroxyl groups on the surface of the quantum dots, leading to the formation of new defect states that results in longer relaxation time. On contrary, using polar aprotic solvent as dimethyl formamide (DMF), that does not form hydrogen bonding with the graphene quantum, see Fig. 7-8.

In summary, graphene quantum dots are unlike semiconductor quantum dots in many perspectives, including the synthesis, and even the size dependent optical properties. Till now there is no strong evidence on the quantum effect of the Graphene quantum dots, and there is no potential difference between the Graphene oxide and Graphene quantum dots except in the size, and the C/O ratio, that directly affects the photoluminescence of the quantum dots. Till now, there is no specific method to engineer the band gap of the Graphene quantum dots except by doping or by changing surface groups or by inducing defects, yet there are potential applications for the quantum dots owing to their considerably small size and their very high stability unlike the semiconductor quantum dots. In addition, the graphene quantum dots are not toxic like the semi conductor quantum dots; as a result they can be used safely for Bio imaging and other biological applications.

We were able to produce graphene quantum dots with a size ranging from 10-30 nm via hydrothermal treatment of graphene oxide. The difference in photoluminescence between

graphene oxide and graphene quantum dots was highlited, and finally we reached a conclusion regarding the origin of the PL of the graphene quantum dots.

7.2 Functionalized graphene quantum dots:

In this part, we functionalized graphene quantum dots with Mercapto propanoic acid (MPA). Fig 7-9 shows the obtained Raman spectra for the functionalized graphene quantum dots, being one of the most sensitive techniques to determine the functionalities on the surface of the quantum dots.

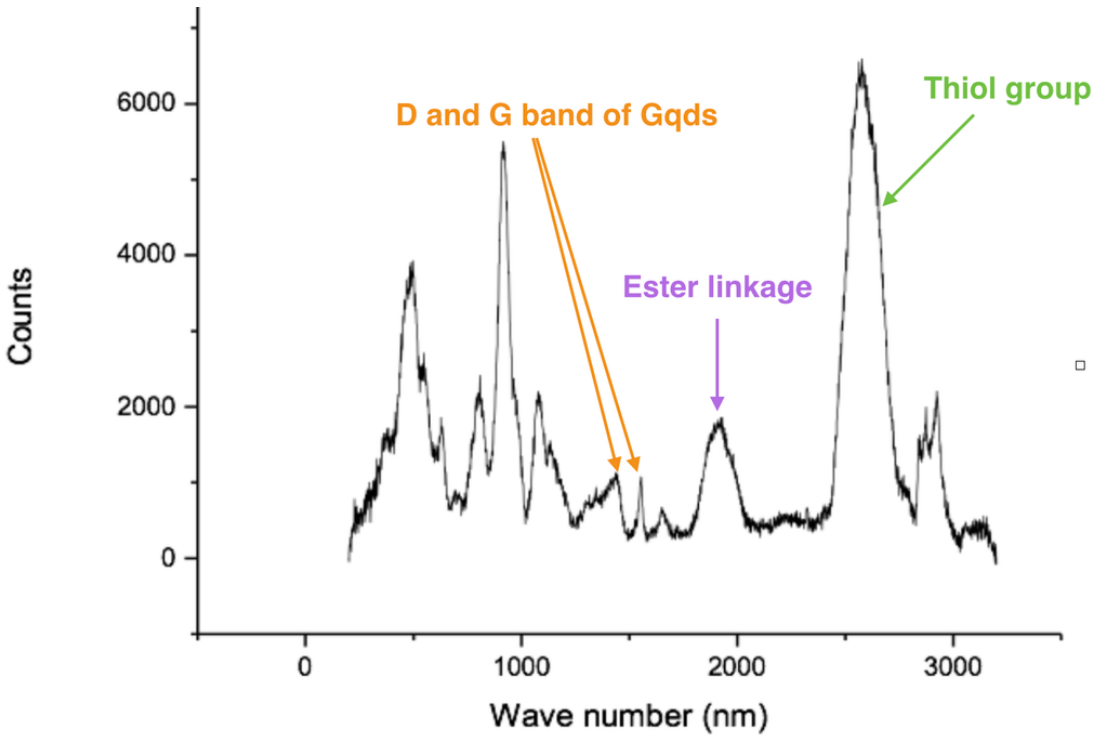

Fig 7-9: Raman spectrum for mercapto propanoic acid functionalized graphene quantum dots.

The D and G bands of Graphene quantum dots appears at their well known positions (1370 and 1570 nm), the ratio between them I_D/I_G equals 1.04, conforming the aforementioned plain graphene quantum dots. We can also define the ester linkage, which appears as a broad peak from 1800 to 2100 nm^{-1}. Also, the thiol group appears prominently at 2750 nm^{-1}.

By applying UV light, we can see the fluorescence produced by the functionalized Graphene quantum dots and how it is difference from Graphene quantum dots before dialysis and after dialysis (fig 7-10). The bleaching that took place indicates the efficient charge transfer between the Graphene quantum dots and the Mercapto propanoic acid. By exciting the electrons of the graphene quantum dots by UV light, they get excited to the conduction band, then the electrons transfer to the linker (MPA), that is why there is no strong fluorescence as seen in other non functionalized graphene quantum dots. This concept was proved by measuring photoluminescence of graphene quantum dots.

The Photoluminescence spectra of the functionalized Graphene quantum dots showed a distinct deviation from the non-functionalized Graphene quantum dots. The $I_{1P,}$ which is reflecting the defect states and surface functional groups, are very prominent compared to I_{2P}. However, in the non-functionalized Graphene quantum dots, the difference between the I_{2P} and I_{1P} was much higher. This increase in the I_{1P} is a solid indication for the functionalization of the Graphene quantum dots with the mercapto propanoic acid, and there is no way to confuse between the I_{1p} peak in the case of functionalized and non functionalized Graphene quantum dots as the difference and the behavior is totally different.

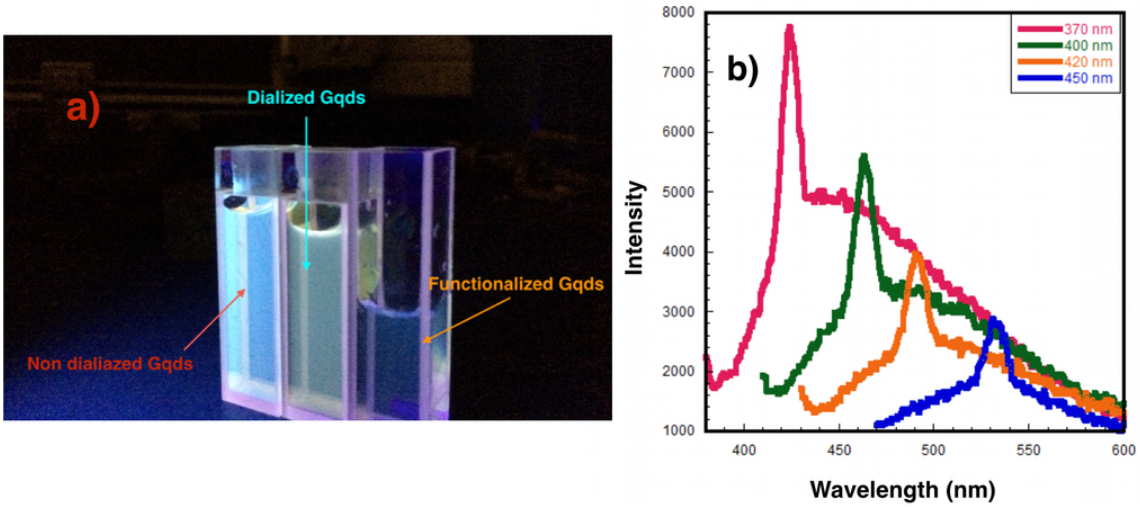

Fig. 7-10: (a) Exciting non dialyzed, dialyzed and functionalized graphene quantum dots with UV light of 345 nm. (b) Photoluminescence of functionalized graphene quantum dots at different excitation wavelengths.

7.3 TiO_2/ Graphene quantum dots:

After we sucsseded to functionalize our graphene quantum dots to make use of the smaller band gap and very high conductivity of graphene quantum dots in solar energy conversion.

Graphene quantum dots act as a photosensitizer on the surface of titania, due to its smaller band gap and very high quantum efficiency. The conduction band of titania is directly below the conduction band of graphene quantum dot, scheme 7-2. This can ensure an efficient electron transfer from the higher energy conduction band of graphene quantum dots to the more stable lower energy conduction band of titania nanotubes. On the other hand, the holes that are produced by excitation of titania nanotubes can directly transfer to the graphene quantum dots, which is higher in energy (holes transfer from lower to higher energy states). As a result, graphene quantum dots are not only photosensitizers, but also they act as a hole sink. This is

expected to directly reduce the recombination rate for titania nanotubes and increase the quantum efficiency.

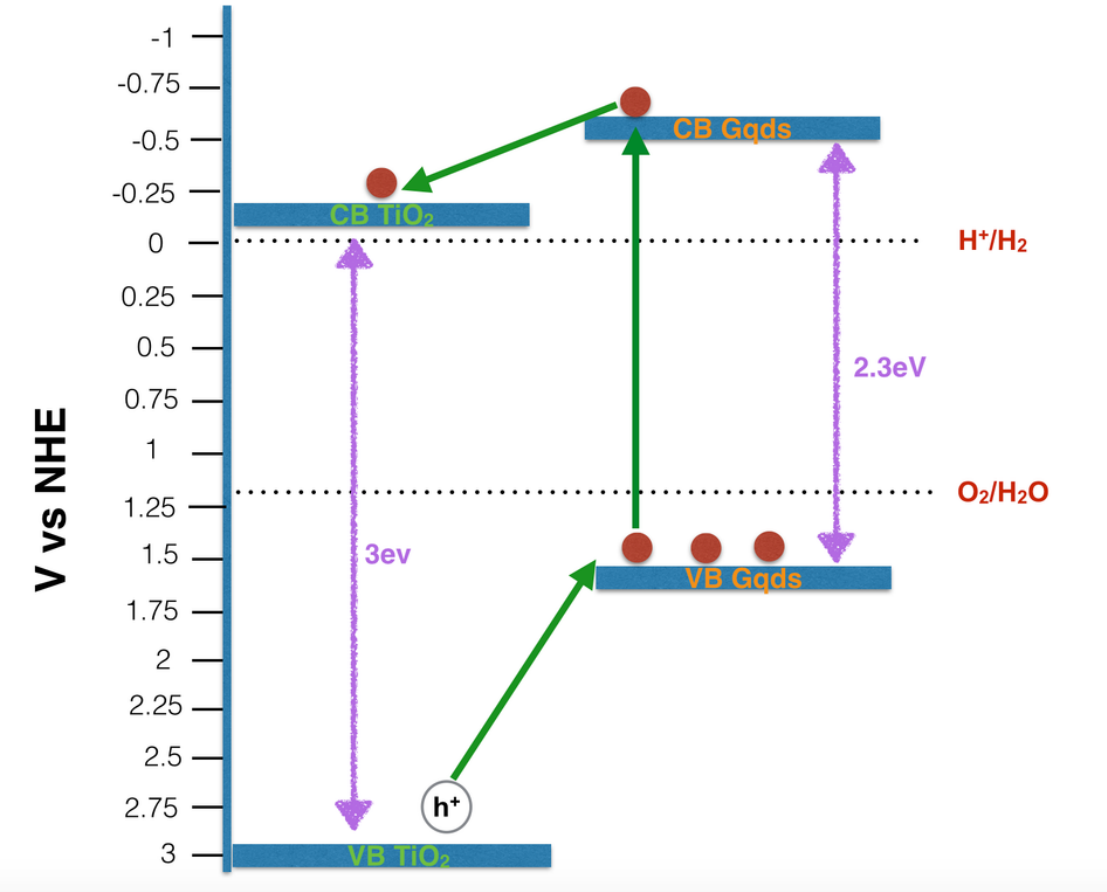

Scheme 7-2: Proposed mechanism for titania/ graphene quantum dots system.

Following the electrophoretic deposition of the functionalized graphene quantum dots on the surface of titania nanotubes, we measured the cyclic voltammetry in order to characterize the functionalization of the graphene quantum dots.

The two prominent reductive desorption peak of the thiol groups attached to the graphene quantum dots appears at -0.9V and -1.5V, and a smaller oxidative deposition peak for thiol also appears at -1.5V.

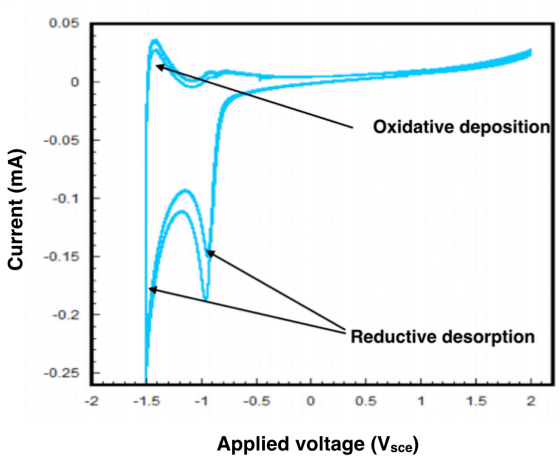

Fig. 7-11: Cyclic voltammetry for the functionalized titania with graphene quantum dots.

XPS was performed for the functionalized titania in order to detect the presence of graphene quantum dots on the surface of the titania. The appearance of two reductive peaks for thiol is indicating that there are two types of thiol configurations on the surface. The presence of defects on the surface reduces the negative potential needed to desorb the molecule, while highly ordered groups requires more negative potential. Its hard to control in such multi step chemical reaction the side reactions that can take place.

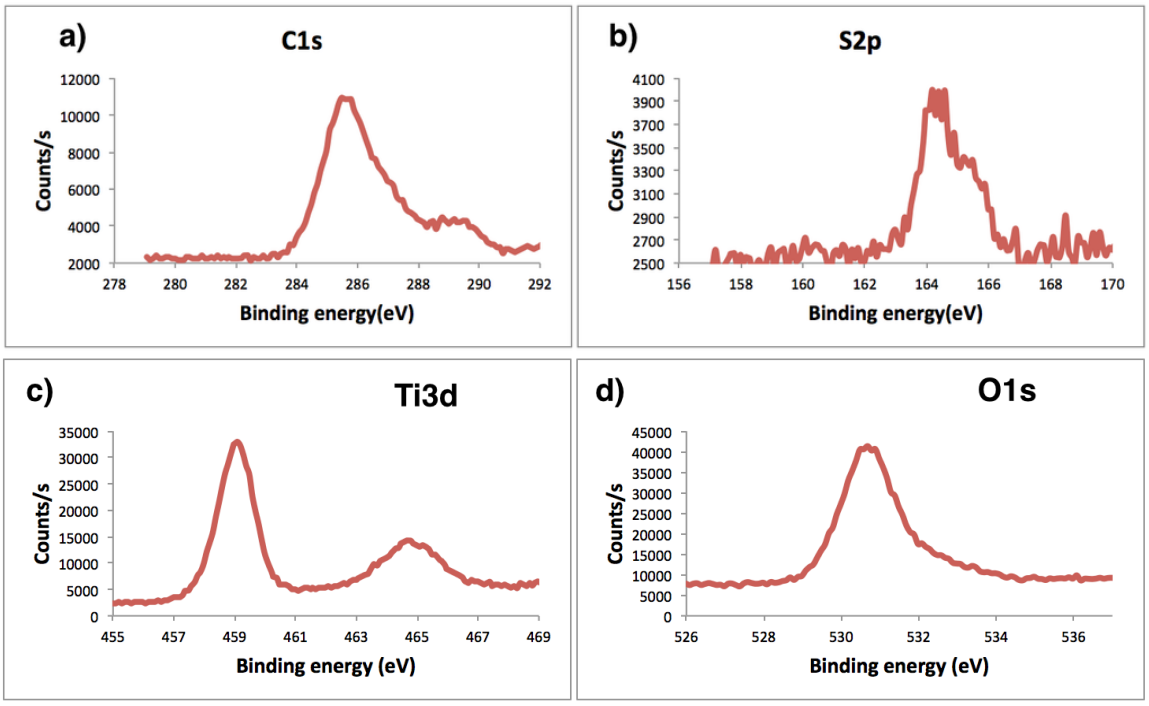

Fig. 7-12: XPS spectra for functionalized titania nanotubes, (a) C1s spectra, (b) S2p, (c) Ti3d, (d) O1s.

We measured the photocurrent so as to understand the role of graphene quantum dots on the surface of titania nanotubes. Surprisingly, nearly a 50% enhancement in photocurrent was achieved when compared to bare titania. This promising result is mainly attributed to the enhanced visible absorption of the graphene quantum dots, and also to the efficient electron transfer from the conduction band of graphene quantum dots to the conduction band of titania nanotube. For sure, that are some charge carrier loss throught the linker. However, MPA is considered one of the most efficient linkers.

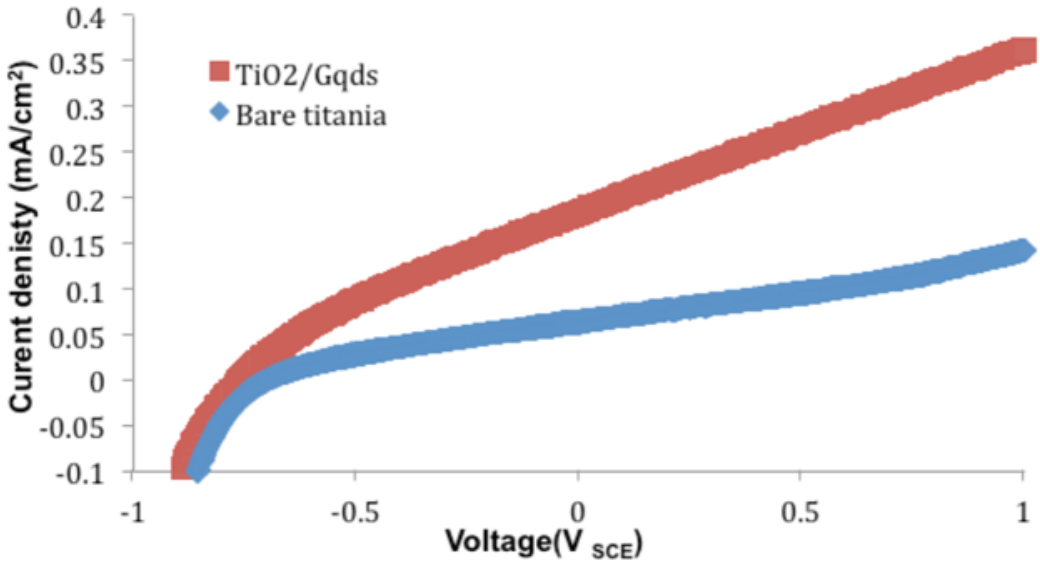

Fig. 7-13: Photocurrent for both bare titania and functionalized titania with graphene quantum dots.

In summary, we were able to synthetize and charactarize graphene quanutm dots, in addition we were able to functionalize graphene quantum dots with mercaptopropanoic acid (MPA) in order to link graphene quantum dots with other systems. In our case we linked graphene quantum dots to titania nanotubes intended for water splitting applicaiton. TiO_2/graphene quantum dots system experienced higher photocurrent by 50%. This promising result will be subjected to further studies to study the efficency of the linking in terms of charge recombination and the best method of deposition.

References:

1. Zhu, S.; Song, Y.; Zhao, X.; Shao, J.; Zhang, J.; Yang, B. The photoluminescence mechanism in carbon dots (graphene quantum dots, carbon nanodots, and polymer dots): current state and future perspective. *Nano Research* **2015***, 8*, 355-381.

2. Tang, L.; Ji, R.; Cao, X.; Lin, J.; Jiang, H.; Li, X.; Teng, K. S.; Luk, C. M.; Zeng, S.; Hao, J. Deep ultraviolet photoluminescence of water-soluble self-passivated graphene quantum dots. *ACS nano* **2012***, 6*, 5102-5110.

3. Kim, S.; Shin, D. H.; Kim, C. O.; Kang, S. S.; Joo, S. S.; Choi, S.; Hwang, S. W.; Sone, C. Size-dependence of Raman scattering from graphene quantum dots: Interplay between shape and thickness. *Appl. Phys. Lett.* **2013***, 102*, 053108.

4. Pan, D.; Zhang, J.; Li, Z.; Wu, M. Hydrothermal route for cutting graphene sheets into blue-luminescent graphene quantum dots. *Adv Mater* **2010***, 22*, 734-738.

5. Li, Y.; Hu, Y.; Zhao, Y.; Shi, G.; Deng, L.; Hou, Y.; Qu, L. An Electrochemical Avenue to Green-Luminescent Graphene Quantum Dots as Potential Electron-Acceptors for Photovoltaics. *Adv Mater* **2011***, 23*, 776-780.

6. Chien, C.; Li, S.; Lai, W.; Yeh, Y.; Chen, H.; Chen, I.; Chen, L.; Chen, K.; Nemoto, T.; Isoda, S. Tunable photoluminescence from graphene oxide. *Angewandte Chemie International Edition* **2012***, 51*, 6662-6666.

7. Gómez-Navarro, C.; Weitz, R. T.; Bittner, A. M.; Scolari, M.; Mews, A.; Burghard, M.; Kern, K. Electronic transport properties of individual chemically reduced graphene oxide sheets. *Nano letters* **2007***, 7*, 3499-3503.

8. Liu, Z.; Zhao, X.; Zhang, X.; Yan, X.; Wu, Y.; Chen, Y.; Tian, J. Ultrafast dynamics and nonlinear optical responses from sp2-and sp3-hybridized domains in graphene oxide. *The Journal of Physical Chemistry Letters* **2011***, 2*, 1972-1977.

9. Yeh, T.; Chan, F.; Hsieh, C.; Teng, H. Graphite oxide with different oxygenated levels for hydrogen and oxygen production from water under illumination: the band positions of graphite oxide. *The Journal of physical chemistry C* **2011***, 115*, 22587-22597.

10. Qu, D.; Zheng, M.; Du, P.; Zhou, Y.; Zhang, L.; Li, D.; Tan, H.; Zhao, Z.; Xie, Z.; Sun, Z. Highly luminescent S, N co-doped graphene quantum dots with broad visible absorption bands for visible light photocatalysts. *Nanoscale* **2013**, *5*, 12272-12277.

Chapter 8

Summary and Future work

From the work presented in this thesis, the following conclusions are drawn:

1. Thin walled titania nanotubes (3-5) nm can be prepared by using a mixture of aqueous and non aqueous solvent in a glycerol based electrolyte, using anodization.
2. Thin walled titania nanotubes proven to be more efficient than conventional thick walled nanotubes in charge separation and efficiency in water splitting application.
3. Hydrogen annealing of titania nanotubes passivates the defect states in titania (4 HRS hydrogen annealing), and increases the defect states in titania (more than 6 HRS hydrogen annealing).
4. Black titania shows only a tail in the absorption spectrum beyond 400 nm, which does not satisfy the clain that black titania absorb from the whole visible spectra.
5. KOH and hydrogen annealing passivates most of the defect states on the surface of titania and increases both the conductivity and the charge carrier concentration.
6. Graphene quantum dots are not so different from graphene oxide, although their PL is quiet different due to their different shape and size, but both of them are having similar band gap and photo activity.

7. Functionalized graphene quantum dots with MPA was anchored to titania nanotubes, and it experienced a 50 % enhancement in photocurrent.

Finally, here are some points that are suggested for the future work:

- Functionalized graphene quantum dots with MPA offers a platform for conjugating the quantum dots with other semiconductor quantum dots, such as CdSe or ZnS, or even with gold nanoparticles for plasmonic effect. Fig. 8-1 shows preliminary XPS results for conjugating CdSe quantum dots with graphene quantum dots.

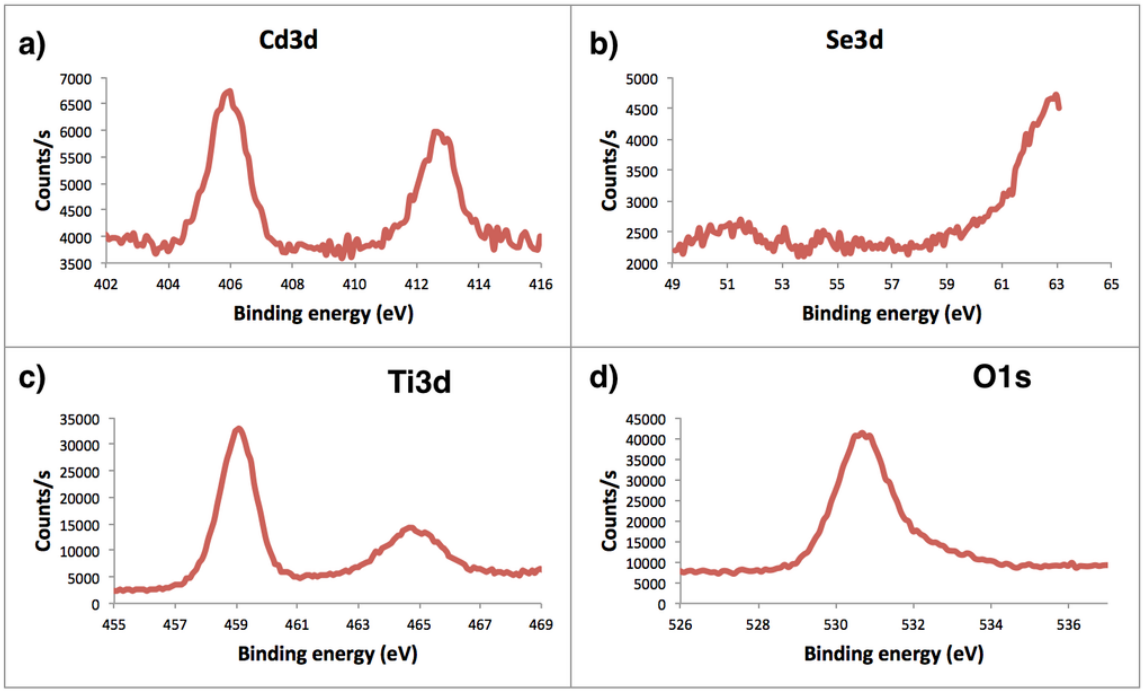

Fig. 8-1: XPS spectra (a) Cd3d, (b) Se3d, (c) Ti3d, and (d) O1s.

- Graphene quantum dots can serve in other fields, due to its very low toxicity, very high stability and luminescence, unlike semiconductor quantum dots, several reports are heading towards using graphene quantum dots for bio imaging. We started working on conjugating graphene quantum dots with malonyl group, that are well known for their binding to nuclear moieties. It is expected that graphene quantum dots would enter the nucleus due to its small size and act efficiently. Fig. 8-2 shows preliminary Raman spectra for the graphene quantum dots conjugated with the malonyl group.

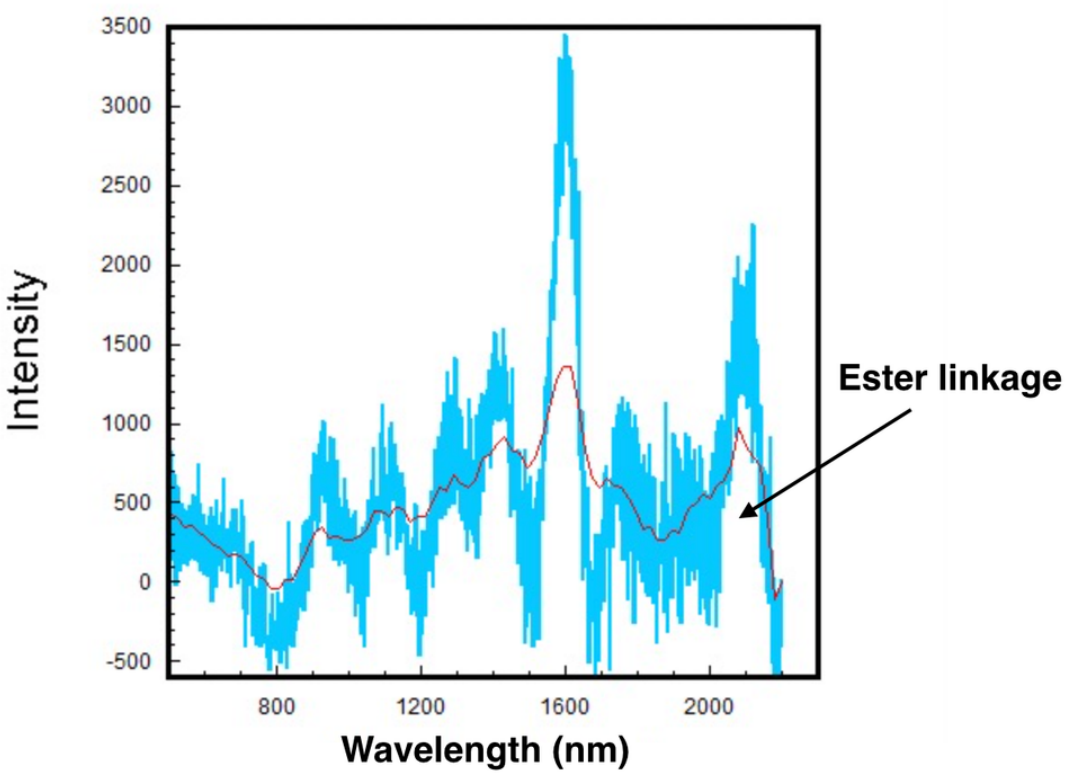

Fig. 8-2: Raman spectra for malonyl-functionalized graphene quantum dots.